

**DISTINCT-ELEMENT MODELLING OF INTERMITTENT
DEFORMATION BEHAVIOUR AND FATIGUE IN TWO
LARGE ROCKSLIDES**

by

MEGAN SMITHYMAN

B.Sc. Queen's University, 2007

**A THESIS SUBMITTED IN PARTIAL FULFILLMENT OF THE
REQUIREMENTS FOR THE DEGREE OF**

MASTER OF APPLIED SCIENCE

in

THE FACULTY OF GRADUATE STUDIES

(Geological Engineering)

THE UNIVERSITY OF BRITISH COLUMBIA

August 2010

© Megan Smithyman, 2010

Abstract

This thesis reports the assessment of two large, slow moving landslides. The Campo Vallemaggia slide is located in the southern Swiss Alps, and has a recorded history of movements dating back hundreds of years. The other slide, Little Chief, is located in British Columbia, and is affected by toe submergence due to the presence of a dam. These slides have well developed sliding surfaces along which the majority of the movement takes place.

A process of modelling the effects of time, involving different water tables to represent the wet and dry seasons of the year, was undertaken using UDEC (Universal Distinct Element Code, Itasca, 2009). The models were run with first the high, then low water tables, alternating repeatedly to represent model years. They were analyzed for signs of fatigue, internal deformations and long term movement trends. The Little Chief Slide was also analyzed using this method to verify the positions and existence of the sliding surface.

Mohr-Coulomb plasticity was applied to both slides, and found to be sufficient for representing the Campo Vallemaggia slide, and developing fatigue indications. A sharp drop in the number of yielded elements in the model was seen at approximately 1300 years. This coincided with a slowing of the model movement and a change in the rate of opening of a fault. This was concluded to be similar to the fatigue effect commonly seen in metal.

However the Little Chief slide did not develop as desired under this constitutive model, therefore the strain softening plasticity criterion was applied to this slide for models that investigated internal deformation of the sliding mass, and those focussing on development of the sliding surface.

Initial strain softening models using the properties expected for the site did not give satisfactory results, likely due to geologic and geometric complications not captured in a two dimensional model using a homogeneous rockmass. Instead, lowerbound properties were applied to the slide, resulting in the development of a sliding surface similar to that interpreted at the site. As well, significant internal deformation was found using these properties, including some suggestive of a fatigue effect.

Table of Contents

Abstract.....	ii
Table of Contents.....	iii
List of Tables	vi
List of Figures.....	vii
Acknowledgements.....	xii
Dedication.....	xiii
1 Introduction	1
1.1 Problem Statement.....	1
1.2 Research Objectives.....	1
1.2.1 Representation of Time in Stress-Strain Models	1
1.2.2 Fatigue Modelling.....	2
1.2.3 Basal and Internal Shear Surface Modelling.....	2
1.3 Thesis Structure	3
2 Literature Review	4
2.1 Slope Monitoring	4
2.1.1 Types of Monitoring Systems.....	5
2.1.2 Monitoring Trends and Discussion.....	8
2.2 Temporal Behaviour of Rock Slopes	9
2.2.1 Creep.....	10
2.2.2 Stages of Material Creep.....	10
2.2.3 Mechanics of Creep	11
2.2.4 Causes of Rockmass Creep.....	12
2.2.5 Creep Considerations.....	15
2.2.6 Fatigue due to Cyclic Loading	16
2.3 Time-dependent Analysis of Rock Slopes.....	16

2.3.1	Predictive Methods of Time of Occurrence	17
2.3.2	Constitutive Modelling	20
2.3.3	Measurements for Time Dependency	22
2.3.4	Strain Softening and Brittle Failure	22
3	Methodology.....	24
3.1	Data Collection and Interpretation.....	24
3.1.1	Campo Vallemaggia.....	24
3.1.2	Little Chief.....	24
3.2	Modelling.....	24
3.2.1	Model Initialization.....	25
3.2.2	Modelling of Rock Mass Fatigue.....	26
4	Case Study of the Campo Vallemaggia Landslide	30
4.1	Geology.....	30
4.1.1	Engineering Geology of the Site	31
4.1.2	Ground Water.....	34
4.1.3	Landslide History and Behaviour.....	34
4.2	The Model.....	34
4.3	Results.....	36
4.3.1	Plasticity and Fatigue	37
4.3.2	Intermittent Displacement Behaviour	50
5	The Little Chief Landslide.....	55
5.1	Geology.....	55
5.2	Engineering Geology and Slide Features.....	55
5.2.1	Basal Detachment	56
5.2.2	Rockmass Properties	58
5.2.3	Fracture Network and Discontinuity Properties.....	63

5.2.4	Water Table.....	63
5.2.5	Assumptions and Implications	64
5.3	Modelling of Initiation and Progressive Development of Failure Surface	65
5.3.1	Model Set-Up.....	65
5.3.2	Initial Results	67
5.4	Fatigue Modelling Based on Interpreted Basal Sliding Surface	82
5.4.1	Model Setup	82
5.4.2	Intermittent Displacement Behaviour	84
5.5	Internal Deformation Modelling	93
5.5.1	The Model.....	93
5.5.2	Internal Deformation Results	94
5.5.3	Movement Patterns and Toe Release	100
6	Conclusions	104
6.1	Fatigue and Internal Shearing for an Unconfined Translational Slide Surface.....	104
6.2	Fatigue and Internal Shearing for a Confined Translational Slide Surface.....	105
6.3	Recommendations for Future Work.....	106
	Bibliography	108
	Appendix A - Time and Computing Requirements	112
	Appendix B - Modelling Code.....	113
	B.1 Annual Cycling – Fish Code	113
	B.2 Campo Vallemaggia Geometry	113
	B.3 Little Chief Geometry	116
	B.4 Plasticity	118
	B.4.1 Campo Vallemaggia Mohr Coulomb	119
	B.4.2 Little Chief Mohr Coulomb.....	119
	B.4.3 Little Chief Strain Softening	119

List of Tables

Table 1: Summary of monitoring instruments and techniques	6
Table 2: Variations used in limit equilibrium assessment of residual values	28
Table 3: Rock mass properties used for modelling, taken from Bonzanigo et al. (2007).....	37
Table 4: Summary of rockmass properties calculated broken down by individual rock units and combined homogeneous slide mass.....	63
Table A1: Computing time requirements for variations of the models.....	112

List of Figures

Figure 1: Standard creep curve derived from a laboratory creep test showing the stages of Primary, Secondary and Tertiary creep (after Jaeger, 1979)	11
Figure 2: Flow chart showing interrelationship between rock slope processes contributing to time-dependent movement and fatigue	17
Figure 3: Sketch of standard curves produced using the Fukuzono method (after Rose and Hungr, 2007)	19
Figure 4: Flow chart showing the progression of steps followed in UDEC to simulate cyclic loading and rock mass fatigue. Those steps shown in pale brown were used to initialize the model to site conditions, while those shown in darker brown were the steps taken	25
Figure 5: Slide results showing all sliding surfaces with factor of safety between 0.95 and 1.05. The surface in black has a factor of safety close to one and matches well with in situ observations of the size and shape of the actual side surface at Little Chief (shown in green). The surface in grey has the lowest safety factor for these conditions. Cohesion =0.05MPa, friction =25 degrees	29
Figure 6: Image of the Campo Vallemaggia landslide. The settlements present on the slide can be seen.	30
Figure 7: Geological cross-section taken longitudinally through the Campo Vallemaggia landslide. Faults shown in bold are those included in the models. (after Bonzanigo et al. 2007).	31
Figure 8: The Campo Vallemaggia landslide, showing the Campo block in bright yellow and green and the Cimalmotto block in pale gray. After Bonzanigo et al. (2007)	32
Figure 9: Disturbed and broken rock at the toe of the Campo Vallemaggia landslide	33
Figure 10: The undisturbed rockmass in the Campo Vallemaggia drainage adit	33
Figure 11: Model of the Campo Vallemaggia slide geometry, showing locations of water tables and movement generated faults (scarps).....	35
Figure 12: Close up of the jointing pattern used in the Campo Vallemaggia models, also showing the lower fault present in the sliding mass.	36
Figure 13: Progression of yielded elements with increasing number of model years for the model with no internal faults.	38
Figure 14: Yield displacements in the unfaulted model compared with fault positions. The box indicates the area shown in later figures. Note that the heavy black lines, which indicate the positions of the mapped faults, are superimposed on this image for comparison. These faults have not be included in the model.	39

Figure 15: Number of yielded elements present in the model at any given year. A sharp decrease can be seen at approximately 1300 years, coinciding with the development of internal shearing and fault scarp generation in the model.....	39
Figure 16: Opening of a fault in the unfaulted model. Shaded areas are openings, white spaces are bricks. See figure 13 for the placement of these figures on the slide.	41
Figure 17: Pore pressure distributions around the area where the fault opens at 10 and 2000 years.....	42
Figure 18: Horizontal stress distributions through the entire slide	43
Figure 19: Horizontal stress distributions in the area of interest around the fault opening. The contours of the stresses are in MPa. Note that the 10 year and 500 year images follow the left legend, while the 1500 year and 2000 year images follow the right legend.	44
Figure 20: Vertical stress distributions through the entire model	45
Figure 21: Vertical stress distributions in the area of interest surrounding the fault opening	46
Figure 22: The number of yielded elements present in the faulted model at any given time.	47
Figure 23: Progression of shear and tensile yield indicators in the faulted version of the model. They are similar to those in the unfaulted version, but tend to localize right on the faults, instead of just in the same general area.....	48
Figure 24: Horizontal displacements are shown for both the a) non-faulted and b) faulted versions of the model. Both show fairly distinct upper and lower block movements, with the faulted model shows a more abrupt transition between these blocks compared to the non-faulted model. The displacements shown are those after 800 modelled years.....	49
Figure 25: Displacement vectors in the area around the opening fault. Note that vectors are scaled for maximum visibility in all models and relative comparison. Magnitudes of vectors cannot be compared between models.....	50
Figure 26: The red stars indicate the locations of the monitoring points used to create Figure 20. The upper star is that used for figures 20 b and d, while the lower star is that used for a and c	51
Figure 27: Displacement vs. modelled years: a) at the toe after 10 years; b) on surface behind the lower fault scarp after 10 years; c) at the toe after 800 years; and d) on surface behind the lower fault scarp 800 years at the surface.....	52
Figure 28: Horizontal velocities at the toe of the slope for the first 10 years.	53
Figure 29: Displacement and velocity data from the Campo Vallemaggia landslide after Bonzanigo et al (2007).....	53
Figure 30: Plan view map of the Little Chief Slide showing slide boundaries and borehole locations, and areas of linear extension, as well as areas experiencing greater degrees of movement. (after Watson, 2006b)	56

Figure 31: Disturbed rock near the top of the headscarp of the Little Chief Slide.	57
Figure 32: Toe bulge at base of the Little Chief Slide.	57
Figure 33: Air photo of the Little Chief Slide. The approximate slide boundaries are shown in green. The road up the slide is the distinct white feature present, and potential extensional features behind the slide are identified in orange.	58
Figure 34: Sketch showing interpretation of internal sliding surfaces relative to the basal detachment and ground surface. Borehole profiles showing gouge zones and areas of movement detected by inclinometers are included.	59
Figure 35: Blocky rockmass outcrop near the top of the Little Chief Slide.....	59
Figure 36: Rockmass outcrop near the bottom of the Little Chief Slide.....	60
Figure 37: GSI chart after Marinis et al. (2005). Superimposed are the ranges in values estimated for the gneisses and schists.....	61
Figure 38: Comparison between non-linear Hoek-Brown failure envelope for the Little Chief mica schist (in red), and linear Mohr Coloumb envelope fit (in blue) through the stress range of interest.....	62
Figure 39: Water tables (shown in light blue) with the borehole profiles from which it was interpreted. .	64
Figure 40: The starting model for the Little Chief Slide when no pre-existing surface is being used. This version is with the presence of valley fill.	65
Figure 41: Joint pattern used in models generating sliding surface.	66
Figure 42: Model setup showing the different water tables used in the fatigue cycling of the Little Chief slide. Shown for the version of the model with no valley fill	67
Figure 43: The Mohr-Coulomb model having been allowed to come to equilibrium with the low water table and then cycled for 30 years. This is just one typical example of Mohr Coulomb results that fail to show landslide initiation.	68
Figure 44: Chart showing strain softening rate for the abrupt strain softening.....	68
Figure 45: Development of toe, and upper part of slide in strain softening model, 70 year simulation	69
Figure 46: Comparison of landslide toe in strain-softening models with and without fill in the valley.....	70
Figure 47: Chart showing the strain softening rate for the lower bound properties.....	71
Figure 48: Strain softening models showing the development of a sliding surface in models with and without valley fill. In both cases this is compared to the sliding surfaces interpreted based on site investigation and monitoring data.....	72
Figure 49: Progression of yielded elements over the course of 750 years. The development of a through going sliding surface can be seen.....	73

Figure 50: Horizontal and vertical stress distribution sin the whole model at 10 and 750 years, with valley fill. Stress contours are in MPa.	74
Figure 51: Horizontal and vertical stresses in the toe of the model at 10 and 750 years, with valley fill. Stress contours are in MPa.....	75
Figure 52: Horizontal displacements in the strain softening model at a) 70 and b) 750 years	77
Figure 53: Velocities of the strain softening lower bound model at a) 70 and b) 750 years.....	78
Figure 54: a) Layering and plasticity indicators, and b) horizontal displacements in the layered model after 30 years of cycling.....	80
Figure 55: Plasticity indicators showing extra damage along the surface and at the toe ten years after the removal of the valley glacier. The glacier is shown in blue.....	81
Figure 56: The Little Chief model used to test the effects of fatigue. The basal sliding surface is shown in green, and the internal sliding surfaces are shown in red.	83
Figure 57: Close up view of the brick pattern of joint spacings used in the slide body in the Little Chief slide model.....	84
Figure 58: Model setup showing the different water tables used in the fatigue cycling of the Little Chief slide.....	85
Figure 59: Displacements at the toe at: a) 10 years, b) 1000 years, c) 3000 years, d) 10 years with one peak 10 year event, e) 1000 years with 10 and 100 year peak events, and f) 3000 years with 10 and 100 year peak events.....	86
Figure 60: UDEC slide model showing location of history monitoring points used to track intermittent displacements and velocities.....	87
Figure 61: Horizontal and vertical displacements as they vary across the slide surface at 10 years. Note that negative vertical values indicate downward movement.....	88
Figure 62: Horizontal and vertical displacements as they vary across the slide surface at 3000 years. Note that negative vertical values indicate downward movement.....	89
Figure 63: Horizontal velocities as the different history points along the slide surface at 10 years.....	90
Figure 64: Displacement vectors (in red) showing movement direction and magnitude. Note that the two parts have different scales for the vectors so that both are visible.....	91
Figure 65: Horizontal stresses in the model at 10 and 3000 years.....	92
Figure 66: Vertical stresses in the model at 10 and 3000 years	93
Figure 67: Yielding as an indicator of the development of internal faults assuming: a) an elasto-perfectly plastic, and b) strain softening constitutive model.....	94

Figure 68: Strain softening model assuming lowerbound properties with the basal sliding surface included, but with no interior sliding surfaces.....	96
Figure 69: Change in the number of yielded elements present in the slide body with cyclic loading up to 1000 years, assuming expected rock mass properties for a strain softening constitutive model.	97
Figure 70: Change in the number of yielded elements present in the toe with cyclic loading up to 1000 years, assuming expected rock mass properties for a strain softening constitutive model.	97
Figure 71: Change in the number of yielded elements present in the slide body with cyclic loading up to 1400 years, assuming the lower bound rock mass properties for a strain softening constitutive model. ...	98
Figure 72: Change in the number of yielded elements present in the toe with cyclic loading up to 1400 years, showing a marked increase after 850 years, assuming the lower bound rock mass properties for a strain softening constitutive model.	98
Figure 73: Horizontal and vertical stresses above the basal detachment surface and 10 and 1100 years...	99
Figure 74: Distribution of horizontal displacement in the down slope direction.....	100
Figure 75: Toe of the landslide showing rotational movement necessary to release and allow movement higher up the slide.....	101
Figure 76: The Prandtl wedge, identified in the yielded elements, horizontal stresses and vertical stresses in the model.....	103

Acknowledgements

Firstly I would like to thank my supervisor, Dr. Erik Eberhardt, for his guidance, and financial support, during this process. His help and support has been invaluable. I would also like to express gratitude to Dr. Oldrich Hungr and Dr. Roger Beckie, my committee members, for their assistance.

I wish to thank the people at BC Hydro, specifically Tom Stewart and John Psutka for providing data and for their time and assistance in bringing this project together.

Thanks to Dr. Luca Bonzanigo for data provided by his work on the Campo Vallemaggia slide.

Finally I would like to express my gratitude to my family. My husband Brendan, without who's love and support this project could not have been completed. My parents, whose emotional, moral and financial support have made it possible for me to pursue my education. And my sister Emily, for always being there.

Dedication

To My Parents

1 Introduction

1.1 Problem Statement

The slow, down slope movement of rock and earth materials may be unnoticeable to the human eye and barely detectable by precision instruments. However, this movement can be the precursor to a large, deep-seated, catastrophic rockslide event. An understanding of rock slope deformation processes can thus be used to gain an understanding of when continuous, or intermittent, slope velocities accelerate indicating increased activity that may potentially lead to failure. These processes are complex; involving components of slip along discontinuities, intact rock yield and creep, and shear localization and progressive failure.

Studying the movement of a rock slope with time can yield valuable information relating to the slope's stability state. Accelerations in the displacement rate (above typical background values) are often seen in advance of catastrophic failure, and these in turn can be used in early warning systems to save lives (Glawe and Lotter, 1996). However, the interpretation of slope monitoring data is highly subjective due to geological complexity and uncertainty. Time-dependent strength degradation processes, oscillating/seasonal external stimuli (e.g. precipitation, snow melt, fluctuating water levels in a dam reservoir, etc.), and elements of progressive failure must all be accounted for to gain a real understanding of the processes under observation.

An improved understanding of slope movements as a function of time, and how to better predict and analyze these, can lead to more reliable early warning forecasting and improved hazard management. This thesis will work towards addressing some of the issues and deficiencies in current modelling practices through the characterization and analysis of time-dependent behaviour and fatigue leading to accelerating slope velocities. Data from two case histories of deep-seated slopes with intermittent sliding behaviour will be used to constrain and calibrate the analyses performed. These case studies are the Campo Vallemaggia landslide, located in the southern Swiss Alps, and the Little Chief slide, located in British Columbia, Canada.

Differentiation is made here between natural slopes for which a fully developed rupture surface already exists, and engineered slopes for which development of the rupture surface may still be required, with focus being concentrated on the former. Displacement-time monitoring data (and other pertinent data) is used to help develop the theoretical framework of the research undertaken and to constrain the numerical models developed for the two case studies. This includes an examination of the means by which time-dependent movement can be reproduced in the models according to the dominant processes involved. Numerical modelling is undertaken using the commercial program UDEC (Universal Distinct Element Code: Itasca, 2009) to specifically investigate strength degradation processes, cyclic loading and material fatigue.

1.2 Research Objectives

1.2.1 Representation of Time in Stress-Strain Models

Numerical modelling of landslides is typically carried out using software that applies stress-strain constitutive models. However, the detailed stress-strain state is often not well understood, or measurable. Instead, what information is available about a given unstable slope often takes the form of

displacement-time data produced through monitoring. One goal of this thesis is to introduce time dependence characteristics to these models. Some work has been done to apply a time-dependent viscoplastic constitutive model to a landslide shear surface interface in a finite element model (e.g. Desai et al., 1995), as well, many commonly used geotechnical software packages (e.g., UDEC; Itasca, 2009) include a creep constitutive model option for intact soil/rock. These, however, do not account for up-scaling issues related to time-dependent properties of a rock mass encompassing both yielding rock and slip along discontinuities.

Instead, this study takes a different, computationally simpler, approach by treating time implicitly through the use of time-dependent effects built into the model. This method is assessed in order to determine whether this is a sufficient analog for time in studies of this nature. This objective can be broken down as follows:

- 1) Use the distinct-element modelling software UDEC to model two deep-seated, slow moving rockslides, with differing basal detachment surfaces. These will be developed to reproduce observed displacement-time records using time-dependent controlling processes built into the models.
- 2) Examine how best to utilize standard displacement-monitoring data. The constitutive models most commonly used in numerical modelling only involve stress-strain relationships and not stress-strain-time relationships. Thus, the data sets most commonly used for monitoring and early warning are disconnected from the stability analyses typically carried out. The data available for model development and calibration are not being used to their full potential. This objective will explore means to make better use of this available monitoring data so that they can be more easily integrated with numerical modelling.
- 3) Investigate the degree of complexity required for the numerical model to adequately represent reality; i.e., is it sufficient to vary the water table position in a model to simulate seasonal changes, or is it also necessary to consider fatigue, brittle fracture, strain softening and rock mass strength degradation processes, etc. Included in this is an investigation of the amount of time, as represented by cycles of load, to cause particular responses in the model such as fatigue failure.

1.2.2 Fatigue Modelling

Metal undergoing cyclic loading will suffer from fatigue failure; this phenomenon has been thoroughly investigated in material sciences. It is therefore reasonable to hypothesize that a rock mass that experiences some form of cyclic loading will likewise suffer fatigue, although the prediction of the number of cycles required to produce failure is less well understood, even when simplified to laboratory testing of intact rock specimens (Bagde and Petros, 2005a).

1.2.3 Basal and Internal Shear Surface Modelling

Modelling of plastic yielding and shear strain localization can be used to investigate the initiation and progressive development of a deep-seated basal shear surface that can then be used to better understand the slope displacement data being collected or to possibly forward model the behaviour of the rockslide in future. Strain-softening models are used to simulate the initiation and development of the basal and internal sliding surfaces for the Little Chief slide case study in order to verify and more fully understand the interpreted surface locations projected through borehole investigations.

1.3 Thesis Structure

The problem statement and research objectives for this thesis are presented in Chapter 1. The objectives break down specific goals under the general topics of time in stress-strain models, fatigue and failure surface prediction.

In Chapter 2, a background literature review for the thesis is presented. General topics covered include monitoring techniques, time-dependent movement of rock, rock fatigue and strain softening in rock masses.

Chapter 3 outlines the methodology used to carry out the research. It separates the collection and interpretation of data related to the study sites from the modelling process used to produce understanding and results related to these sites.

Chapter 4 presents the setting and results for the Campo Vallemaggia landslide, used as a conceptual model in which the sliding surface is largely unconstrained at the toe of the slope (i.e. it daylight in a translational manner without a passive resisting block forming). These results compare and contrast internal shearing that develops through differential movements along the translational slide surface between models that incorporate known/interpreted complexity and those that are simplified. As well, displacement results are given and compared to those recorded for the site.

Chapter 5 presents the setting, behaviour and results for the Little Chief slide. The results are again divided between those in which all known features are included in the model, comparing displacement and plasticity results, and those without the features included. This case study also involves a more complex toe release mechanism, for which strain-softening modelling is undertaken to better establish the development of the basal failure surface.

Lastly, Chapter 6 summarizes the major conclusions from this thesis study, and provides recommendations for future work that could be done to continue this work.

2 Literature Review

This review is intended to cover the most important topics required for the completion and understanding of this thesis. It begins with a review of the current practice in slope monitoring and the measurement of time-dependent movement and then proceeds to discuss the causes of this movement in section 2.2. The effect of fatigue a particular focus of this thesis is considered at the end of this section. The work already undertaken in studying and modelling time-dependent behaviour is discussed in section 2.3. Finally, section 2.4 covers strain softening behaviour and models used in this thesis to study time-dependent behaviour.

2.1 Slope Monitoring

Slope monitoring to obtain information about a slope and its behaviour requires a program involving different instruments to detect changes in the slope, in most cases, displacements and pore pressures. The type of change detected depends on the instrument used. When dealing with unstable rock slopes, monitoring is one of the few means to gather the data needed to assess when the slope may fail (Glawe and Lotter, 1996).

The Mine Monitoring Manual (Franklin, 1990), released by the Canadian Institute of Mining and Metallurgy lists six reasons to monitor in mines. These are:

- To prevent accidents and protect personnel, i.e. by giving warning of a rockfall
- To obtain data for design
- To verify design data and assumptions
- To investigate ongoing instability and failures; useful in both back analysis and planning of remedial work
- To evaluate ground treatment
- To check the impact that mining has on the surrounding environment

The first four of these also apply to natural slopes. For many of these purposes surface displacement is often of interest to the engineer as its measurement provides the simplest and most cost effective way to observe the evolution of a landslide and analyse the kinematics of movement (Gili et al., 2000). There are many options when designing a monitoring program. The required accuracy and frequency of monitoring information will determine which type of instrument is most suitable for the slope in question. For landslides, or rock slope failures in general, accuracy should be on the order of centimetres, if not smaller (Gili et al., 2000). Pore pressure levels in a slope can also be very important and Bhandari (1988) describes common monitoring practices including comparing measurements of rainfall to variations in piezometric pressures or visible changes on the landslide surface (e.g. opening tension cracks, etc.).

Even the best monitoring set up is of limited use when not used properly. There are many cases where monitoring information has been diligently recorded but the readings, or their implications, not fully considered (Salt, 1988). Well trained operators, who understand the instruments and the meaning of the readings, are a vital part of any monitoring program.

Monitoring is an important source of input data for numerical modelling and rock slope design, providing constraints on the in situ behaviour of the material. Laboratory tests are another source of design data, but can be problematic, especially for creep modelling, due to scale issues and because the

short time duration of testing prevents real creep behaviour from being observed (Cristescu et al., 2002). For this reason information from in situ measurements is preferable wherever possible for modelling purposes.

2.1.1 Types of Monitoring Systems

There are two major categories into which monitoring schemes, or systems, may be divided: continuous and intermittent. Continuous systems, as the name suggests, involve readings or measurements being constantly taken, thus creating an uninterrupted data record of the measurement of interest. Intermittent systems on the other hand take readings at different time intervals. The interval depends on the set up of the system, and on operational and accessibility constraints. Continuous schemes have many advantages but tend to be high cost compared to intermittent schemes (Bhandari, 1988).

Monitoring systems available vary widely in what they measure, accuracy, frequency of measurements, and usefulness. An appropriate monitoring system should be chosen based on the type of slope failure anticipated or of concern. Early warning systems and the placement of monitoring equipment cannot be decided without a basic understanding of the mode of failure, an important consideration in system design (Eberhardt, 2008).

As an example, infrequent measurements are unlikely to record a rockslide that suddenly accelerates, while high precision instruments would be necessary for measurement of small creep movements in the range of mm per year (Bhandari, 1988). Due to variation both in rock behaviour and in monitoring equipment, it is necessary to carefully consider the options available. A summary of the more common types of slope monitoring equipment is presented in Table 1 with typical precision, advantages and disadvantages of each type listed.

2.1.1.1 Monitoring examples

A few examples of the implementation of monitoring systems are listed below, highlighting issues that arose in the use and maintenance of the systems.

- Geodetic monitoring was carried out for the Tessina Landslide in Italy. Benchmark prisms were monitored every 1-3 hours during emergency periods; at normal times they were monitored every 6 hours (Angeli et al., 2000). In this case, the prisms were surveyed intermittently, and this system demonstrates the necessity of increasing the frequency of monitoring during times of concern when employed for early warning purposes. The Campo Vallemaggia landslide provides another detailed case history involving over 100 years of geodetic monitoring, from survey monitoring using triangulation (1897 until the 1940's), to polygon levelling using theodolites (until 1984), to laser-based distance measurement from 1986 to present (Bonzanigo et al., 2007).

Table 1: Summary of monitoring instruments and techniques

Instrument	Type of Measurement	Typical Precision	Advantages	Disadvantages	Continuous or Intermittent
Geodetic	displacements	variable, typically mm scale	<ul style="list-style-type: none"> • very common • easy to use • can use local features as markers or targets • can monitor relative movements between blocks within landslide body (Bonzanigo et al., 2007) 	<ul style="list-style-type: none"> • must choose targets wisely to get total representation • must ensure instrument (e.g. total station) is set up on stable ground 	either
Extensometer	displacements	mm or less (Bhandari, 1988)	<ul style="list-style-type: none"> • many varieties suitable for different purposes • simple, reliable and low cost • can be combined with inclinometers and piezometers (Corominas et al., 2000) • can measure separate but related movements in slide mass (Angeli et al., 2000) when set up with multiple points 	<ul style="list-style-type: none"> • can develop complex systems with allowing opportunity for error • provide only relative movements (Furuya et al., 1999) • borehole methods can be very expensive • surface methods (wireline) sensitive to temperature change • they are 1-D sources, must use multiple setups to get 2-D or 3-D 	either
Inclinometer	angle of inclination of borehole used for subsurface movements	0.5-1mm/m of borehole (Franklin, 1990)	<ul style="list-style-type: none"> • can be very precise • allow a profile of displacement with depth to be created • can be used to identify subsurface sliding surfaces • in-place inclinometers can be used for continuous monitoring of displacements along known shear surface 	<ul style="list-style-type: none"> • if bottom of hole is not fixed below sliding surface, readings may incorrectly indicate no movement • borehole can be distorted and sheared off, rendering the instrument unusable • may have systematic errors related to instrument drift, depth positioning and spiralling of casing (Mikkelsen, 2003; 2008a; Willenberg et al., 2008b) • boreholes are very expensive 	either

Instrument	Type of Measurement	Typical Precision	Advantages	Disadvantages	Continuous or Intermittent
Piezometer	groundwater levels pore pressures	variable by type	<ul style="list-style-type: none"> • can be simple or complex • can have very quick response times (electrical) • several can be installed in one hole to create multipoint/profiles (Franklin, 1990) 	<ul style="list-style-type: none"> • can have very slow response times (standpipe) • borehole method - very expensive 	either
Seismic Monitoring	measures small ground motions related to the occurrence of seismic events	variable by system and ground type	<ul style="list-style-type: none"> • common in mines for rockbursting activity • can aid in detection and location of joint slip, fracture initiation and other subsurface processes (Franklin, 1990) 	<ul style="list-style-type: none"> • high volumes of data may require onsite storage (Eberhardt, 2008) • large open fractures can lead to signal attenuation 	monitors intermittent events
GPS	displacements (mainly horizontal)	mm to cm	<ul style="list-style-type: none"> • similar to geodetic • can track absolute movements in relation to a set of targets (Gili et al., 2000) 	<ul style="list-style-type: none"> • targets must be chosen that represent mean behaviour of slope 	intermittent
Visual Inspection and Vegetation	presence of movement	N/A	<ul style="list-style-type: none"> • can give early warning of developing instability (tension cracks, tilted trees) • allows first detection of slopes requiring more detailed investigation and monitoring 	<ul style="list-style-type: none"> • gives only very general information 	intermittent

- Extensometers are highly effective and reliable as demonstrated by their use for the Siroo slide, where fibre optic borehole extensometers were able to detect continuous micrometer movements over long periods of activity (Angeli et al., 2000), and Checkerboard Creek where 60 m long multipoint borehole extensometers were used providing a ten year record with incremental displacements detectable in the 0.05-0.1mm range (Watson et al., 2004; Watson et al., 2006).
- Piezometers not only provide useful data regarding the groundwater levels in a slope or surrounding an open pit, but also can be used to monitor rises in piezometric pressure that may trigger accelerating landslide movements, such as in the case of the Giau Pass Landslide (Angeli

et al., 2000), or potentially catastrophic failure. A correlation between precipitation amounts (including antecedent levels), piezometric readings and measured slope displacements is quite common in many cases, including that of the Campo Vallemaggia landslides (Angeli et al., 2000).

- Rockslide investigators have experimented with the use of geophones to measure seismic activity related to rock slope movements. However many difficulties exist with the deployment and use of such systems. Microseismic systems can produce high volumes of data requiring onsite computer storage, as in the case of the 1991 Randa rockslide (Eberhardt, 2008). Also in this study, the investigators showed that the presence of large open fractures typical of many active rock slope instabilities, leads to attenuation problems in which the signal quality is degraded through energy loss making it difficult to locate the seismic source with any accuracy. Still, as demonstrated by its common and successful use in deep mines to monitor for rockbursting activity (Franklin, 1990), seismic monitoring offers much potential in the detection and location of joint slip, fracture initiation and other subsurface processes related to active rocksliding processes.

2.1.2 Monitoring Trends and Discussion

When designing a monitoring system, the choice of instruments is controlled by the nature of the landslide, as well as the type of information desired, the budget, the accessibility of the slide surface and other practical concerns. The location of monitoring instruments must be chosen carefully to ensure that the maximum valuable information is obtained from each installation. For example, when dealing with geodetic systems, in order to represent the overall movement of the slope, it is important that a representative point or series of points be chosen on the slope. Generally several reflectors are used as a means to filter out localized movements that may be related to the reflector being located on an isolated block (i.e. rock fall) that is not indicative of the overall slope movement trend. The presence of several reflectors also allows for the relative movements of various blocks within a larger slide body to be measured as discussed by Bonzanigo et al. (2007). Similarly with inclinometers, or any downhole instrument that must cross the shear plane in order to be effective, it is important to consider the lifetime of the installation. If the shear movement across the borehole is too great, it will distort and possibly shear off the inclinometer hole, rendering it useless as the probe will not be able to pass across this point.

Of the instruments discussed in table 1, some are more useful than others in typical rock slope environments. Inclinometers are often excellent when movement is occurring along a pre-existing plane, as they can isolate this movement within their measurements. Geodetic measurements are relatively simple and inexpensive (no bore hole is required) and so are a popular choice. Piezometers are excellent on slopes where water is thought to be a major contributor to the movement, but of little use in drier slopes.

Current trends in monitoring are moving toward the combination of several of these methods. This, along with in-place probes to give warning of changes, can be combined into an automatic data acquisition system to give continuous monitoring of changes in slope behaviour (Watson et al., 2004). Moore et al. (1991) outline a monitoring strategy that includes both investigative monitoring to provide an understanding of the slope, thus enabling an appropriate action to be implemented, and predictive monitoring to provide a warning of a change in behaviour, allowing mitigative efforts to be carried out to limit damage or intervention to prevent hazardous sliding. (Moore et al., 1991) GPS surveys can be a valuable complement to conventional surveying. This is done by measuring the GPS coordinates of

reference points on the slope and comparing the change between readings of the same point at different times. When used this way, field surveys should be carried out with regular frequency (Gili et al., 2000). In order to be a truly useful movement indicator, selected GPS targets must reflect the mean behaviour of the surrounding slope. Any GPS target network should include within the control network several fixed points outside the landslide area to act as a reference (Gili et al., 2000).

There is a continued trend in using remote sensing for slope monitoring, including both terrestrial and satellite radar. Differential Interferometric Synthetic Aperture Radar (DInSAR) is a rapidly growing technique that provides both high-resolution monitoring and full area spatial coverage of a slope as opposed to relying on geodetic point measurements. The advantages and application of InSAR are described in more detail in Eberhardt (2008)

Another important aspect of creating early warning systems is the idea of investigative monitoring, to create the system. It is not always clear as to what the underlying causes or mechanisms are promoting slope movements, and therefore what the best choice for a permanent monitoring system may be. In the Watson et al. (2004) case study of Checkerboard Creek, the small displacements present meant that it took several years for the distinct annual displacement cycle to become obvious. The most valuable data in this case was largely from extensometers, as it took nearly half a year for the slope to move enough to exceed the sensitivity of the inclinometers. Once the displacement cycle was recognized and the correct instruments to record it were in place, the investigators began considering the cause of the cycles. They placed piezometers and compared this data to the movements, but as it did not match up perfectly alternative mechanisms were considered. At this time temperature cycles are speculated to be a major contributing factor. This development of the monitoring systems based on earlier findings is important to avoid wasting time and money. This idea of investigative monitoring as a first step toward predictive monitoring, or monitoring to find out what to monitor, is discussed in more depth in Eberhardt (2008).

2.2 Temporal Behaviour of Rock Slopes

The slow, down slope movement of rock and earth materials is generally referred to as creep. These movements may be continuous or intermittent, although this determination depends on the precision of the displacement monitoring instruments and/or the frequency of the measurements. The causes and nature of this type of movement are not always obvious, and are often quite obscure. This section will address the common factors and behaviours contributing to the time-dependent movement of many rock masses that have been studied in the literature.

A review of the literature on the topic of rock mass time-dependent behaviour and rock creep suggests that some confusion or disagreement exists on what the term creep refers to. Some use it only to refer to time-dependent internal deformation of intact rock, others to refer to very small movements of a rock mass over time, disregarding whether these are continuous or discontinuous over time.

Within this thesis the following definitions are used:

Rock creep refers to the time-dependent internal strain of intact rock under a constant load (accommodated through grain boundary diffusion, dislocation, glide, etc.);

Rock mass creep refers to the continuous, time-dependent downhill movement and deformation of the rock mass, including slip along joints, under the constant self-weight of the material. Rock mass

creep therefore is actually a combination of rock creep and joint slip. This may refer to either continuous or intermittent movement, the distinction will be made, as below, when necessary.

Time-dependent Movement refers to all of the above, and any other movement that is dependent directly on time. Movement that is dependent on time indirectly is referred to as apparent time-dependent movement, and is often intermittent

Intermittent movement refers to the apparent time-dependent movement of a rock slope, but where velocities accelerate and decelerate in response to external stimuli. The apparent time dependency of the displacements is usually due to the frequency of the measurements relative to the periodicity of the external stimuli, for example seasonal patterns in precipitation.

2.2.1 Creep

Creep is commonly defined as the time-dependent deformation of mineral, rock or soil particles under a constant load. In a slope, this may develop as the slow, imperceptible downhill movement of the soil or rock under gravity.

Leroueil et al. (1996) state that slope movement and related phenomena are the consequences of the stress-strain-time behaviour of the slope forming materials. This sums up the considerations necessary for any creep analysis: stress, strain and time. Creep can occur in both sliding and toppling modes (Goodman, 1993), although sliding is more commonly considered. Clays will creep under constant effective stresses, for small strain conditions. For higher stress conditions that cause larger strains, strain rates accelerate to failure more quickly. This behaviour appears to be applicable to most geomaterials, including rocks (Leroueil et al., 1996).

2.2.2 Stages of Material Creep

Material creep is generally divided into three stages: primary, secondary and tertiary creep. Figure 1 shows a sketch of a typical creep curve. Primary creep involves the strain hardening of the material. Here the strain rate is initially high, but slows with increasing strain reaching a minimum as hardening and annealing in the material balances. This transitions into secondary creep, also known as steady state creep, where the strain rate becomes constant. Tertiary creep, also called accelerating creep, represents accelerating strain as dislocations, microfracturing and shear localization develops leading to failure (Jaeger, 1979). Tertiary creep tends to occur in specimens stressed near peak strength, and the resulting failure is often referred to as creep rupture (Goodman, 1980).

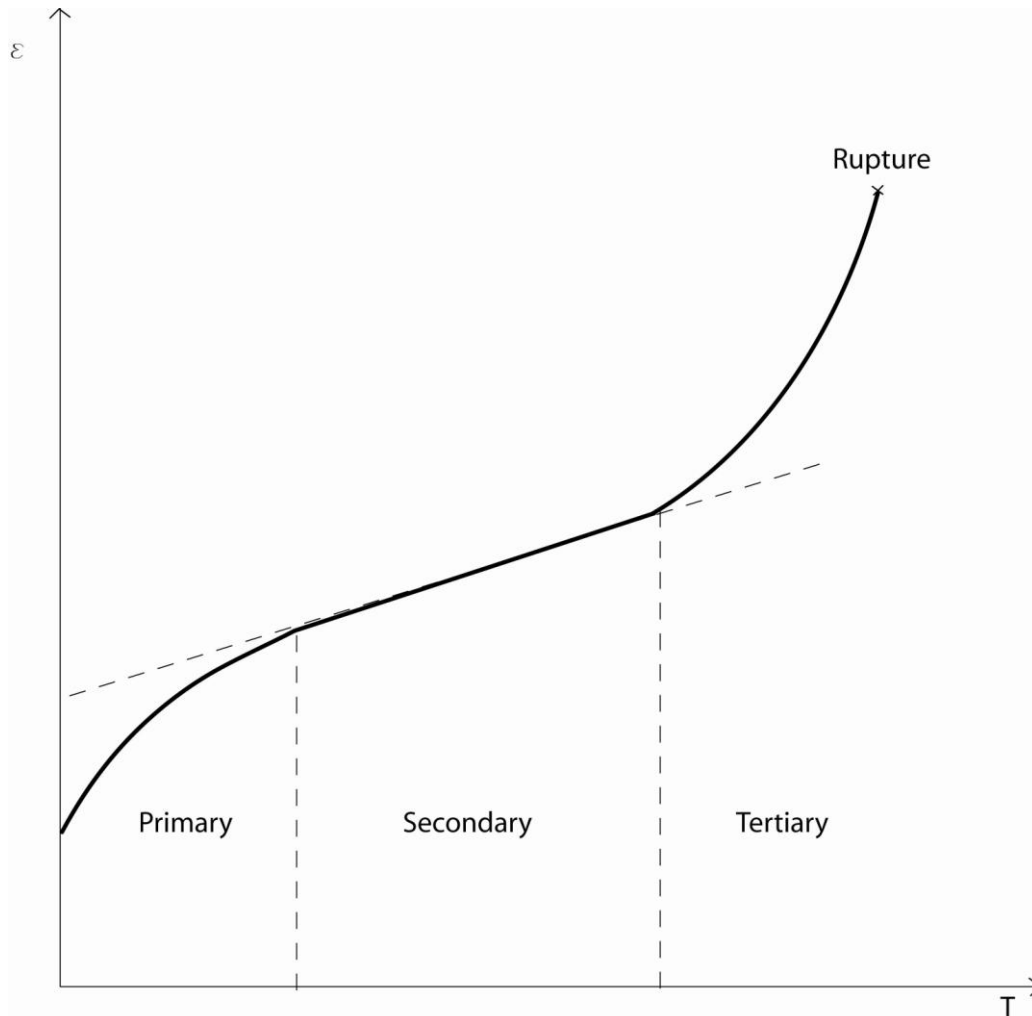


Figure 1: Standard creep curve derived from a laboratory creep test showing the stages of Primary, Secondary and Tertiary creep (after Jaeger, 1979)

2.2.3 Mechanics of Creep

There are two main mechanisms of creep in rocks: mass flow and brittle microfracturing (Goodman, 1980). Some rocks, like rock salt and potash, will creep even without the presence of fissures through intercrystalline gliding and movement of dislocations. In uncemented clay, creep is explained by the movement of water and clay particles. Some bituminous rocks are simply inherently viscous (Goodman, 1980).

2.2.3.1 Fracture Initiation and Propagation

Brittle rocks are likely to experience creep when the deviatoric stress is high enough to cause new crack formation. Stress will cause changes to the crack network. This is a nonlinear process because each new increment of crack development (initiation and propagation) has an irreversible effect on the rock fabric. Accordingly, it is unlikely that any rock exhibits truly linear elastic behaviour under all levels of observation (Goodman, 1980).

An example of the effects of fracture initiation and propagation on rock mass strength degradation and increasing slope movements is described by Eberhardt (2008) for the case of the 1991 Randa rockslide; down slope gravitational forces acting on a steep rock slope generated yielding at the toe of the slope resulting in movement and extensional strains in the upper slope, leading to the opening of numerous, sub vertical tension cracks and development of internal shears. These in turn served to weaken the rockmass, enabling localization and formation of a shear plane for failure stepping along existing joints and yielded rock bridges.

2.2.3.2 Intercrystalline Glide and Dislocation

Other common causes of creep in intact rock include intercrystalline glide, which is defined as movement of grain boundaries relative to one another. This response includes dislocation creep, which is the diffusion of dislocations through and within a crystal. These dislocations are minor imperfections or flaws within the crystal. The rate of dislocation creep is dependent more on the stress applied than on the grain size. In diffusion controlled creep (Nabarro-Herring, Coble, etc.), atoms diffuse through the crystal, either through the lattice or along grain boundaries. These atoms line up along the stress axis, elongating the grain in that direction (Goodman, 1980).

2.2.4 Causes of Rockmass Creep

Aside from intrinsic material creep, there are other displacement generating mechanisms at work that may cause slow down slope movements within the larger-scale volume of a rock mass. This makes it important to distinguish between intrinsic material creep, as discussed above, and other rock mass scale mechanisms such as slip on joints, shear localization and fracture initiation and propagation. Many rock mass failures involve both of these micro- and macro-scale mechanisms, although the latter usually dominate in most large rock slope failures (Eberhardt, 2008).

2.2.4.1 Effective Stress and Water

The presence of water in joints (and faults) reduces the effective stress acting along the joint surface reducing its frictional strength; this can cause slip and small movements along the joint, which when added together for the entire discontinuity network and over time, may lead to rock mass creep or intermittent displacements.

Sometimes large inputs of water will take the movement beyond creep, into larger scale failure. When the peak borehole water level in the Zentoku landslide in Japan reached critical heights, large movement occurred; below this level, small creep-like movements occurred (Furuya et al., 1999). This study demonstrates that borehole water levels can sometimes be used to define a critical threshold that distinguishes between pore pressures at depth that might cause accelerating behaviour, potentially to catastrophic failure, and those that will merely cause the slope to creep.

A similar threshold was observed for the Campo Vallemaggia landslide in Switzerland (Bonzanigo et al., 2007). In addition, data from this study suggests that the rate at which water is introduced to the slope also has an important effect. At the Campo Villamaggia landslide, it was noted that large sudden rainfall events would cause movement of blocks near the surface, while slower but prolonged rainfall events would penetrate deeper and raise the groundwater pressure along the basal sliding surface, thus contributing to larger, continuous movements as long as the water pressures at depth were elevated (Bonzanigo et al., 2007).

2.2.4.2 *Strength Degradation and Progressive Failure*

The rationale behind the idea of strength degradation and progressive failure is described by Eberhardt (2008). Many natural rock slopes have existed in a relatively stable state for periods of hundreds if not thousands of years. Periodically, however, one of these rock slopes will collapse, meaning that an element of time-dependent rock mass strength loss must be at work as the morphological characteristics of the slope contributing to most of the driving forces (e.g. steepness of the slope) have changed little if at all over the same time period. Strength degradation through extensional strain, creep, fracture propagation, stress corrosion, weathering etc., must be present to act to destroy intact rock bridges between non-persistent, non-systematic discontinuities and (or) asperities between locked joint surfaces over time.

As strength reduction progresses with time, resistance to the driving forces likewise decreases, until the factor of safety drops below one and failure occurs. This is referred to as progressive failure (Eberhardt, 2008). Within the context of progressive failure, it is important to note that triggering events which are often ascribed to large landslides, for example a heavy rainfall, are often not sufficient in themselves to explain the occurrence of most mass movements. With the exception of a large earthquake, which temporally is a non-frequent reoccurring event, it is very unlikely that an often repeating trigger type event like a heavy rainfall or snowmelt was the largest of its kind to have occurred over the last hundred or thousand years (Eberhardt, 2008). Instead, previous trigger-type events would likely have contributed to the strength degradation process and progressive failure of the slope, weakening it to the point where the next large rainfall tips the balance of forces and failure occurs.

2.2.4.3 *Apparent Time Dependence*

Apparent time dependence of rock slope creep may actually be influenced by meteorological affects (Glawe and Lotter, 1996), and especially in situations such as mine slopes, by anthropogenic effects and activity. Freeze-thaw cycles, mining excavation/blasting schedules, fluctuating water tables (i.e., seasonal precipitation cycles), temperature changes and vegetation changes all may have effects on the movement of a rock slope. While these events may be time-dependent, it would not be accurate to say that the rock slope deformations are continuous or time-dependent in the same context as creep. Instead, these movements are often both spatially discontinuous and temporally intermittent .

When rock slope movement rates are given over larger time spans (e.g., mm/year) or with low sampling intervals (e.g., one measurement per month or year) this may give the appearance of time dependance. However, if the displacements are temperature or precipitation dependent, then monitoring on a more frequent time scale such as mm/day or month, depending on the periodicity of the climate pattern allows variations that are clearly not continuous to be more clearly seen.

2.2.4.4 *Joint Slip*

The acting slope shear stresses are often lower than the shear strength of intact rock, and therefore behaviour of the slope is analyzed based on the presence of discontinuities, and their properties, as these serve to weaken the overall rock mass (Leroueil et al., 1996). In these cases, although it is possible to cause internal yield and deformation of the intact rock, and therefore movement, localized slope movements are more easily accommodated by slip along the joints. Joint slip may happen simply due to the effects of gravity and strength degradation along asperities, or it may be influenced by external factors

as discussed below, the primary factor being the role of joint water pressures in reducing the effective stress along the fracture.

2.2.4.5 Ice Loosening and Thermal Effects

Freezing can exacerbate slip along a joint through asperity breakdown and dilation of the joint due to the volume increase when water freezes. The effect of forcing open the joint may also break rock bridges and cause new cracks to initiate, i.e., frost shatter (Goodman, 1993).

Frost creep, or solifluction, is another known phenomenon common in periglacial environments. It originates from heaving that occurs normal to the slope during freezing, followed by vertical settling during thawing. This combination of normal expansion and vertical settling results in a small net downslope movement, which then accumulates over multiple freeze thaw cycles (Font et al., 2006).

This expansion and contraction of rockmass material due to freezing/thawing (and in some cases wetting/drying) can also contribute to rock mass creep. This has been observed at sites like Checkerboard Creek in British Columbia (Watson et al., 2004) and Randa (Willenberg et al., 2008a), where high resolution displacement monitoring indicated a small thermal signal in addition to displacements related to rainfalls and/or snowmelts.

The effect of temperature on rock mass creep is still not fully understood, but can best be described using the example of Checkerboard creek as discussed by Watson et al. (2004; 2006). Here an annual displacement cycle was dominated by an active phase with displacements in early autumn to late winter, and an inactive phase with limited to no displacements in spring to early autumn. Although at first these were correlated to seasonal precipitation patterns, the cycle proved to be remarkably repeatable regardless of precipitation amounts or repeated in years that were especially dry. Instead, the cycle is more strongly correlated to seasonal temperature variation than it is to piezometric elevation (groundwater level).

Although the measured slope deformations extend to over 50m into the slope and temperature fluctuations penetrate to only 10m, the data suggested that thermally-induced strains are the primary cause. UDEC (Universal Distinct Element Code;(Itasca, 2009) analyses indicated that thermal contraction during seasonal cooling (winter) introduces deviatoric stresses into the slope which can cause slip on discontinuities. This results in downward and outward displacement of the slope. During warming (summer) the normal stresses increase, and these work to prevent further slip (Watson et al., 2006). The models also confirmed that although displacements would be greatest at the surface, they could penetrate to depths of 80m. This suggests that the reaction is plausible as a component of the overall displacement mechanism. The conclusion from this study was that an annual creep mechanism controlled by temperature fluctuations would be repeatable each year regardless of precipitation (Watson et al., 2004).

Other examples were noted by Gunzburger et al. (1997) who found that thermally induced deformations can be sufficient to cause the gradual downward creep of a rock block located in an awkward position.

2.2.4.6 Erosion Effects

River erosion removing material from the toe of a slope, or glacial erosion resulting in oversteepening and debuttressing of a slope can also lead to rock mass creep over time. At La Clapiere in France, glacial erosion is believed to have led to the initiation of creep deformation, which progressed until weakening of the rockmass enabled shear localization and the development of a failure surface (Leroueil et al., 1996).

Although less commonly observed, Furuya et al. (1999) report creep of a crystalline schist rock slope in Japan, the Zentoku landslide, caused by internal erosion caused by piping along and above weak shear zones within the slide body. Sediment discharge measured from springs was correlated to landslide activity, explaining why the landslide is active not only during heavy rain but creeps throughout the year (Furuya et al., 1999). Erosion was increased by heavy precipitation, which in turn led to increased landslide creep and further erosion (Furuya et al., 1999).

2.2.4.7 Earthquake Shaking and Seismic Effects

Earthquakes are well known triggers of landslides. In fact there are several methods for determining the amount of displacement on a landslide to be expected during an earthquake, for example the Newmark Method (Newmark, 1965). Typically the landslides considered when studying earthquake triggers are those that fail catastrophically during large shaking events; however the same change in stresses that can trigger failure may instead only lead to large movements. Shaking of a slope can add an inertial force to an otherwise equilibrium state, increasing the gravitational down slope driving forces, alternating with reductions in the normal force and therefore frictional strength of the slope. This disequilibrium leads to down slope movement of the slope materials.

2.2.4.8 Open Pit Excavation

In natural slopes the shape, height and many other factors that contribute to the slope's stability state do not change. This is not the case for open pit slopes as the mining process continuously alters the height, and sometimes angle, of the slope. Active mining and excavation will deepen and widen the pit, as well as change the shape and steepness of the slope walls. It is possible that after each excavation stage, the pit walls will move slightly to re-establish equilibrium (Franklin, 1990). Thus pit slope movements may appear to be continuous until or unless there is a pause in the excavation schedule.

2.2.4.9 Vegetation

Vegetation changes are more commonly a problem on natural soil slopes, but they may affect rock slopes if they serve to minimize water infiltration into the subsurface. The removal of large, older trees and the subsequent death of large root systems may lead to a rising water table, as well as decrease the cohesion present in the near surface. Tree roots can also contribute to crack propagation within a slope by forcing themselves into small cracks and expanding.

2.2.5 Creep Considerations

The creep behaviour of landslides is not well understood (Furuya et al., 1999), and can introduce many complications when trying to correct for survey errors or interpret displacement signals in monitoring data that are very small (Goodman, 1993). The conditions under which creep may progress to a point where slope velocities accelerate leading to catastrophic failure are equally not well understood. Creeping is likely to create larger landslides because the accumulated creep is often deep-seated.

The tendency to creep is often particularly pronounced in terrain with strongly foliated rockmasses, especially those with adversely oriented schistosity dipping towards the valley, but also in the case of flexural toppling, where foliation dips steeply into the slope (Goodman, 1993). In both cases, the foliation provides a directional plane of weakness along which slip may occur.

2.2.6 Fatigue due to Cyclic Loading

Many of the factors that contribute to time-dependent movements previously discussed affect the rockmass in a cyclical manner. Simple examples of this include seasonal climatic factors like precipitation, snow melt and freeze-thaw behaviour. These cyclic affects can lead to a degradation of the rock mass strength, generally referred to as fatigue, that increases the tendency toward time-dependent movement (Goodman, 1980).

This breakdown due to cycling can be seen in situations such as the occurrence of highly weathered rock in regions where thermal and/or moisture cycling are the obvious causes (Hall, 1999; Halsey et al., 1998), or where the initiation and propagation of brittle fractures leads to the degradation of rock mass strength and development of tension cracks and internal shearing. In both cases, these processes may lead to down slope movements.

Because changes in temperature, pore pressures and other factors cause expansion and contraction of the rock, compressive and tensile stresses occur within the intact rock between non-persistent joints. The frequency of these stress changes, greatly affects the extent of the fatigue effect upon the rock (Halsey et al., 1998). The number of cycles and the magnitude of cyclic stresses induced are also extremely important (Bagde and Petros, 2005a; Bagde and Petros, 2005b). Figure 2 shows the primary causes of fatigue and time-dependent movement as identified in this thesis study.

2.3 Time-dependent Analysis of Rock Slopes

A detailed search of the literature for time-dependent slope analyses produced a very small number of examples. In contrast, numerous examples could be found reporting stress-strain modelling of open pit and natural rock slopes, as stability analyses and factor of safety calculations represent the key index for determining how close to failure a slope may be (Hammah et al., 2005). Similar problems exist in the availability of time-dependent constitutive models incorporated into commercial software. For example, Itasca has created a constitutive model for creep in UDEC (Itasca, 2009), but this is restricted to the intact blocks. No models exist for time-dependent movement along joints.

Most methods proposed for the study of time-dependent behaviour are extrapolation methods, which are limited in accuracy and cannot be used to predict sudden movements (Leroueil et al., 1996). In some cases, for example open pit mining as discussed by Rose and Hungr (2007), stress relief associated with mining may lead to false alarms triggered by pit wall movements in the form of elastic rebound and ground relaxation that dissipate with time instead of movements that have the potential to accelerate to failure.

Still, studying rock slope movements with time can yield valuable information and in several cases has proved successful. Some methods which have shown success are discussed below.

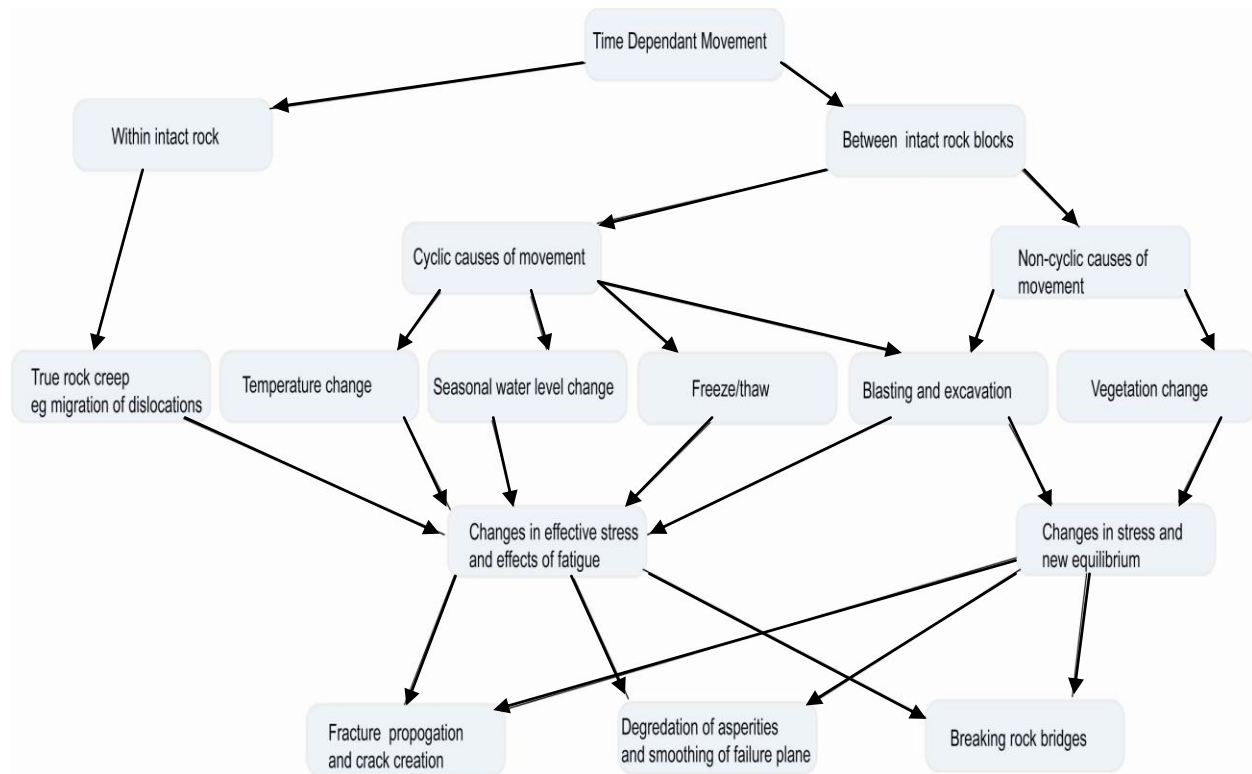


Figure 2: Flow chart showing interrelationship between rock slope processes contributing to time-dependent movement and fatigue

2.3.1 Predictive Methods of Time of Occurrence

Time-predictive methods of slope analysis, as the name implies, are those that attempt to predict a time of failure based on creep behaviour of rock or soil. This is usually done with the aim of preventing damage or loss of life. Accurate prediction, especially in open pit mines, is necessary in order to provide a safe working environment, as well as minimizing the economic impacts of closing down a ramp or pit area much sooner than planned due to accelerating slope movements.

Federico et al. (2002) divides all predictive methods into three groupings: i) those that relate displacement rates to tertiary creep and the time remaining to failure, ii) those that take into account all stages of creep behaviour, and iii) others which do not fall into these two categories

Saito (1965) introduced one of the first methods to use lab measurements of strain rates during secondary creep. He stated that the time remaining until tertiary failure is inversely proportional to the strain rate at the present time. This method was devised for soil but was successfully applied to predict collapse of a rock cliff on National Highway 327 in Saigo, Japan (Federico et al., 2002; Saito, 1965).

2.3.1.1 Inverse Velocity Method (Fukuzono Method)

The Fukuzono method of determining time of failure is based on the forward projection of a line or curve to cross the time axis on an inverse velocity vs. time plot. The method and basic equations are summarized here, with a full description being provided by Fukuzono (1985).

In simple terms the method is based on the observation that slope velocities will increase rapidly as a creeping slope approaches failure. The line on a velocity-time graph will approach vertical at this

point, the transition to which, however, can be difficult to identify. Instead, this transition point is more easily picked out on a plot of inverse velocity vs. time, with the line being extended until it intersects the time axis marking the predicted date or time of failure.

The basic principle of this method, which is based on Saito's method mentioned above, is that the logarithm of time to failure is proportional to the logarithm of strain rate (Fukuzono, 1985). In Equation (1) below, t_r is time to failure and $\dot{\epsilon}$ is the strain rate:

$$\log(t_r) = c - m \cdot \log(\dot{\epsilon}) \quad (1)$$

Assuming values for m and c , which are empirical constants, (Saito, 1965) applied the equation to predict time to failure:

$$\log(t_r - t) = c - \log(\dot{\epsilon}) \quad (2)$$

Equations (1) and (2) only really apply for secondary creep. In order to really account for tertiary creep Fukuzono found the need to generalize by replacing c and m with the unknown constants A and B .

Many experimental models were run testing variations of surface displacement caused by rainfall. As a result the following relationship was found (Fukuzono, 1985):

$$\frac{dx^2}{dt^2} = a \cdot \frac{dx^\alpha}{dt} \quad (3)$$

where x is the downward slope movement. Constant a is then set to 0 and the equation integrated. The resulting equation depends on the value of α (see Figure 3).

Using these equations, the curve for inverse velocity vs. time is linear if $\alpha=2$, convex if $\alpha>2$ and concave if $1>\alpha>2$ (Fukuzono, 1985). See Figure 3 for a typical example of these curves. Using these curves, failure can be predicted. For the straight line case ($\alpha=2$), the failure time can be exactly predicted by finding the point where it crosses the time axis; this matches the time predicted by Saito's method. When α does not equal 2, the failure time may be estimated by drawing a tangent to the curve as close to the end of the data series as possible. An exact time may also be predicted by differentiation of the intermediate equation by t , which gives the following relationship, in which v represents velocity:

$$\frac{\left(\frac{1}{v}\right)}{\left(\frac{d(1/v)}{dt}\right)} = -(\alpha - 1)(t_r - t) \quad (4)$$

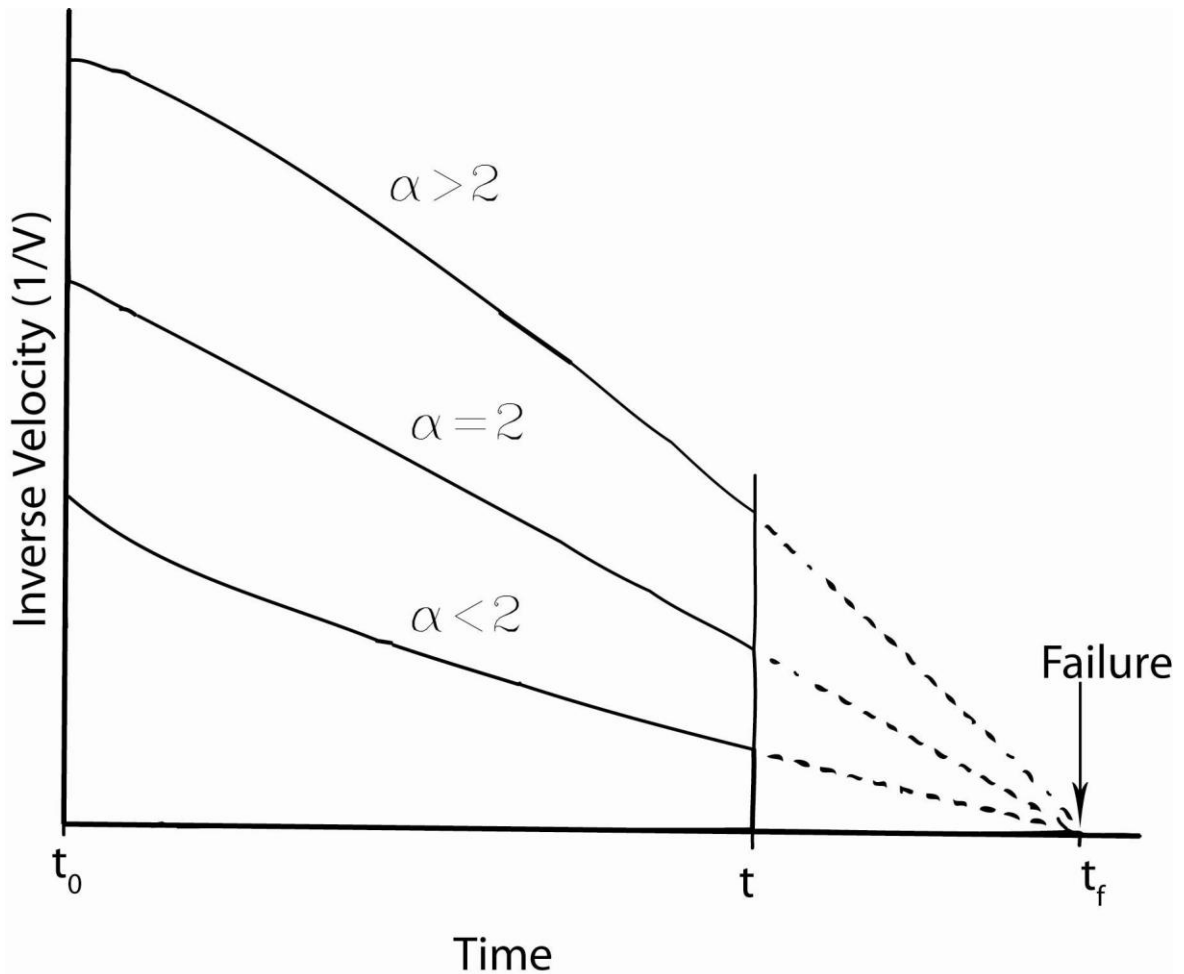


Figure 3: Sketch of standard curves produced using the Fukuzono method (after Rose and Hungr, 2007)

This method has been successfully applied to several examples. Fukuzono himself applied the method to loam slopes and predicted the time of failure to within 1 minute of actual failure. This method was also successfully applied by Fukuzono (1985) to a series of model slopes. Rose and Hungr (2007) successfully used the inverse velocity method to predict three large open pit slope failures, ranging from two weeks to three months ahead of failure.

Despite these successes, care must be taken and consideration given to the fact that these and other empirical methods are holistic, disregarding the underlying mechanisms and controlling processes (Eberhardt, 2008). They look at the behaviour of the system as a whole, which may lead to ambiguities in the data interpretation. This prevents long term prediction of failure from being an absolute. Monitoring that continues right up until the time of failure, and careful analysis to watch for any deviations from the predictive trend are therefore required (Eberhardt, 2008).

2.3.1.2 Empirical Creep Laws

Displacement vs. time curves are generally referred to as creep curves. These curves may be fitted empirically using exponential or power functions (Goodman, 1980). To do this it is typical to consider the contribution of each of the three stages of creep over the creep curve separately. This is discussed in this section and can be found in greater detail in Jaeger (1979) and Goodman (1980)

There are two empirical laws that are used to represent primary, or transient, creep in rocks. These are the power law and the logarithmic law (Jaeger, 1979). The general power law is:

$$\varepsilon_1 = At^n, \quad 0 < n < 1 \quad (5)$$

in which ε_1 is transient creep, t is time, and A is a constant. The general logarithm law is:

$$\varepsilon_1 = A \ln t \quad (6)$$

A common form of the power law is Andrade's 1/3 power law in which $n=1/3$ and A is a constant that varies depending on conditions such as temperature and pressure (Jaeger, 1979).

These laws do not model the form of primary creep perfectly as they continue to increase with time rather than levelling off to steady state and secondary creep. They also have the mathematical anomaly that the velocities approach infinity for very small time values (Jaeger, 1979). Many modifications have been made to the logarithm law particularly to minimize this problem. One example is the modified Lomnitz law, where a and α are parameters of the material:

$$\varepsilon_1(t) = A[(1 + at)^\alpha - 1] \quad (7)$$

The logarithm law (6) has been popular for experimental interpretation as it has provided a good fit in a number of examples. It is important to remember however that these laws are essentially empirical, and while they are useful as representations and provide reasonable extrapolations over short time periods, they are extremely limited as theoretical prediction methods when applied to complex systems (Jaeger, 1979).

Steady state or secondary creep takes the form of:

$$\varepsilon_2 = Vt \quad (8)$$

Where V is the creep velocity and ε_2 is secondary creep. There are also empirical laws that represent the value of V . Many of these, governed by studies involving metals, are based on stress dependence.

2.3.2 Constitutive Modelling

2.3.2.1 Distinct Element Modelling

The Distinct Element Method (DEM) is a numerical method specifically derived to simulate the response of a jointed rock mass, modelling the problem domain as an assemblage of deformable blocks, accounting for complex non-linear interactions between the blocks including slip and opening/closing along discontinuities (Hart, 1993). With respect to material creep, the method has not been widely used with only one case looking at joint slip using a Kelvin viscoelastic creep model to simulate viscous deformation of joints in slopes experiencing excavation unloading (Jin et al., 2003). This was carried out for analyses applied to the Three Gorges Dam shiplock slopes and shows excellent agreement with recorded data (Jin et al., 2003). Their methodology and reasoning is summarized below.

The finite element method is commonly used to model creep deformation due to its simpler formulation when adopting a continuum treatment (isotropic or anisotropic). However, for jointed rock

masses, much of the time-dependent movement may be taken up along the joints. Therefore the distinct element method, which can analyze jointed rock masses, is better suited for this application (Jin et al., 2003).

In order to calculate creep displacement, Jin et al (2003) developed a numerical scheme to apply incremental contact forces, which they equated to producing creep displacements (Jin et al., 2003). Creep deformation can be a lengthy process, and so typical DEM time steps of $10e-5$ seconds are not suitable. Time steps on the order of days to months are more appropriate; therefore using the same calculation scheme and time steps for creep and regular equilibrium is not efficient (Jin et al., 2003).

This then requires the definition of the equivalent incremental contact force. For each time step that force is added to the previous force and equilibrium calculation automatically carried out (i.e. displacement). The computation steps that follow are:

- 1) Unloading - this is done starting with the initial time step, then the prescribed forces are added and the model iterates until equilibrium. This process uses very small time steps.
- 2) Creep deformation - here the incremental contact forces are calculated and updated for a creep time step, then very small time steps are run again until the model reaches equilibrium with the changed forces. This is repeated for multiple large, creep time steps.
- 3) Steps one and two are repeated until excavation is complete and creep vanishes (Jin et al., 2003).

This procedure was necessary because UDEC contains constitutive models for block creep, but not creep along the joints in the model.

2.3.2.2 Interface modelling

As well as work done studying creep within intact rock and within joints between rock blocks of the same type, work has been done to study creep movements along interfaces. Desai et al, (1995) propose a constitutive model in which a creeping mass is moving at an interface above an essentially stationary rock mass below it. This involves a finite interface zone within which the variation of translational displacements is much greater than that found in the mass above the interface. The model, based on the theory of elastoviscoplasticity by Perzyna (1966), is implemented using finite element analysis in the study by Desai et al (1995) producing predictions that compare well with displacement and velocity profiles for the study sites. The model does not however include full coupling between mechanical and fluid effects. It is also a two dimensional model, and therefore valid for central regions of slides which do not incorporate lateral spreading. Finally, this model does not allow for catastrophic landslides (Desai et al., 1995)

Further work presented by Samtani et al. (1996) describes the interface as a thin smeared zone between moving and stationary bodies. The model primarily involves shear deformation under the effect of normal and shear stress. This is developed into an elasto-viscoplastic model which relies upon the assumption of small strains wherein the total strain vector may be decomposed into elastic and viscoplastic strain components (Samtani et al., 1996). The elastic component is then assumed to be independent of time. A series of ultimate and current yield surfaces are generated for the model (see Samtani et al, 1996 for derivation) and the proposed model is characterized based on behaviour relative to the. For a stress state inside the yield surface only elastic deformations are seen. Outside the yield surface

viscoplastic strains are generated, which in turn modify hardening parameters, changing the current yield surface. A point between the current and ultimate surfaces will give a transient creep phenomenon while a stress point outside the ultimate yield surface gives a secondary creep response (Samtani et al., 1996). The Samtani et al (1996) model requires elastic, plastic and viscous parameters. The model validation is then presented in the paper.

2.3.3 Measurements for Time Dependency

In order to constrain numerical models of creep behaviour it is necessary to have data sets which meet certain criteria. Even with the best data sets, rock slope instabilities are highly complex (Bhandari, 1988), and involve a number of integrated factors that are not always simple to reliably assess. For this reason the timing and spacing of measurements is very important.

According to Bhandari (1988) the frequency of displacement measurement must be high relative to the frequency of occurrence. Otherwise, critical increases in displacement rates, occurrence of surges or short spells of deceleration, etc., may be missed if intervals between observations are too long. Furthermore, not only may information be missed but the nature of slide movement may be disguised if the time between measurements is long enough to smooth out an otherwise irregular displacement-time curve (Bhandari, 1988).

Another important aspect of studying time-dependent failure is knowing what is meant by failure. The traditional idea is that failure occurs when the factor of safety (FOS) is less than 1, and that the degree of instability can be considered to be governed by the rate of drop of FOS with time (Bhandari, 1988). However, some slopes creep at more or less sustained levels of gravitational stresses which may be considerably lower than critical levels of shearing stresses (Bhandari, 1988). Therefore to define failure it is important to know the acceptable amount of total displacement.

2.3.4 Strain Softening and Brittle Failure

Numerical modelling enables changes a rock mass may undergo as a result of stress changes and movements to be accounted for. For this, a strain-softening model can be used to account for strength degradation in the rock mass as a result of brittle fracturing and plastic yielding, but the corresponding input parameters are difficult to establish or constrain. This method of reducing the rock mass shear strength, especially the cohesion, as plastic strain increases, has been used with some success in studies of large rockslides (Eberhardt, 2008).

The Mohr-Coulomb yield criterion represents the most commonly used constitutive model for elasto-plastic modelling due to the simplicity of the criterion. However, it has been shown by experimental observation that the linear strength envelope used in this criterion is not applicable to many rock materials (Lee and Pietruszczak, 2008). One viable alternative to better represent the post-peak behaviour of rock is a strain softening model, which represents a decrease in strength with increasing plastic strain (Hajiabdolmajid et al., 2002).

The brittle failure process in rocks often follows the initiation, growth and accumulation and concentration of microfractures leading to progressive rockmass strength degradation, and in many cases to localization and development of a shear surface (Eberhardt et al., 1999). As a result of this an important component of brittle rock mass failure is strain softening, which involves the weakening of cohesion as a function of rock damage or plastic strain (Hajiabdolmajid et al., 2002). This decrease in

cohesion is often accompanied by frictional strengthening, as the full mobilization of frictional strength occurs only after initial cohesion has been reduced (Hajiabdolmajid et al., 2002; Martin, 1997). Unless the loss of cohesion can be compensated for by increased frictional resistance, the stress-strain curve for the rockmass under consideration will show a softening behaviour (Zhang et al., 2009).

Lajtai (1969) showed that frictional strength mobilization occurs in direct shear tests when there is a high normal load. However with low normal stresses, the failure is by tension-induced damage, or cohesion loss.

This process of strain softening concentrating on cohesion occurs because cohesion is often the dominant component of strength at early stages of brittle failure. Tensile cracking and crack coalescence which occur due to strain in the rock mass lead to a gradual destruction of this cohesive strength, and from this comes the observed strain softening brittle behaviour of many rock masses (Hajiabdolmajid et al., 2002). This can help to explain the lower strength seen in situ compared to laboratory testing of rock samples (Hajiabdolmajid et al., 2003).

Mechanistically, what happens during brittle failure is a destruction of strength from the bonds between grains. This is the cohesive strength of the rock. This differs from ductile failure in which continuity of the material is largely maintained (Hajiabdolmajid et al., 2003). Due to the heterogeneity of rock, this loss is progressive, rather than instantaneous (Hajiabdolmajid et al., 2003). Although many accept microcracking as the contributing cause for strain softening, Pichler et al. (2007) note that macroscopic damage and its evolution on a larger scale also involves fractures at the macroscopic level (e.g. natural joints).

In work done by Lee and Pietruszczak (2008), models taking into account strain softening assumed that post-failure state of rock materials involved all strength parameters changing as a function of plastic strain, decreasing linearly to residual values. This differs from Hajiabdolmajid and Kaiser's (2002) approach where cohesion and friction responded inversely to one another.

The effect of strain softening, within a rock mass is to gradually localize deformation along a narrow zone (Vitale and Mazzoli, 2008). This makes it an ideal criterion to model the localization and formation of shear surfaces. The opposite effect, strain hardening, will serve to diffuse deformation through a rockmass (Vitale and Mazzoli, 2008).

3 Methodology

Two case studies involving large deep-seated rockslides in crystalline rock were examined to investigate the modelling of time-dependency and fatigue, as outlined in the thesis objectives. The first, the Campo Vallemaggia slide, was selected as a case where the basal sliding surface is roughly translational and daylighted near the valley floor. This case was used to establish the modelling methodology for simulating rock mass fatigue due to seasonal variations in pore pressures (cyclic loading) given its relatively simple 2-D problem geometry. The rockmass fatigue modelling methodology developed was then expanded and applied to the second slide, the Little Chief Slide, which involves a more complex deep-seated rupture surface in which the toe is partially confined. The details of the techniques used are explained in the sections below.

3.1 Data Collection and Interpretation

In general, deep-seated landslide failure surfaces cannot be easily located, especially when limited to surface observations. Geomorphological features may provide some constraints, but otherwise, borehole data is necessary in order to create a reasonable prediction for the location of the sliding surface along which monitored movements are taking place.

3.1.1 Campo Vallemaggia

The Campo Vallemaggia landslide, located in southern Switzerland, was chosen as the initial case study to model for this project in large part because of the detailed investigations, monitoring and analyses of the slide that have already been carried out (Bonzanigo et al., 2007; Eberhardt et al., 2007). Based on these detailed investigations, the slide kinematics and deformation behaviour is relatively well understood; little additional interpretation of the slide surface or other parameters was required for this site. A description of the Campo Vallemaggia slide and its geological setting can be found in Chapter 4.

3.1.2 Little Chief

For the Little Chief Slide, located near the Mica Dam, north of Revelstoke, British Columbia, detailed site investigation data was made available through a series of reports provided by BC Hydro, which contained detailed borehole, core log, and inclinometer and piezometer data. Interpretation of the slide surface at Little Chief has evolved with the different investigation campaigns carried out over the past 40 years, supplemented by testing results of the sheared materials along the failure surface. Based on this data, a cross-sectional profile of the sliding surface was constructed, and interpretation of the likely internal shear surfaces within the slide profile made. During site visit made in July 2009, a general site reconnaissance and Geological Strength Index (GSI) assessment of the rockmass was performed. A description of the Little Chief slide and its geological setting can be found in Chapter 5.

3.2 Modelling

The procedure adopted for the numerical modelling involved bringing the models to an initial equilibrium for a given water table and friction angle assigned to the basal sliding surface. From this equilibrium state, the water table was then varied in a cyclic manner to simulate annual fluctuations. The procedure developed is shown as a flow chart in Figure 4 and described in more detail below.

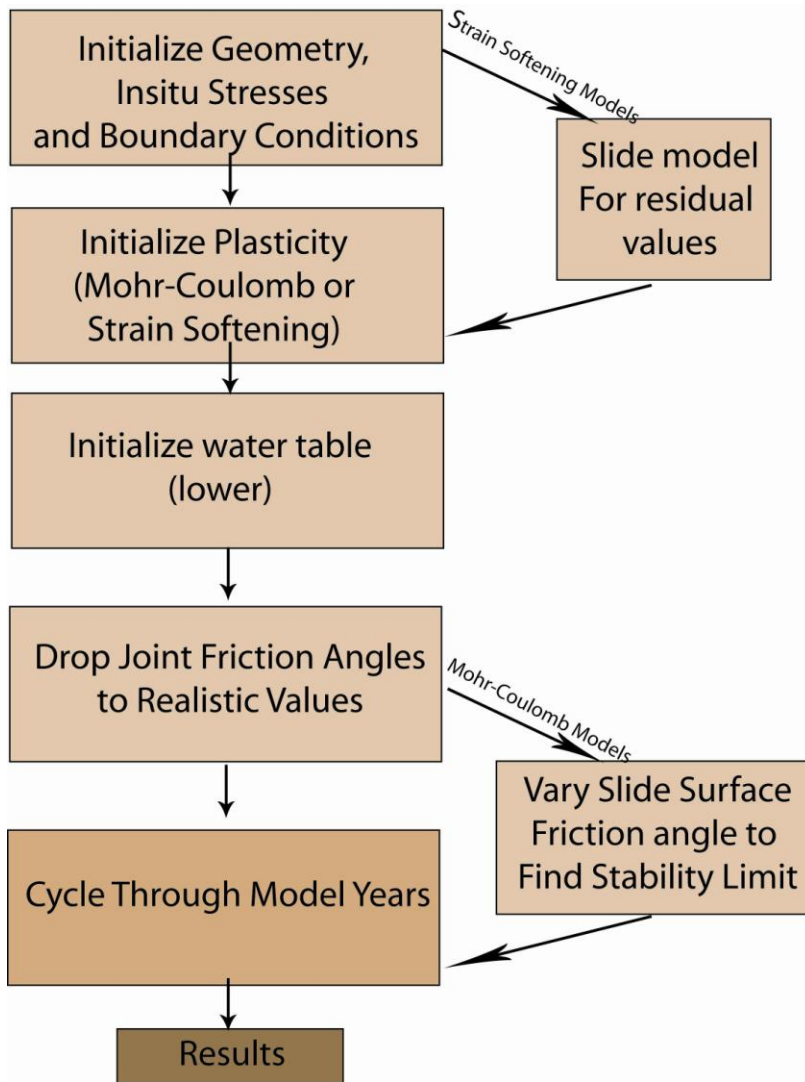


Figure 4: Flow chart showing the progression of steps followed in UDEC to simulate cyclic loading and rock mass fatigue. Those steps shown in pale brown were used to initialize the model to site conditions, while those shown in darker brown were the steps taken

3.2.1 Model Initialization

The first step in the modelling procedure was to build the model geometry, specifying the joint patterns identified for each case study and exterior boundary conditions. Zero horizontal velocity boundaries ($x_{vel}=0$) were specified for the exterior vertical lateral boundaries, and a zero vertical velocity boundary ($y_{vel}=0$) was set for the bottom of the model. The material properties were initially assigned assuming an elastic constitutive model and the joint friction angles were intentionally set to very high values to prevent movements during the initialization of gravity and solving for the initial in-situ stress conditions. The model was then run to equilibrium.

The second step was to introduce plastic yielding by applying either a Mohr-Coulomb or strain-softening constitutive model, and again bringing the model to equilibrium. The constitutive model used

was chosen depending on the objectives of that particular model series. The Mohr-Coulomb elasto-plastic model was used for cases where the basal rupture surface was explicitly represented in the model. Where modelling was carried out to simulate the initiation and progressive development of the basal rupture surface, a strain softening model was used. This was mainly carried out for the Little Chief slide to help identify and verify the location(s) of the sliding surface(s) projected from the site investigation data. To help establish the rock mass properties to be used, the RocScience limit equilibrium program Slide 5.0 (RocScience, 2003) was used to determine the appropriate residual values of cohesion and friction angle to begin with. This is explained in section 3.2.2.2 below.

The third step was to introduce a water table. Typically the water table used for this step was that representing the seasonal low conditions; i.e. those where the slide would be in a lower state of activity. The model was again run to equilibrium, allowing joint water pressures to equilibrate without significant displacements occurring. Permeability and fluid flow in the UDEC formulation are controlled by the input for fracture aperture based on the cubic law relationship (Priest, 1993); the blocks are treated as being impermeable, with flow confined to the joints.

Step four was to then lower the friction angles for the different joint sets to values that were more representative of those estimated based on site investigation data. The models were once again time-stepped to an equilibrium state (or as close as possible). This is the first step that allowed significant displacements to develop along the joint surfaces if the conditions permitted. In most cases these were minimal as the slide conditions were modelled to be more stable for the lower bound water tables.

Finally, the fifth step involved determining the limiting friction angle along the detachment surface for which sliding begins. For the Little Chief Slide, this was done by starting with a friction angle of 26 degrees and lowering it in one degree intervals to a friction angle of 19 degrees. For the Campo Vallemaggia Slide a range of 29 to 22 degrees was tested. A friction angle was then selected based on the value which produced a meta-stable model under the lower bound water table conditions.

3.2.2 Modelling of Rock Mass Fatigue

Once the meta-stable slide conditions were determined for each model, rock mass fatigue was introduced through a procedure that alternated between applying a higher water table representing the “wet season” and the lower water table under which equilibrium was established representing the “dry season.” This cycle was then equated as representing one year, which could then be repeated to simulate any number of years limited only by time and computational hardware.

The appropriate number of computation cycles to be used to represent one season was determined as follows: Time stepping was carried out until the slide displacements observed in the model equalled the average annual yearly displacement seen in the monitoring data. For Campo Vallemaggia the monitored slide velocity was approximately 2-6 cm per year (prior to construction of a drainage adit that stabilized the slide body), while for Little Chief, the velocity was much smaller at several mm per year. Coincidentally, for both models the number of computation cycles (time steps) required to reproduce one year of slope displacements was approximately 1000 cycles per season, for a total of 2000 cycles per year. The only limitation to the number of years that may be modelled was controlled by real time and computing availability. See Appendix A for a summary of time requirements.

The combination of number of computation cycles and water table is not unique to achieve the appropriate amount of movement in a single year. However, for both slides, the positions of the water tables were determined using piezometric and observational data from the landslides. Within these restrictions the choice of number of cycles was unique. In both cases a model with the wet season water table was run to 100000 computation cycles, and determined not to reach a static equilibrium at that point.

In addition, a second-order perturbation was run for the Little Chief models adding a higher table every 10 years in place of the regular high water table, and an even higher one every 100 years. This was to test the response of the models to the occurrence of less frequent extreme rainfall/snowmelt events, as are normally experienced over the years, rather than repeating the same high point every year.

3.2.2.1 Sensitivity to joint spacing

For both landslides, early models were run assuming much wider joint spacings than were used in the final models. This was done to allow much faster modelling in the stages where geometry and other variations were being assessed.

In later models, the spacings were reduced; multiple models were run for relatively short times (2000 to 10 000 computation cycles, depending on the model) to find the simplest model that allowed for appropriate geometric and kinematic behaviour of the slide.

All versions of the models included dense jointing in the unstable slide body and upper model near the areas of interest, and much sparser jointing below. The joints continued below the area of interest to allow for modelling of fluid flow through the model. The sparser jointing below the slide body was used to speed up the model as deformation and movement within the slide body was the goal of investigation

Different geometries were experimented with for the two landslides. Models were run both with and without an established sliding surface. Models were also run with and without internal shear surfaces, as mapped in the field, but with the basal sliding surface in place. Joint patterns were also varied but the orientations of the joints were kept the same, as these were based on mapping and borehole data. However, the persistence and spacing were varied. Some models included joints that were fully persistent through the slide body; however, non-persistent joints, forming a brick like pattern, were more typically chosen as a more limited persistence better fit the field observations. See chapters 4 and 5 for these details.

3.2.2.2 Limit equilibrium analysis to estimate initial strain softening properties

The method of slices program Slide 5.0 (RocScience, 2003) was used to back calculate the limit equilibrium state of the slide surface properties for the Little Chief slide. These were then used as a first estimate of residual strength values to be used in the strain softening modelling of the initiation and progressive development of the Little Chief slide surface. The advantage of starting with the limit equilibrium analysis over beginning with a trial and error approach in UDEC was that Slide could quickly solve for multiple potential failure surfaces and the factor of safety along these surfaces. This allowed for an easy comparison of critical slide surfaces (F.S. <1) for different combinations of cohesion and friction values. In terms of differences in computational speed, a typical Slide analysis for Little Chief could be undertaken in less than one minute, whereas running a similar UDEC analysis could take 48 hours or

more. Therefore Slide was used as a quick method for narrowing down the range of initial strength values to be tested in UDEC.

The profile of the Little Chief slide and the level of the lower water table were input into Slide. Then peak strength parameters of friction and cohesion were lowered either individually or together until values were found in which a Factor of Safety (FoS) of approximately 1.0 was found for a slide surface similar in shape and size to that interpreted from the surface and subsurface borehole site investigation data. The limit equilibrium method of slices trial-and-error variations used are shown in Table 2.

Table 2: Variations used in limit equilibrium assessment of residual values

Cohesion (MPa)	Friction Angle (degrees)	Size and shape of critical sliding surface (Factor of Safety=1) relative to that interpreted from site investigation data
3	35	No critical slide surface produced
1	30	No critical slide surface produced
0.5	30	No critical slide surface produced
0.5	25	Too large
0.4	25	Too large
0.3	25	Too large
0.2	25	Slightly too large
0.1	25	Slightly too large
0.05	25	Best Fit
0.05	30	Too small
0.05	30	Too small
0.01	25	Very close
0.01	28	Too small
0.01	27	Too small
0.01	26	Slightly too small

Good agreement was found with the field data as the residual friction angle that provided the best fit in the Slide analysis (25 degrees) falls within the range of values determined based on testing of slide material at the Little Chief slide (19 to 26 degrees) (Watson, 2006a). Figure 5 shows the results of the best-fit Slide trial. From this, the values selected as a starting point for the strain softening models in UDEC were a cohesion of 0.05 MPa and friction angle of 25 degrees. This was not expected to serve as an exact match for the UDEC Model, but merely as a more efficient means to narrow down the initial estimate of values required to reproduce the basal slide surface; the trial and error assessment required to carry out this modelling was significantly much faster in Slide than UDEC.

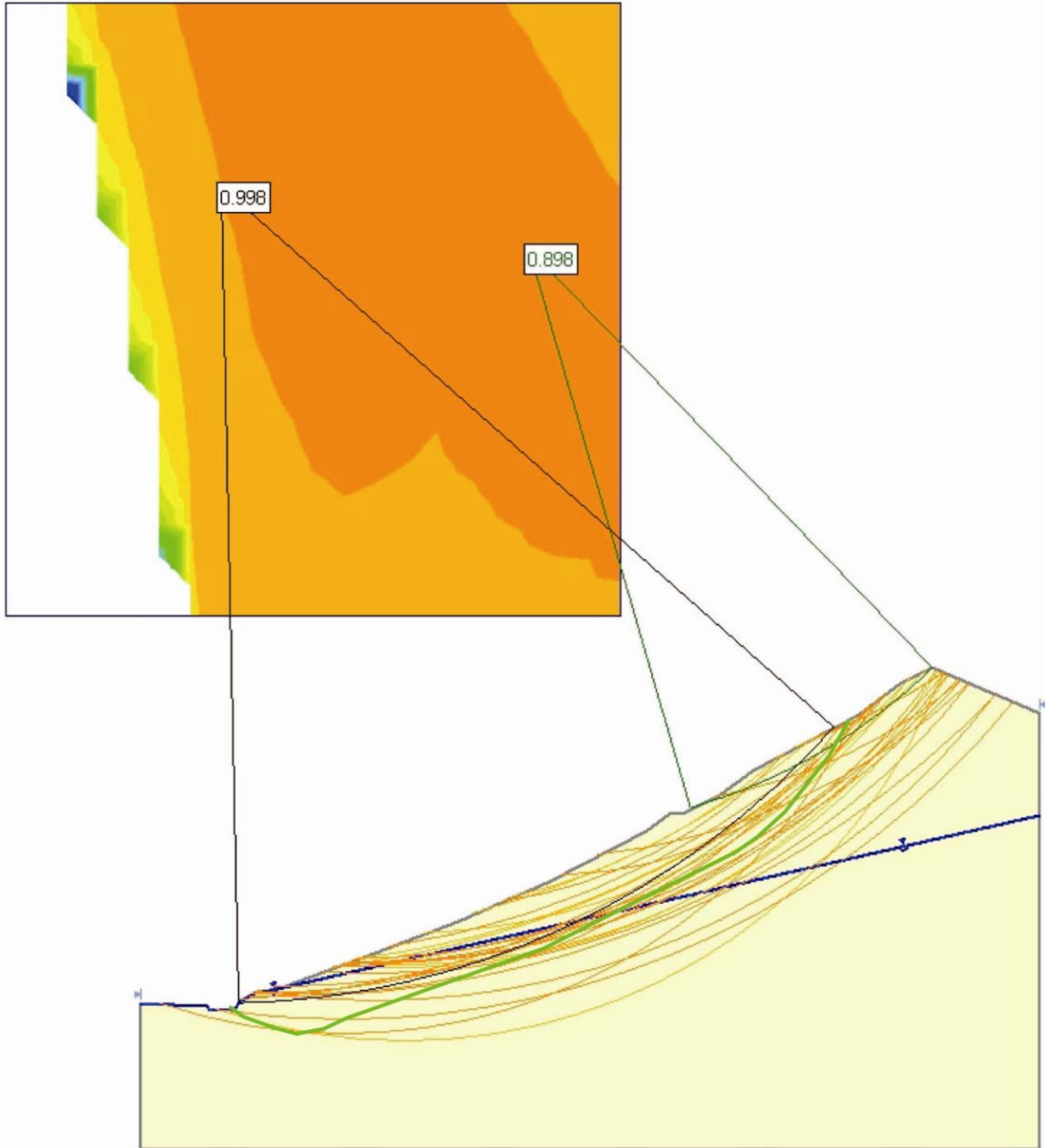


Figure 5: Slide results showing all sliding surfaces with factor of safety between 0.95 and 1.05. The surface in black has a factor of safety close to one and matches well with in situ observations of the size and shape of the actual side surface at Little Chief (shown in green). The surface in grey has the lowest safety factor for these conditions. Cohesion =0.05MPa, friction =25 degrees

4 Case Study of the Campo Vallemaggia Landslide

In order to investigate the role of fatigue in deep-seated rock slope failures, a conceptualized model of a large landslide was used as a basis for analyzing the effects of cyclic loading on down slope movements. The Campo Vallemaggia landslide in the southern Swiss Alps, in the canton of Ticino, is a well-documented 800 million m³ sliding mass in fractured crystalline rock. It is known to have complex compositional layering and artesian pressures which contribute to the temporal sliding characteristics of the mass (Bonzanigo et al., 2007). A detailed study by Bonzanigo et al. (2007) reports the 200 year history of measured slope movements, as well as the geometry, geology and subsequent stabilization of the landslide in 1995 through the construction of a drainage adit. Documentation of this can be found in Bonzanigo et al (2007) and Eberhardt et al. (2007). For purposes of this investigation, the pre-stabilized state of the landslide is examined.

The Campo Vallemaggia slide was chosen to help develop the rockslide fatigue modelling procedure because its behaviour is well understood and there is detailed site investigation data available in the public domain. This made it the ideal conceptual model with which to test methods and modelling procedures. A photograph of the lower half of the sliding mass and the two communities situated upon it are shown in Figure 6.



Figure 6: Image of the Campo Vallemaggia landslide. The settlements present on the slide can be seen.

4.1 Geology

The primary rupture surface of the Campo Vallemaggia landslide dips at approximately 20°. This is believed to be a well-defined basal detachment zone at the base of the slide along which the landslide moves. There are several internal shear surfaces present within the slope that complicate the movement pattern.

A geologic cross section of the landslide taken from Bonzanigo et al. (2007) is provided in Figure 7. The basal shear surface and internal faulting of the mass can be identified in this figure. Within the Campo block, shown in Figure 8, the deformations and displacements are concentrated along these

internal shear surfaces. The primary sliding surface reaches depths of up to 300 m, and the volume of slide material is approximately 800 million m³.

4.1.1 Engineering Geology of the Site

Interpretations of the geology and geometry done by Bonzanigo et al. (2007) of the Campo Vallemaggia landslide are based largely on a series of detailed site investigations that began in 1983. These include geophysical surveys, borehole drilling and instrumentation including both inclinometers and piezometers, geodetic measurements, surface mapping and sample testing.

The jointed crystalline rock mass is highly fractured and disturbed, especially in the lower half of the slide. Figure 9 is an image of the disturbed rock seen at the slide toe, showing its broken and weathered nature. Figure 10 shows the undisturbed rock in the drainage adit, which is significantly more intact and competent. There are two dominant joint sets important to modelling, one that is sub-horizontal and one that is sub-vertical. The subhorizontal set runs parallel to the schistose zones, dipping between 20 and 30 degrees SE. This is consistent with the sliding direction, indicating that this feature likely contributed to the formation of the sliding surface. The subvertical fractures are far less frequent and persistent. They dip at 70-80 degrees to the North and East (Bonzanigo et al., 2007)

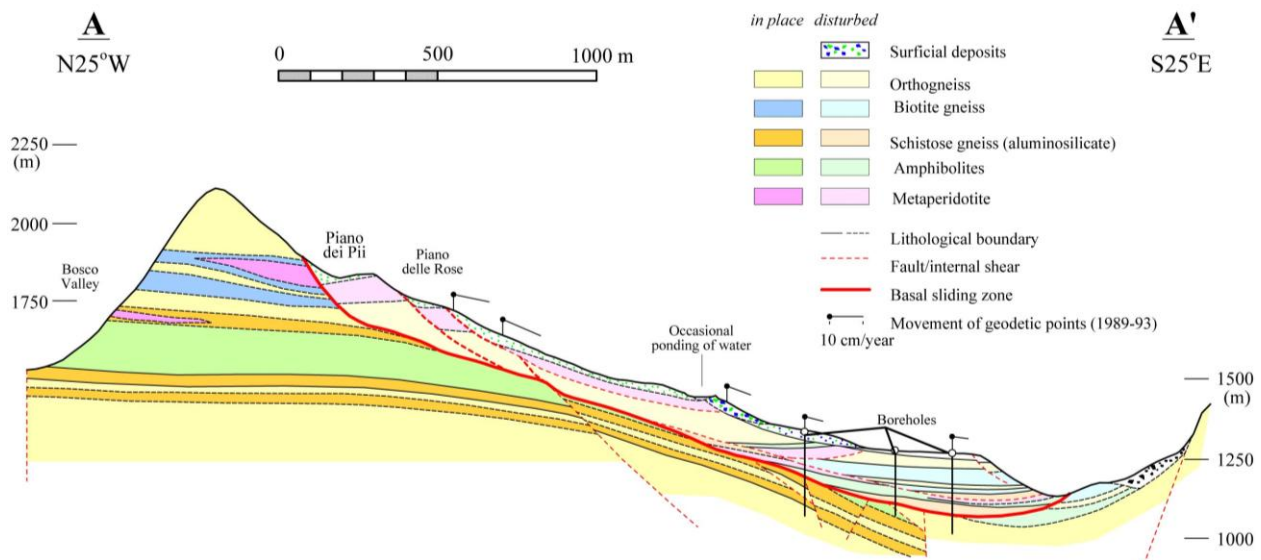


Figure 7: Geological cross-section taken longitudinally through the Campo Vallemaggia landslide. Faults shown in bold are those included in the models. (after Bonzanigo et al. 2007).

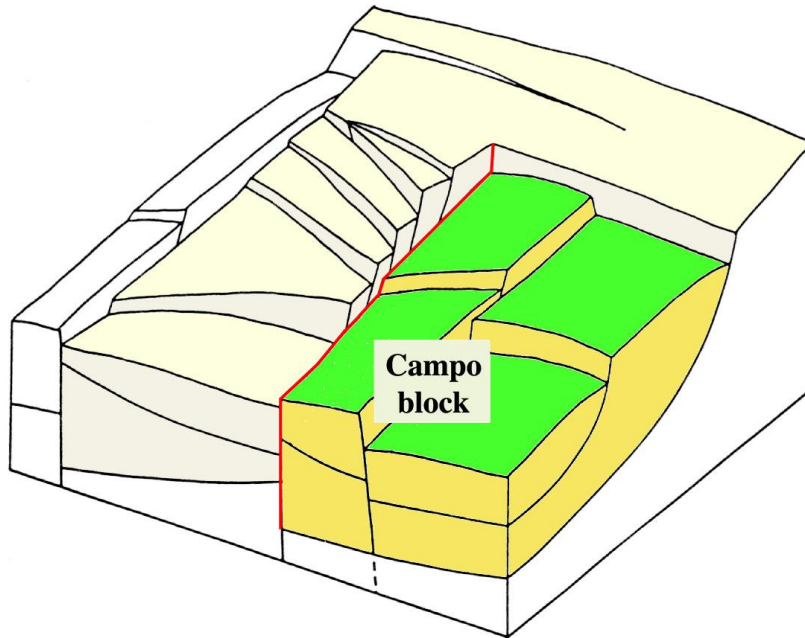


Figure 8: The Campo Vallemaggia landslide, showing the Campo block in bright yellow and green and the Cimalmotto block in pale gray. After Bonzanigo et al. (2007)

The local geology consists of a metamorphic series of amphibolites, micaceous schists, gneiss, ultramafic metaperidotites and metacarbonates. Compared to the surrounding host rock, the slide body shows a greater degree of weathering and is more disturbed (Bonzanigo et al., 2007). This highly disturbed nature is attributed to the long history of sliding and very large amount of movement the slide has undergone.

There are four general zones, geomorphologically, within the slide: the headscarp area with large blocks and open tension cracks; the upper and central slide with large intact blocks that are highly disturbed and partially covered with a thin veneer of till; the lower terrace which is highly fractured and represents the most disturbed and deformed area; and the slide toe which is the erosional front of the landslide (Bonzanigo et al., 2007).



Figure 9: Disturbed and broken rock at the toe of the Campo Vallemaggia landslide



Figure 10: The undisturbed rockmass in the Campo Vallemaggia drainage adit

4.1.2 Ground Water

Within and below the slide body, artesian water pressures have been found through borehole drilling. Numerous surface springs also exist. As is typical of crystalline, metamorphic environments, jointing and faulting are the main controls on hydraulic conductivity and fluid flow, with schistosity playing a smaller role (Bonzanigo et al., 2007). To stabilize the landslide, a drainage adit was constructed below the slide body and drainage holes drilled upwards into the basal sliding zone to relieve the groundwater pressures. This was followed by a significant reduction in slide velocities. Based on the analysis of the pre- and post- drainage monitoring data by Eberhardt et al. (2007), high pore pressures were found to be the primary destabilizing mechanism with seasonal variations in the groundwater table closely matching periods of acceleration and deceleration in the slide body.

In addition to the artesian conditions, there is a large river at the toe of the landslide for which toe erosion has been alternatively identified by some as the destabilizing mechanism. Modelling work presented by Eberhardt et al. (2007) suggests that this is not the case, pointing instead to the artesian conditions. However given that remediation of the toe through diversion of the river was coincident with drainage, toe erosion cannot be conclusively ruled out.

4.1.3 Landslide History and Behaviour

The Campo Vallemaggia landslide consists of several blocks, subdivided by subvertical fault zones. This results in a rather complex slide motion, difficult to represent with simple models. The landslide can be divided generally into two lobes (see Figure 10) based on a major fault scarp. One, the Campo block (on the right in Figure 10), exhibits primarily translational, downslope motion while the other, the Cimalmotto block (on the left in Figure 10), is partially restricted in its movement by the first mass (Bonzanigo et al., 2007). The Cimalmotto block is moving both down and towards the Campo block, rather than directly downslope. The translational Campo lobe has been used for this study as the simpler motion and kinematics were more suitable for a two-dimensional analysis.

The movements described above have a history of being both intermittent and related to changes in hydraulic heads at depth. The intermittent movement has a history of accelerations that correspond with intense periods of precipitation. The nature of this movement has been described as “forward pulsing” (Bonzanigo et al., 2007), making it an ideal case for this study. The slope movements have been reported for over 200 years with an average slide velocity of 5 cm/yr recorded for the time between 1892 and 1995 (Bonzanigo et al., 2007).

4.2 The Model

The modelling work presented here takes into consideration the pre-drainage/pre-stabilized behaviour of the landslide, in order to study its response to fatigue in the form of seasonal fluctuations in the modelled water table. In this sense, the Campo Vallemaggia case history serves as a more generalized example of a large slow-moving landslide affected by cyclic loading and progressive localized strength degradation and shearing.

The distinct-element program UDEC (Itasca, 2009) was used to model the problem geometry as an assemblage of deformable interacting blocks. The discontinuity network was generated based on that used by Eberhardt et al. (2007) to portray a strong horizontal anisotropy within the slide body and vertical anisotropy below it as mapped during construction of the drainage adit used to stabilize the landslide.. The modelling performed involved a multi-stage cycling procedure. Once initial model equilibrium had

been established, a simulated water table was raised and then lowered for 1000 time-steps each. These combined 2000 time-steps represent a period of one year, made up of one wet and one dry season. The 1000 time-step limit was selected based on calibration testing as to the number of time-steps required to reproduce the velocity trend of 2-5 cm/year established for the landslide through long-term monitoring. Various versions of the model were tested for durations of up to 3000 “years”. The basic model, and the two water tables representing annual lows and highs, can be seen in Figure 11. A closer look at the close joint spacing in the sliding mass is seen in Figure 12. Table 3 provides the joint and block properties used in the model, the upper and lower sliding bodies mentioned in Table 3 are identified in Figure 11. As with the discontinuity network, the properties in Table 3 were based on the work already done on the Campo Vallemaggia landslide by Bonzanigo et al. (2007) and Eberhardt et al (2007).

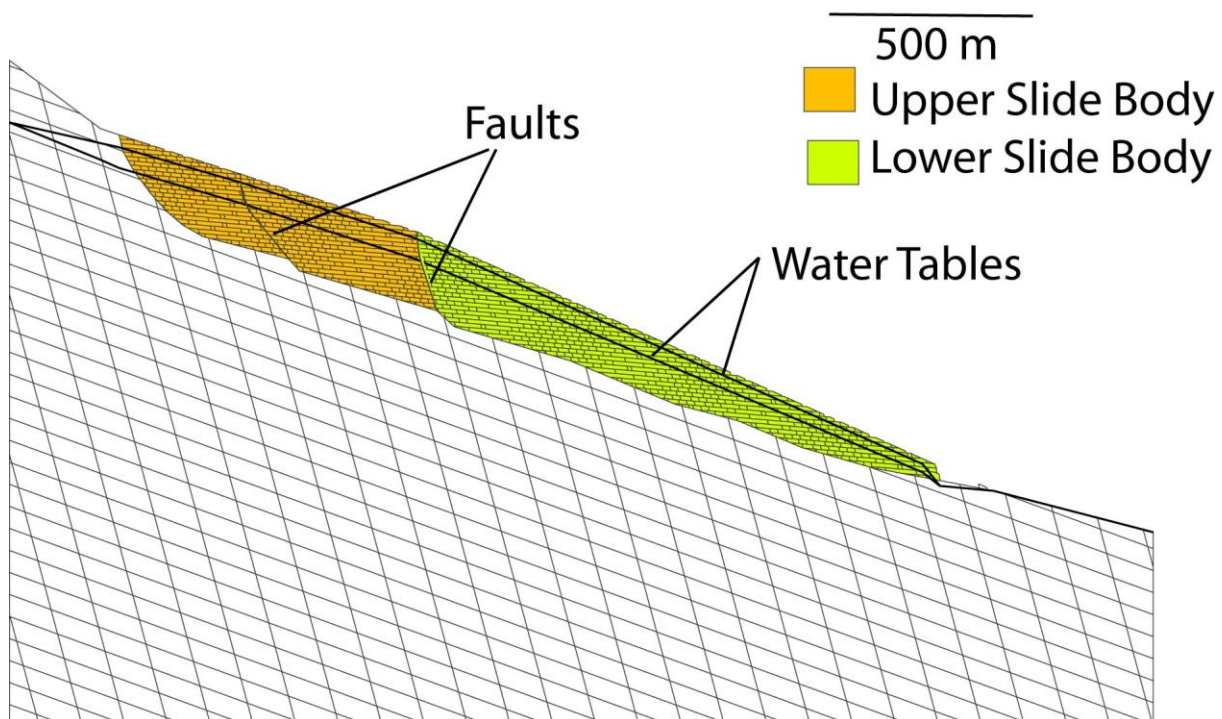


Figure 11: Model of the Campo Vallemaggia slide geometry, showing locations of water tables and movement generated faults (scarps).

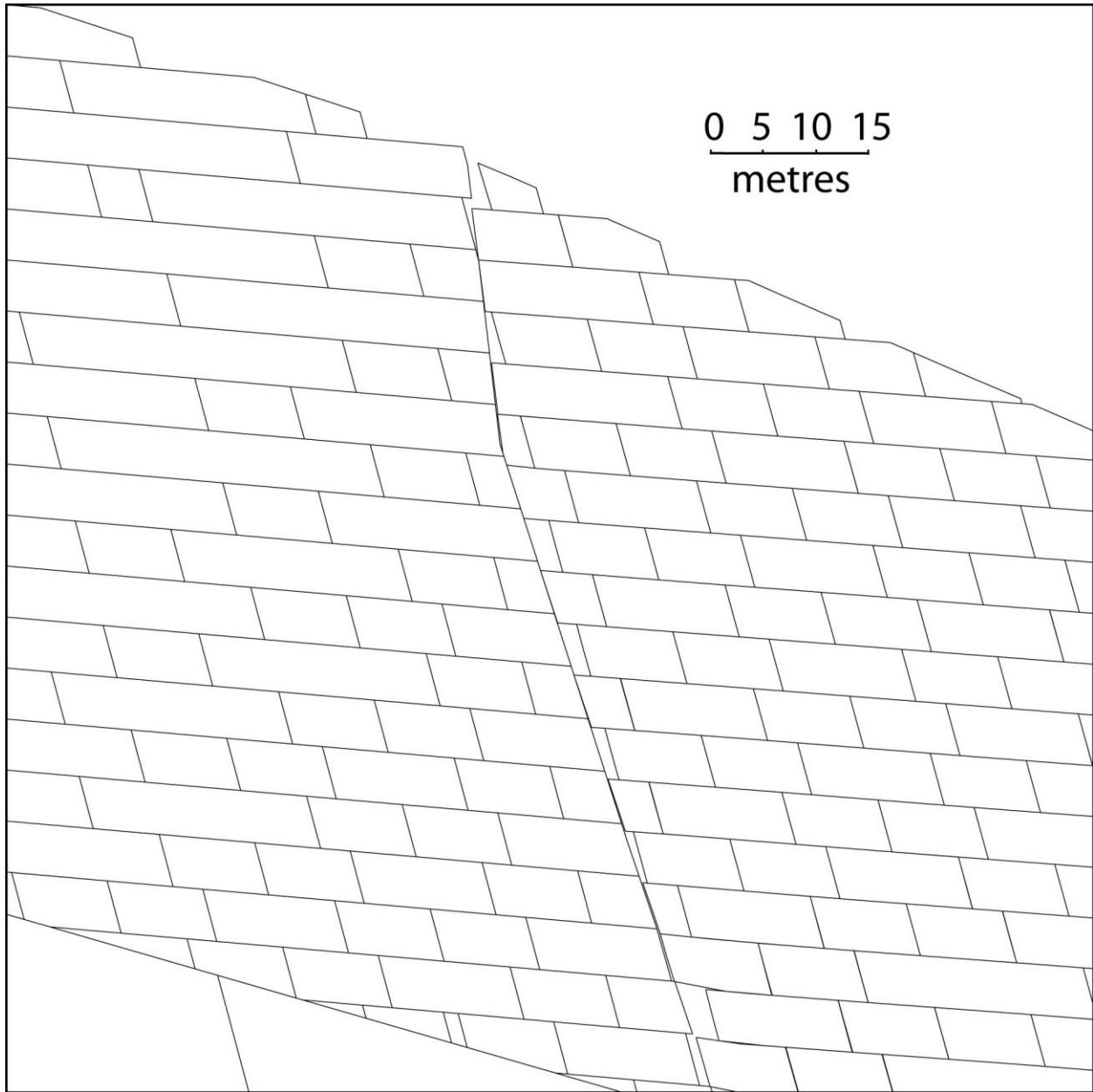


Figure 12: Close up of the jointing pattern used in the Campo Vallemaggia models, also showing the lower fault present in the sliding mass.

4.3 Results

Results for the model fall into two categories. The first is the comparison of the model with and without internal shear surfaces, and the results were compared. The purpose was to determine whether the method would generate the same internal surface when they were not placed explicitly in the starting model. Preliminary results from these models were presented by Smithyman et al. (2009). These results have been expanded on in this thesis, but there are no results that invalidate the findings.

Table 3: Rock mass properties used for modelling, taken from Bonzanigo et al. (2007).

Property	Below Slide	Upper Sliding Body (see Fig. 11)	Lower Sliding Body (see Fig. 11)
Density (kg/m ³)	2600	2300	2250
Young's Modulus (GPa)	30	20	5
Poisson's ratio	0.25	0.3	0.35
Block cohesion (MPa)	n/a	1	0.2
Block internal friction angle (°)	n/a	45	30
Block tensile strength (MPa)	n/a	0.5	0.1
Joint friction angle (°)	45	40	35
Joint cohesion (MPa)	0	0	0
Zero joint aperture (mm)	2	1	1
Residual joint aperture (mm)	1	0.5	0.5
Sliding surface friction angle (°)	25	n/a	n/a

4.3.1 Plasticity and Fatigue

The model was first run with only the basal sliding surface and the representation of the meso-scale joint network explicitly included. Major faults mapped across the landslide body were not included in this first series of models. A parallel set of models with these features included (Figure 11) were also tested in order to examine their influence on the landslide behaviour and its evolution. The most prominent of these faults crossing perpendicular to the 2-D cross-section (Figure 7), form upper and lower scarps in the upper half of the slide body below the Piano dei Pii and Piano delle Rose.

The initial non-faulted model was examined at multiple stages of cyclic loading in order to observe the development of plastic yielding in the form of shear and tensile damage indicators. These damage indicators and their progression with each load cycle (i.e. raising and lowering of the water table) were interpreted as representing rock mass damage and fatigue and are presented in Figure 13. In particular, it was noticed that yielding tended to localize around the regions of the modelled slide where the mapped major fault and scarp features are found. This comparison of yielded elements to fault locations is shown in Figure 14. Note that the faults shown in this figure are those mapped in the field superimposed on the model results for comparison. It can be seen that the majority of the yielding occurs slightly below the lower fault, with a collection of tensile failure locations clustering around the projected fault scarp at surface. The upper fault shows significantly less yielding, and the match up is not as good, but again there is localized yielding near to the fault location

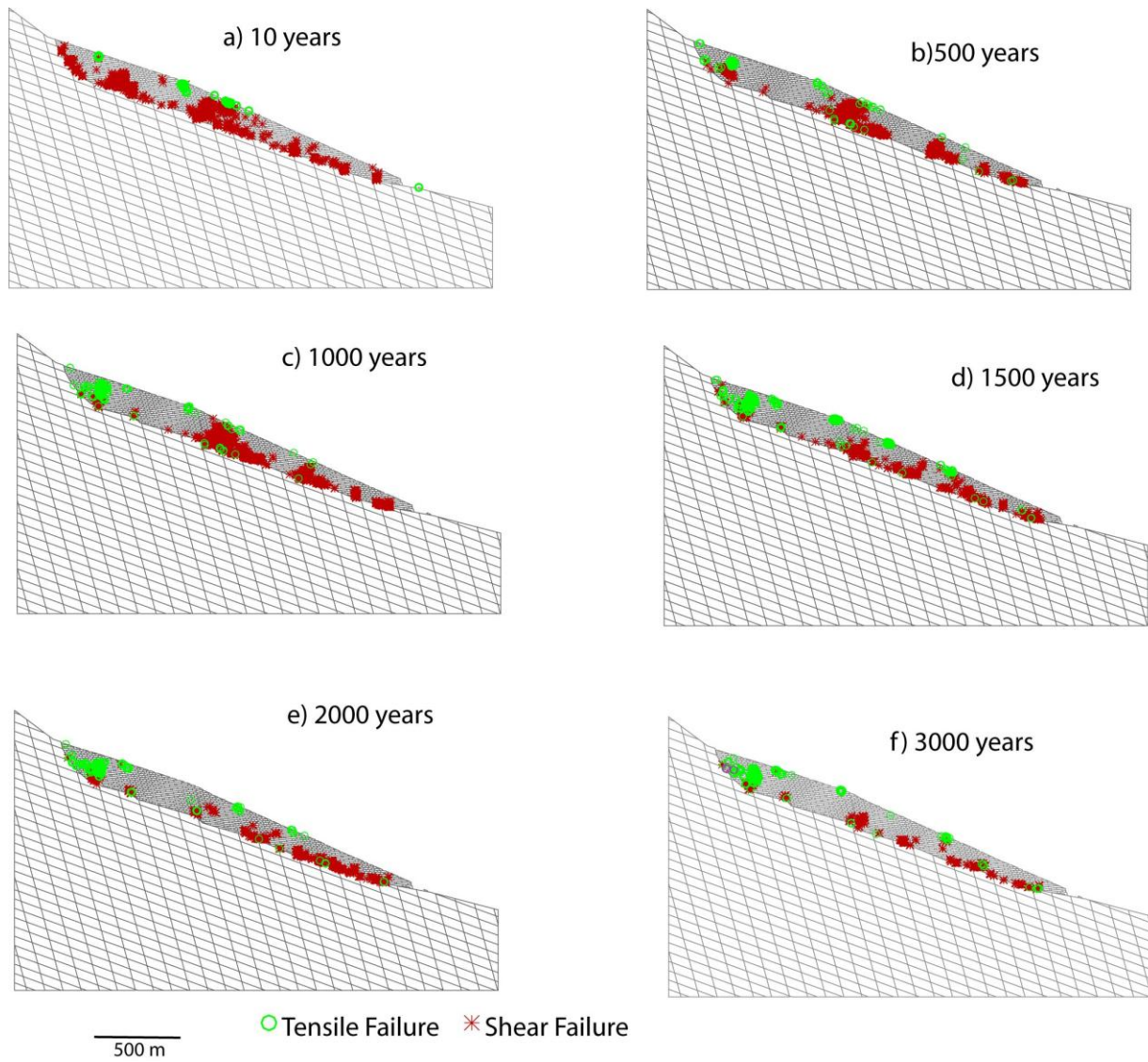


Figure 13: Progression of yielded elements with increasing number of model years for the model with no internal faults.

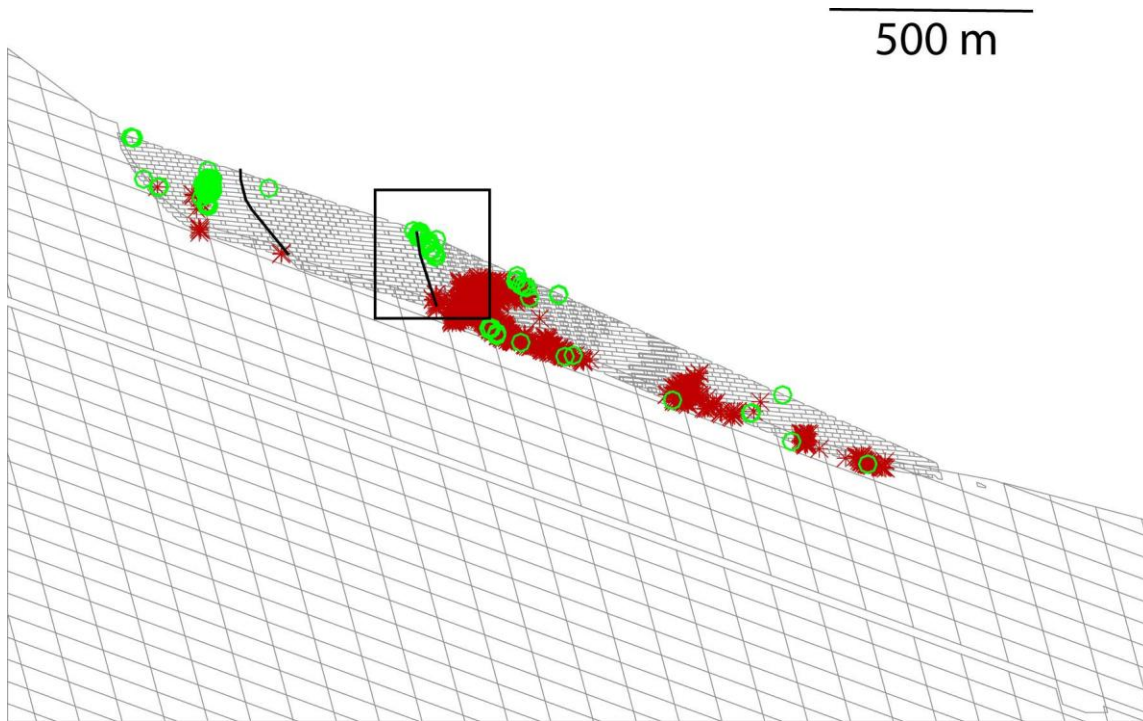


Figure 14: Yield displacements in the unfaulted model compared with fault positions. The box indicates the area shown in later figures. Note that the heavy black lines, which indicate the positions of the mapped faults, are superimposed on this image for comparison. These faults have not be included in the model.

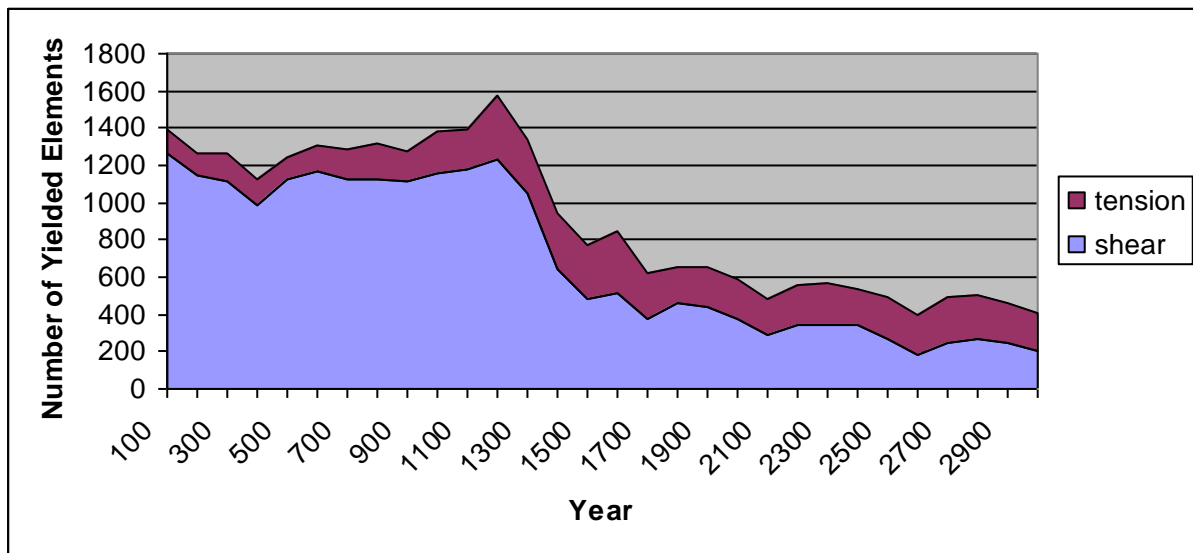


Figure 15: Number of yielded elements present in the model at any given year. A sharp decrease can be seen at approximately 1300 years, coinciding with the development of internal shearing and fault scarp generation in the model.

Although these concentrations could be partly attributed to the characteristics of the uneven basal sliding surface, the shape of which was partially interpreted based on the presence of these faults (Bonzanigo et al., 2007), the model results suggest that deep-seated sliding activity is not likely without some internal yielding and shearing at these points. Figure 13 shows the progression of yielding over 3000 modelled years, or fatigue cycles, of raising and lowering the groundwater table. The results show

that after only 10 years of displacement, stress and strain concentrations had already begun to focus around these areas.

After 200 years (Figure 13), there are fewer yielded elements localized around the upper fault due to the redistribution of stresses enabled through the previous yielding of elements and accommodation of slip along the discontinuities. However, throughout the model there are increasing numbers of yielded elements developing downslope of the lower fault. A scattering of yielded elements can also be seen throughout the lower part of the slope. These represent the more general trend of fatigue within the slope, and the need for internal rearrangement and/or yielding of the rock mass in order to kinematically enable downslope movement. The 400 and 800 year yielding patterns (Figure 13) continue to follow this trend of increased overall yield. However, a change is noticed in the 3000 year pattern. There has been a significant decrease in overall yield. Figure 15 shows this progression of increased yield and then decrease, and Figure 16 shows the corresponding formation of an opening positioned just below the lower fault.

This behaviour agrees with that expected for fatigue-driven progressive failure. A consistent high amount of yielding, and increasing rock mass dilation (opening where the fault is developing) is seen up until a point around 1300 years, after which the number of yielding elements drops significantly and the fault stops opening. This can be associated with the break point in the progression of fatigue failure. As one bends a paper clip repeatedly, the metal cracks more and more, until the clip breaks apart completely and there is no connection left to damage. In a similar manner, the number of yielded elements increased as the rockmass accommodated the breaking, and then decreased sharply once the fault is opened and blocks need no longer adjust around it. The fact that the number of yielded elements does not drop off to nothing, as it would if a piece of metal broke under cyclic loading, is due to the fact that the landslide is a complex system of blocks, and the breaking of this fault is not accompanied by catastrophic failure. Instead, further yielding is still required to accommodate continued movement.

Figure 17 shows the pore pressure distributions, and the dry season water table, for the model both before and after the opening of the fault. Away from the fault itself the two pore pressure distributions are identical. This is logical and expected given that the water table, and therefore pore pressures are manually reset every 1000 computation cycles. There is a difference seen at the fault. The joints immediately around the fault, and the fault opening itself, show small or no pore pressures. Again this is expected as the fault opens and UDEC can no longer determine contacts between the blocks, and therefore pore pressures. This is likely similar to reality, where faults often form conduits through which water escapes the general rockmass.

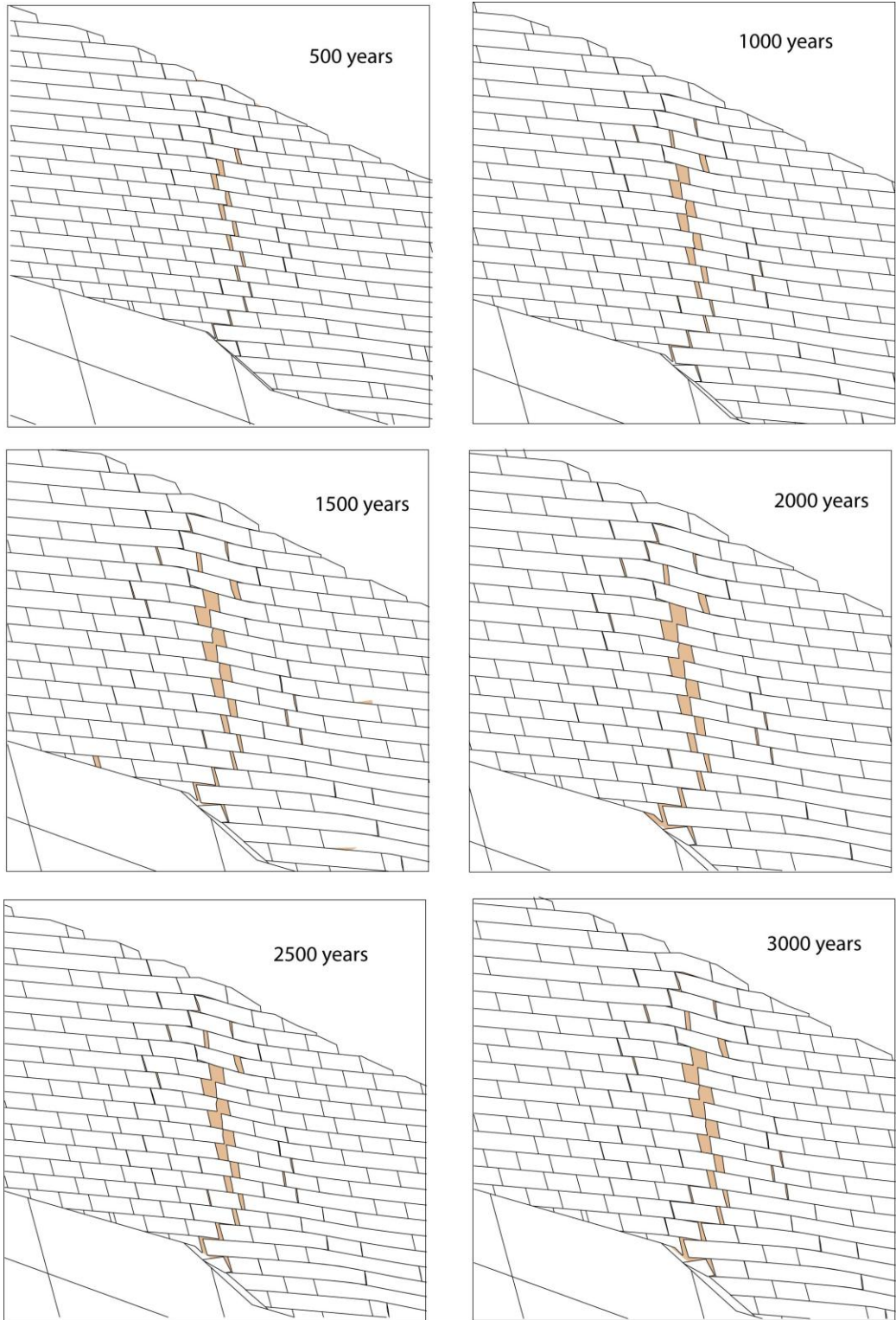


Figure 16: Opening of a fault in the unfaulted model. Shaded areas are openings, white spaces are bricks. See figure 13 for the placement of these figures on the slide.

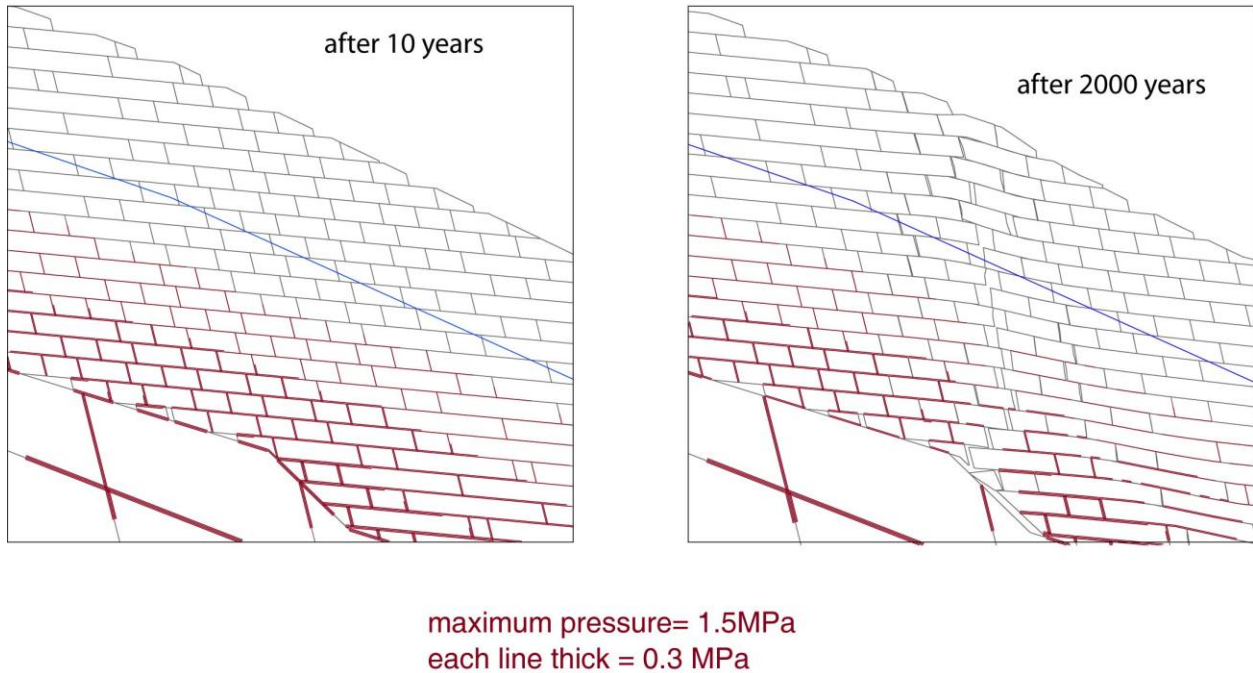


Figure 17: Pore pressure distributions around the area where the fault opens at 10 and 2000 years

Figures 18 and 19 show the distribution of horizontal stresses through the model before and after the opening of the fault. Figure 18 shows the whole model while Figure 19 shows the area immediately around the fault. In Figure 18, very little change is seen in the overall stress distribution with time; however one notable change is that there is significantly less horizontal tension after the opening of the fault. This is logical based on the fact that the movement of the downslope portion of the slide, when blocks were interlocking with the upper portion, would have a drag effect of pulling the upper portion toward the right. As the fault opens this effect is reduced significantly, as the downslope blocks are no longer in contact with those upslope to affect them. Note that this is likely a slight effect with very small tensile stress values. Once the fault opens, those blocks are no longer interlocking, and so the effect of the downslope portion of the slide on the upslope portion is greatly reduced.

In Figure 19 it can be seen that there is very little change in the horizontal stress distribution around the fault with time. However it is possible to see the development of a high stress zone along the basal detachment just to the left of the fault. This zone becomes higher stress, and more localized with time. As it is situated at the step in the basal detachment surface, it is likely that this localization is related to the movement of blocks down at the step. This would create a downward force on the surrounding rockmass, which could cause these high stresses to form behind the fault. This build up of becomes more localized as the fault opens, and less movement is taking place in the upslope half. As the blocks are no longer moving, they are not adjusting to a more favourable stress distribution around this location.

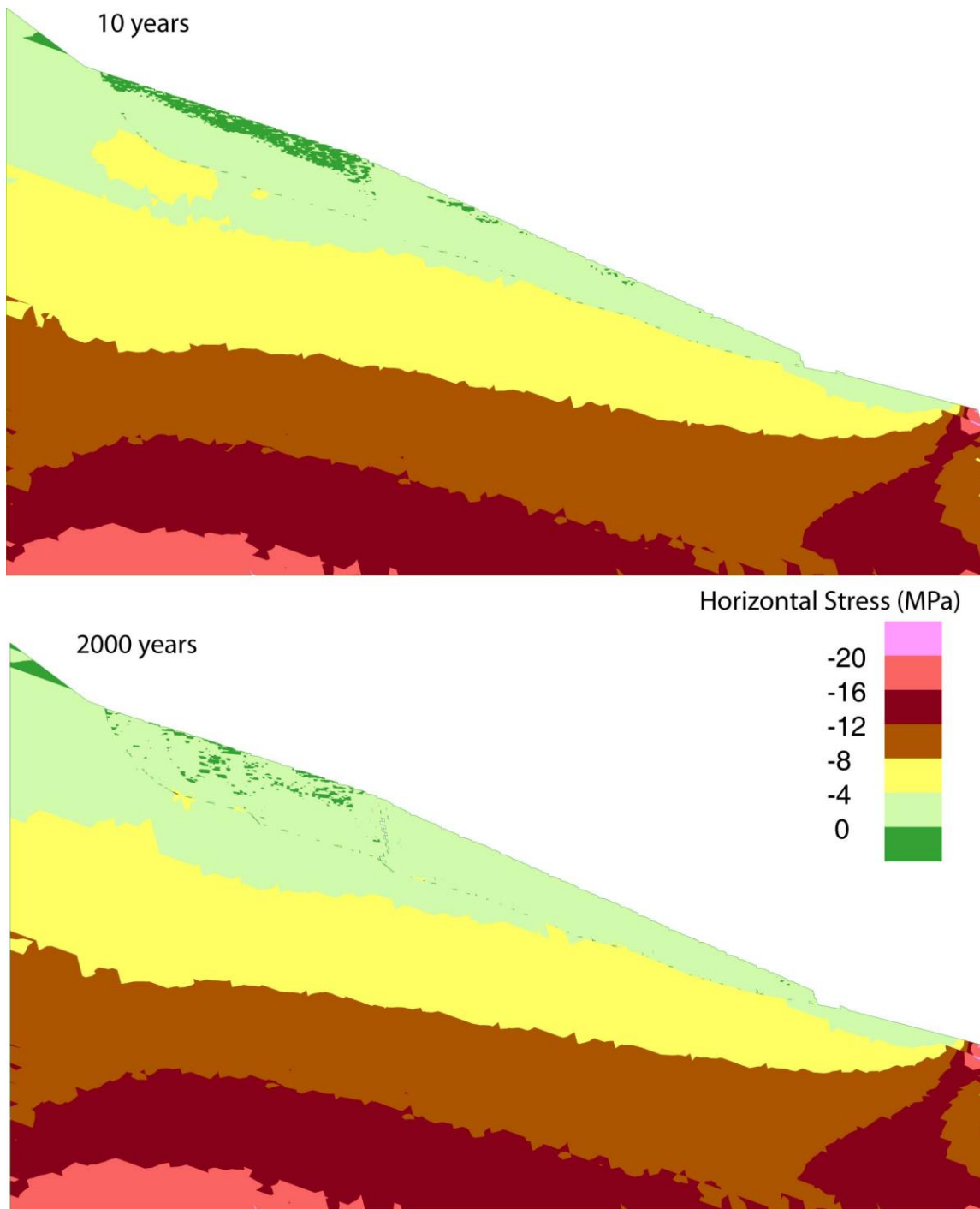


Figure 18: Horizontal stress distributions through the entire slide

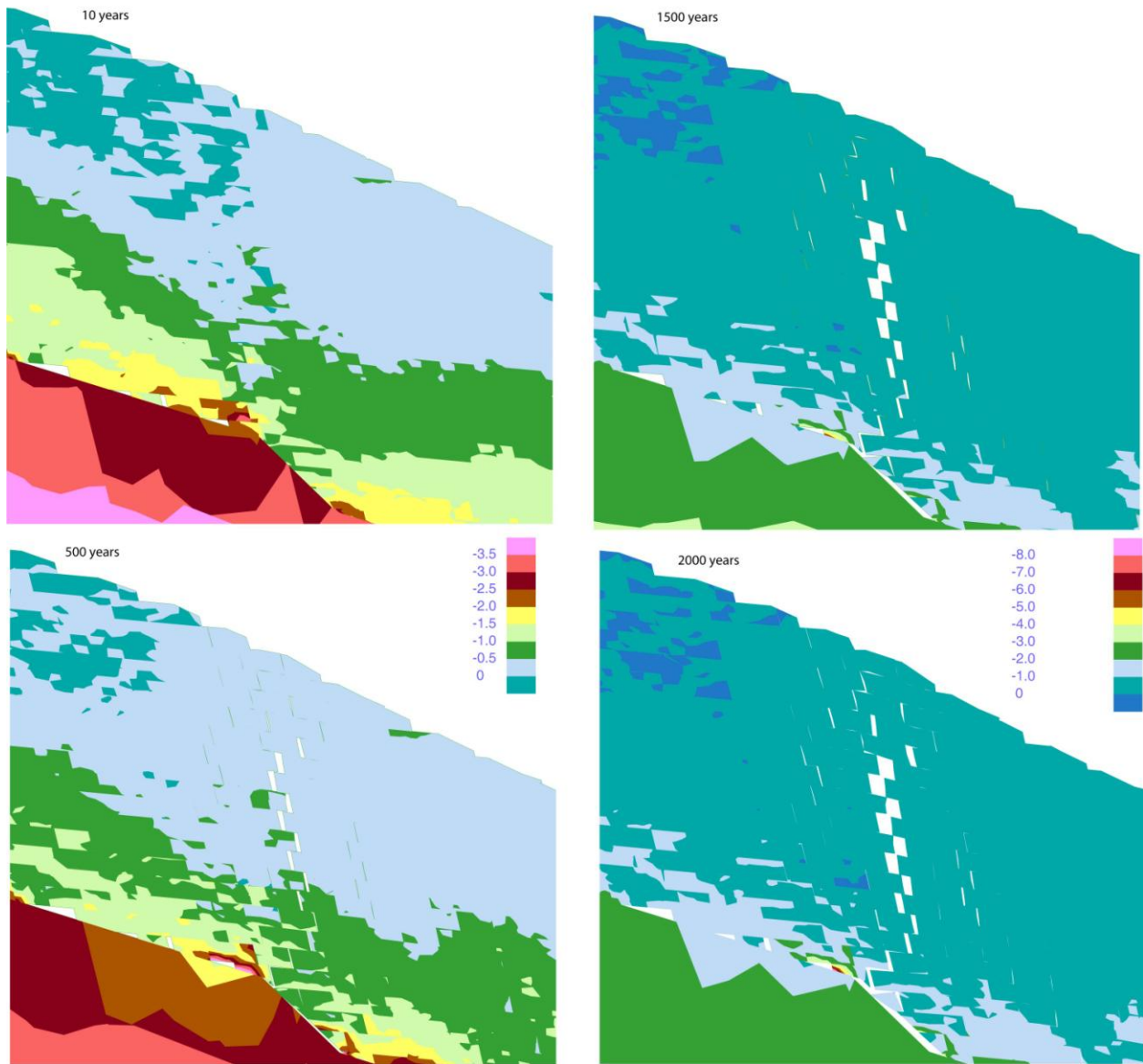


Figure 19: Horizontal stress distributions in the area of interest around the fault opening. The contours of the stresses are in MPa. Note that the 10 year and 500 year images follow the left legend, while the 1500 year and 2000 year images follow the right legend.

Figures 20 and 21 show the vertical stress distributions in the model before and after the opening of the fault. Figure 20 shows that there is very little difference at the whole model scale between before and after. In the 2000 year slide, there is a slight localization along the basal surface near the top of the slide, likely related to the transition from curved to nearly planar sliding surface. This localization is not large in terms of stress value. Figure 21 shows the vertical stresses in the area immediately around the fault. As with Figure 19 there is a localization of high stresses forming on the basal detachment surface to the left of the fault. Again this is likely due to the step shape of the surface at this point. An interesting feature is the stress in the blocks immediately on either side of the fault. From as early as 10 years, these blocks show a lower stress than the surround blocks, suggesting that the opening fault is a weak zone, with the blocks there carrying a smaller load than the others. From 500 years on a second vertical section

of low stress forms on the other side of the high stress localization. This general weakening of the upper block near the fault is logical, and expected given that much of the yielding for the fault to form happened upslope of the opening. This yielded rock is unlikely to carry as much load as the unyielded rock around it.

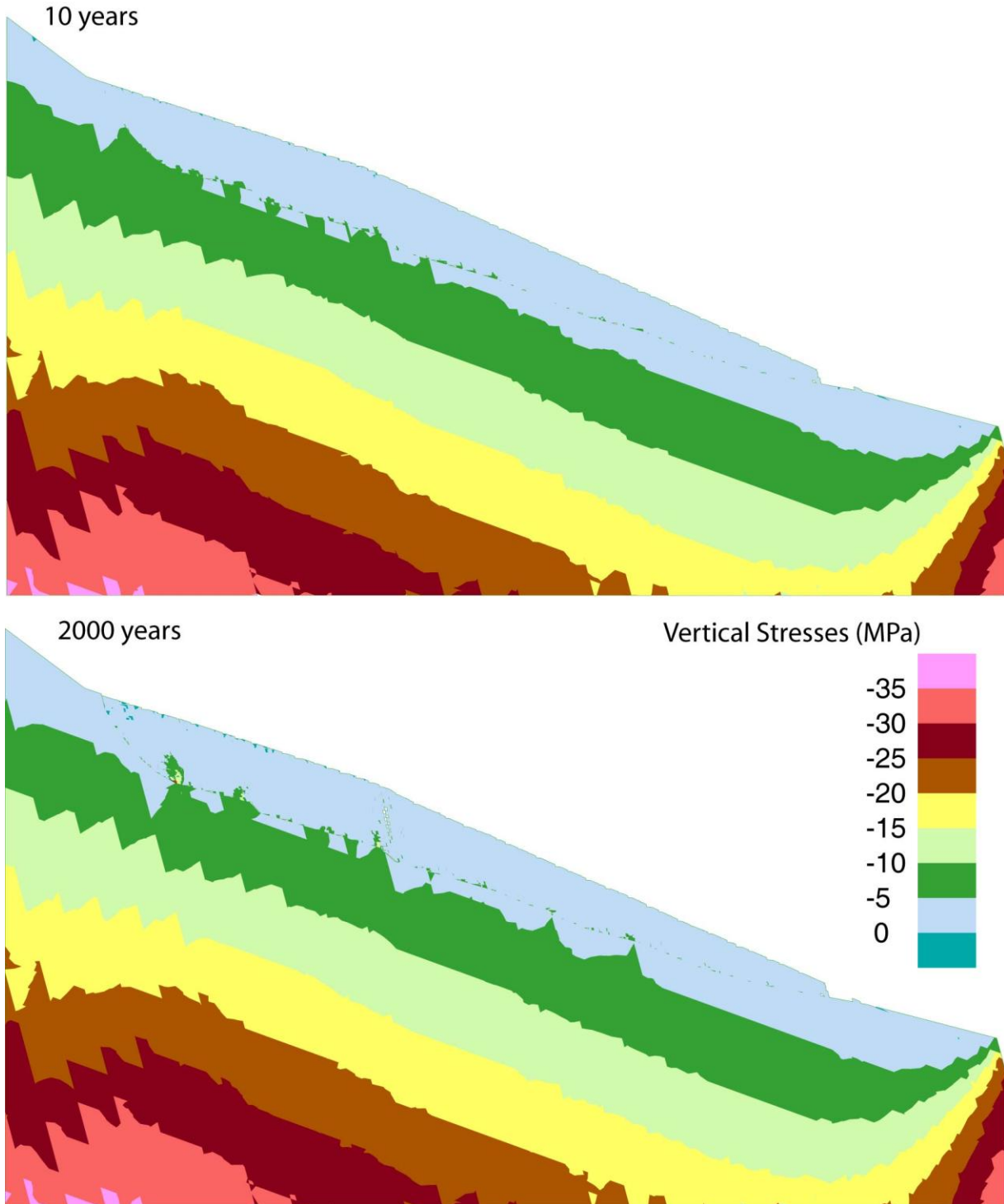


Figure 20: Vertical stress distributions through the entire model

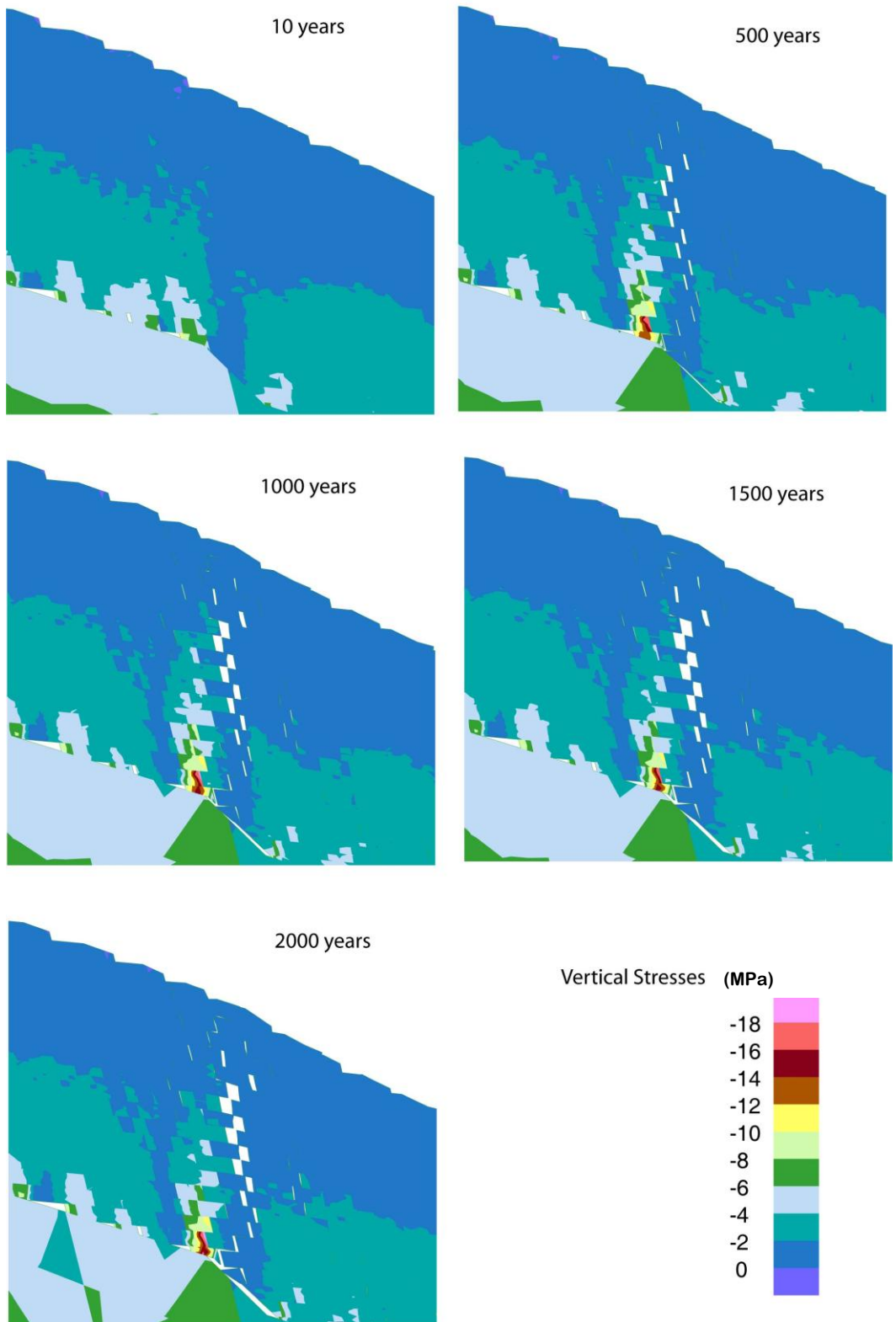


Figure 21: Vertical stress distributions in the area of interest surrounding the fault opening

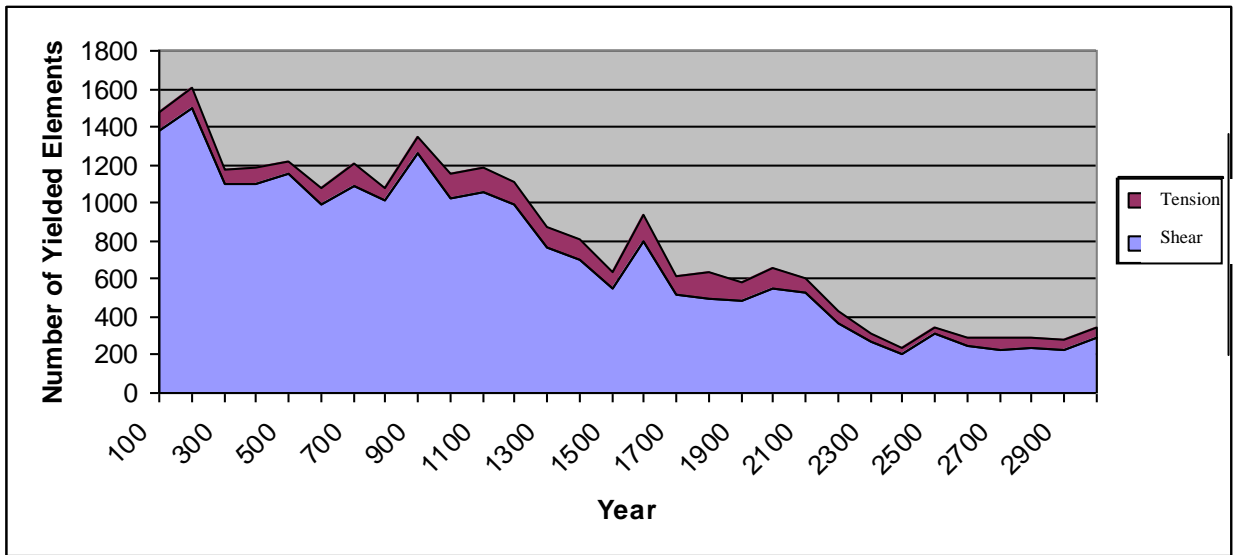


Figure 22: The number of yielded elements present in the faulted model at any given time.

The model results confirm the development and position of major faulting leading to compound sliding for the problem geometry. A second set of models were then constructed to explicitly include these faults, as they represent dominant features in the surface morphology of the landslide. The models were then solved for 800 years and examined to assess the continued evolution of internal yielding and fatigue, and the characteristics of the downslope deformation patterns.

Figure 22 shows the number of yielded elements present in the model at each time. As with the unfaulted model it can be seen that there is a decrease in the number of yielded elements between 1100 and 1500 and then a smaller one between 2100 and 2500 years. The larger of these correlates to the breaking and fatigue effect seen in the unfaulted model. The major difference is that there are fewer yielded elements in the faulted than unfaulted model, and the decrease is more gradual. This is to be expected given that the difference between the two models is that by explicitly including the fault, localized shearing, dilation and movement are more easily accommodated. Therefore the surrounding rock mass does not need to yield to allow movement. Figure 23 shows that the same type of localization of yielding occurs in the internally faulted model as in the unfaulted version. The difference is that the yield indicators localize right at the faults instead of near them as occurs in the unfaulted model.

For both the faulted and unfaulted models, a very large number of cycles (over 1000 years) are needed to see the fatigue effects. This indicates that it is likely that a large number of cycles will be needed in other models in order to see signs of fatigue, something addressed in objective 3 (Chapter 1).

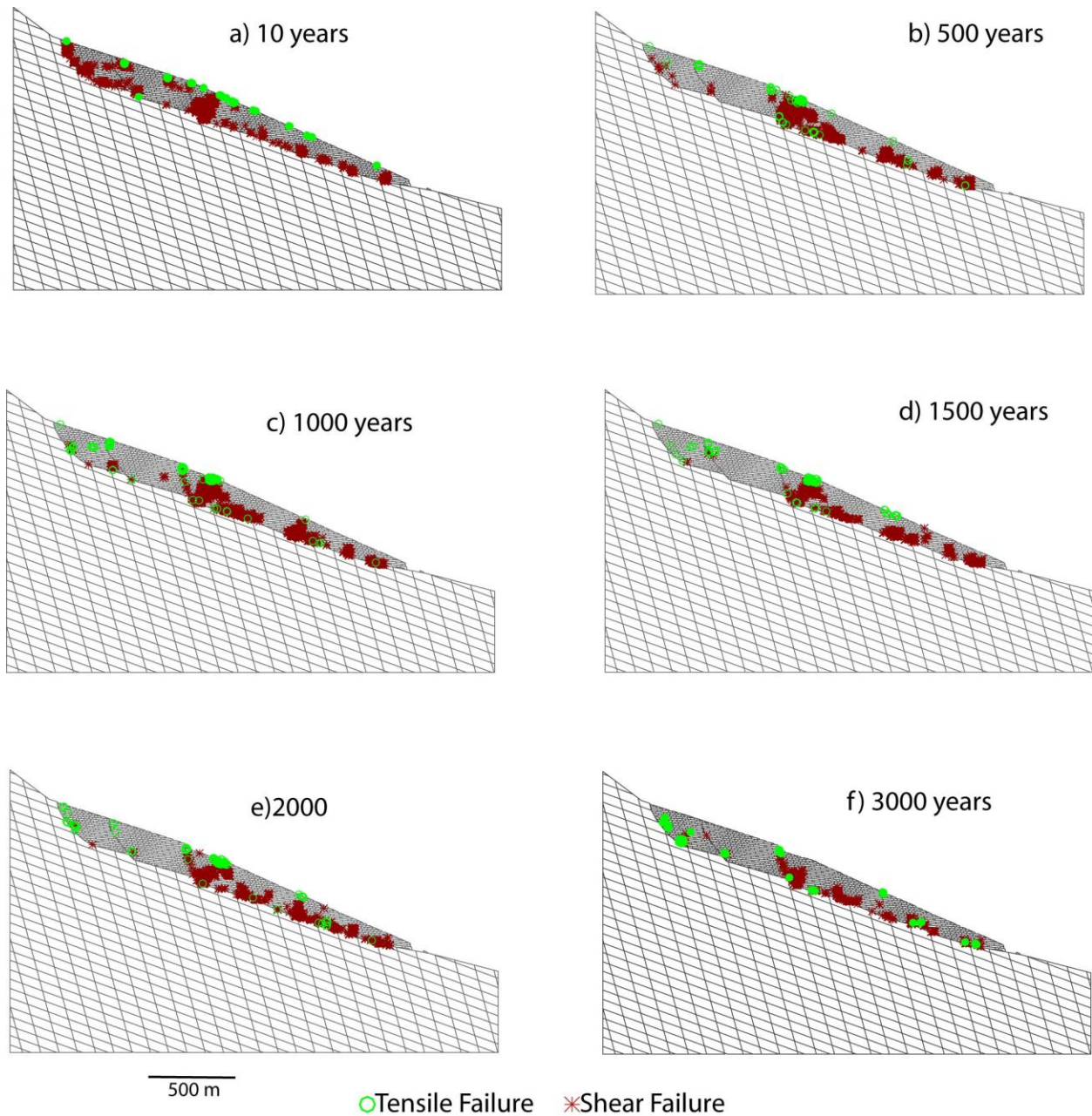


Figure 23: Progression of shear and tensile yield indicators in the faulted version of the model. They are similar to those in the unfaulted version, but tend to localize right on the faults, instead of just in the same general area

Figure 24 shows the tendency of the lower half of the model to move more than the upper half. This difference in displacement accommodates some of the internal rearrangement seen through the yielding within the model. Figure 24 shows that this is true to a greater extent in the faulted version of the model than the non-faulted. This indicated that the presence of these faults gives the lower part of the slope increased kinematic freedom to move at different rates than the upper half of the slide. Otherwise, the only key difference between the two sets of models is that the velocity difference between the upper and lower halves of the slide body is more abrupt when the faults are explicitly included.

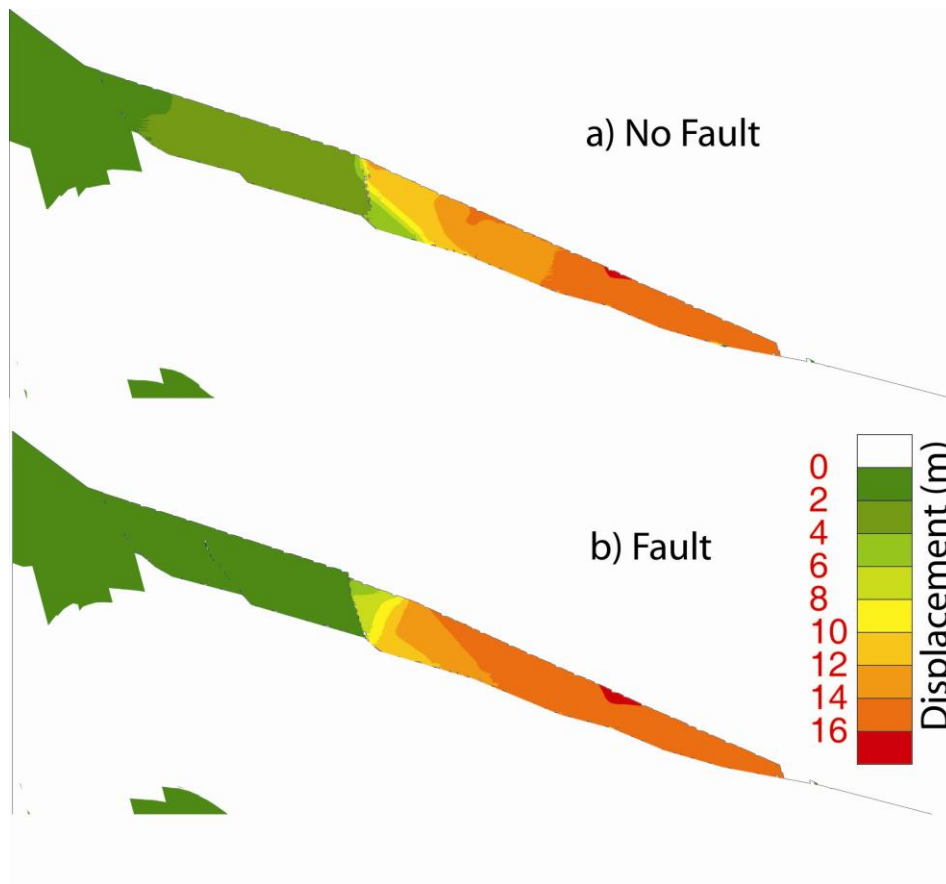


Figure 24: Horizontal displacements are shown for both the a) non-faulted and b) faulted versions of the model. Both show fairly distinct upper and lower block movements, with the faulted model shows a more abrupt transition between these blocks compared to the non-faulted model. The displacements shown are those after 800 modelled years.

Figure 25 shows the displacement vectors for the unfaulted model at four times throughout the opening of the fault. Note that the scale of the vectors is different for the 10 year model than for the other three. This was necessary in order for the vectors to be visible in the 10 year model. At 10 years, there is somewhat more movement to the right of the step in the basal detachment surface than there is to the left, but no clear point of change can be seen. It is a gradual transition. There is also no noticeable variation with depth. For the models beyond 10 years, there is a distinct change from small to large movements at the opening fault. This difference is a logical result of the fault opening. There is also a distinct variation in the amount of movement with depth. The blocks in the deeper part of the model near the fault are moving less than those above them. This demonstrates that not all movement in the model takes place along the basal detachment surface, some displacements are occurring along the various joints in the rockmass.

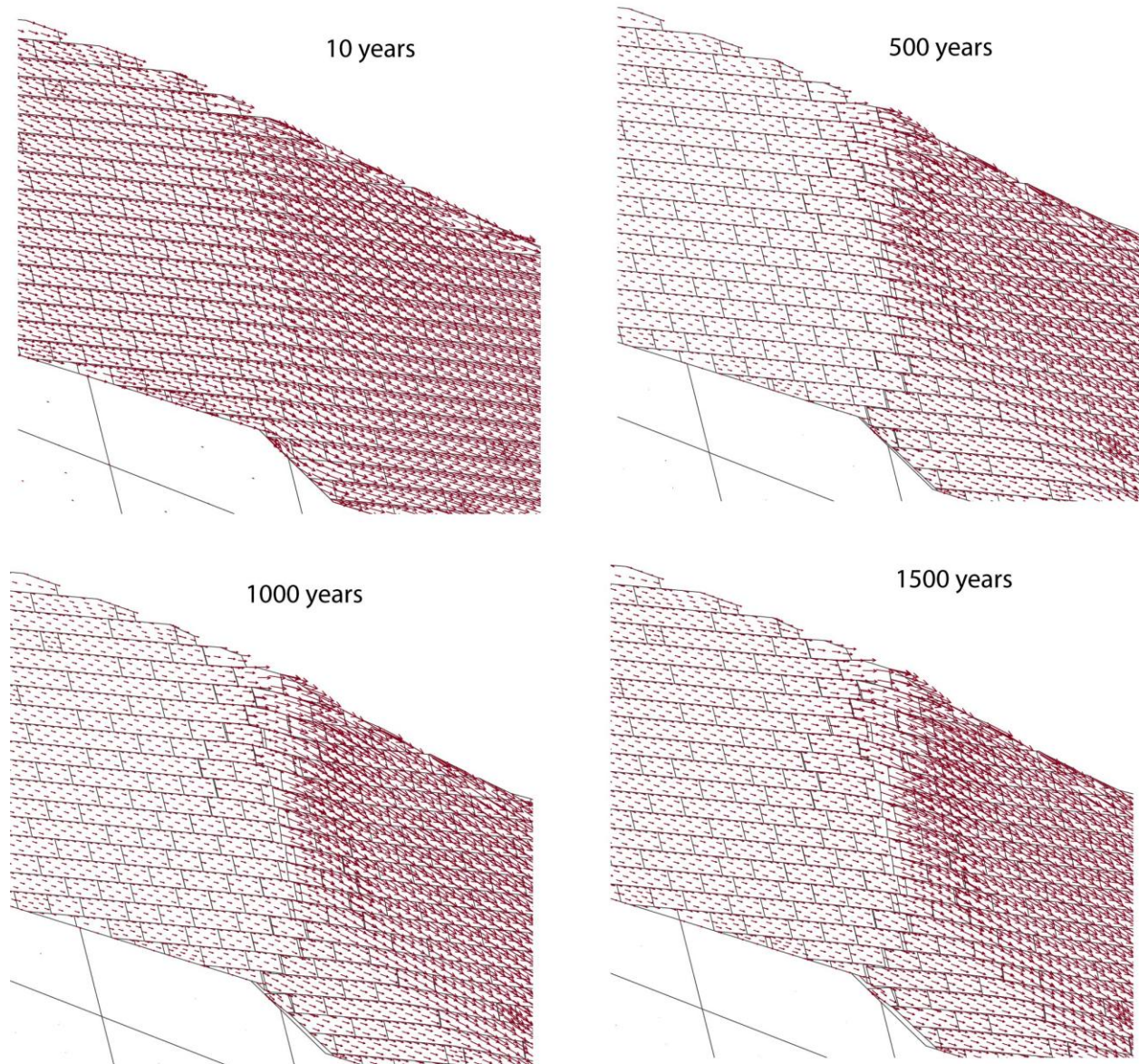


Figure 25: Displacement vectors in the area around the opening fault. Note that vectors are scaled for maximum visibility in all models and relative comparison. Magnitudes of vectors cannot be compared between models.

4.3.2 Intermittent Displacement Behaviour

To further evaluate the model results, a series of history points were tracked in the model to simulate surface geodetic and borehole inclinometer measurements in the modelled slope. These provide a means to compare the different model responses to fatigue cycling to the actual monitored temporal response observed at Campo Vallemaggia. Figure 26 shows the locations of the two monitoring points referred to in this section.

A typical example of the modelled movement pattern is shown in Figure 27. Figure 27a, c shows the horizontal displacement of the toe for the first 10 and 800 years, respectively. Figure 27b, d shows the same time intervals, but for a surface point approximately halfway up the slope (i.e. representing the behaviour of the landslide above the secondary slide scarp fault).

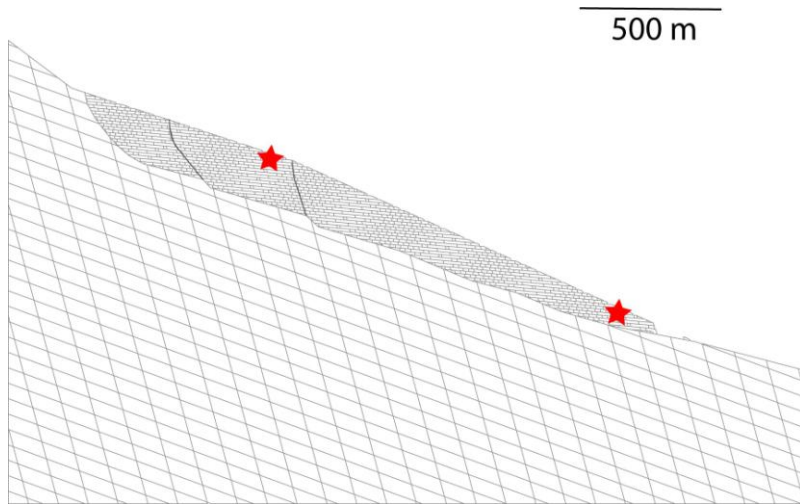


Figure 26: The red stars indicate the locations of the monitoring points used to create Figure 20. The upper star is that used for figures 20 b and d, while the lower star is that used for a and c

The periodic intermittent trend seen in these graphs correspond to one model year. The steep portion of each step corresponds to a period of increased precipitation and groundwater level, while the flattened portion represents the dry season and lowered groundwater table. The amount of displacement, seen mainly in the slip period, is on the order of 2-4 cm/year, similar to displacements recorded at Campo Vallemaggia (Eberhardt et al., 2007). It can be clearly seen that the displacements measured at the toe have a very regular pattern, while those in the upper part of the slide show more variation with each cycle. This is logical given that the toe is unconstrained and would be free to move in response to the changing effective stress conditions along the basal sliding surface. Downslope displacements in the upper part of the slope would also be promoted by the changing pore pressures, but would be constrained in part by the buttressing effect of the lower half of the slide. This can be clearly seen in Figure 24.

Figure 28 displays the horizontal velocities in the slide for the first 10 years. This shows a periodic pattern of acceleration and deceleration that corresponds to the wet and dry seasons. These velocities were found by dividing the 1000 cycles that represent the season up evenly into one half of a year, and then calculating velocity based upon the change in displacement for every 0.005 years. With the exception of the 1990 and 1994 peaks in the real data, it can be seen that the high value of approximately 0.2 mm/day present in the model is similar to the typically high values seen in all other years in Figure 29

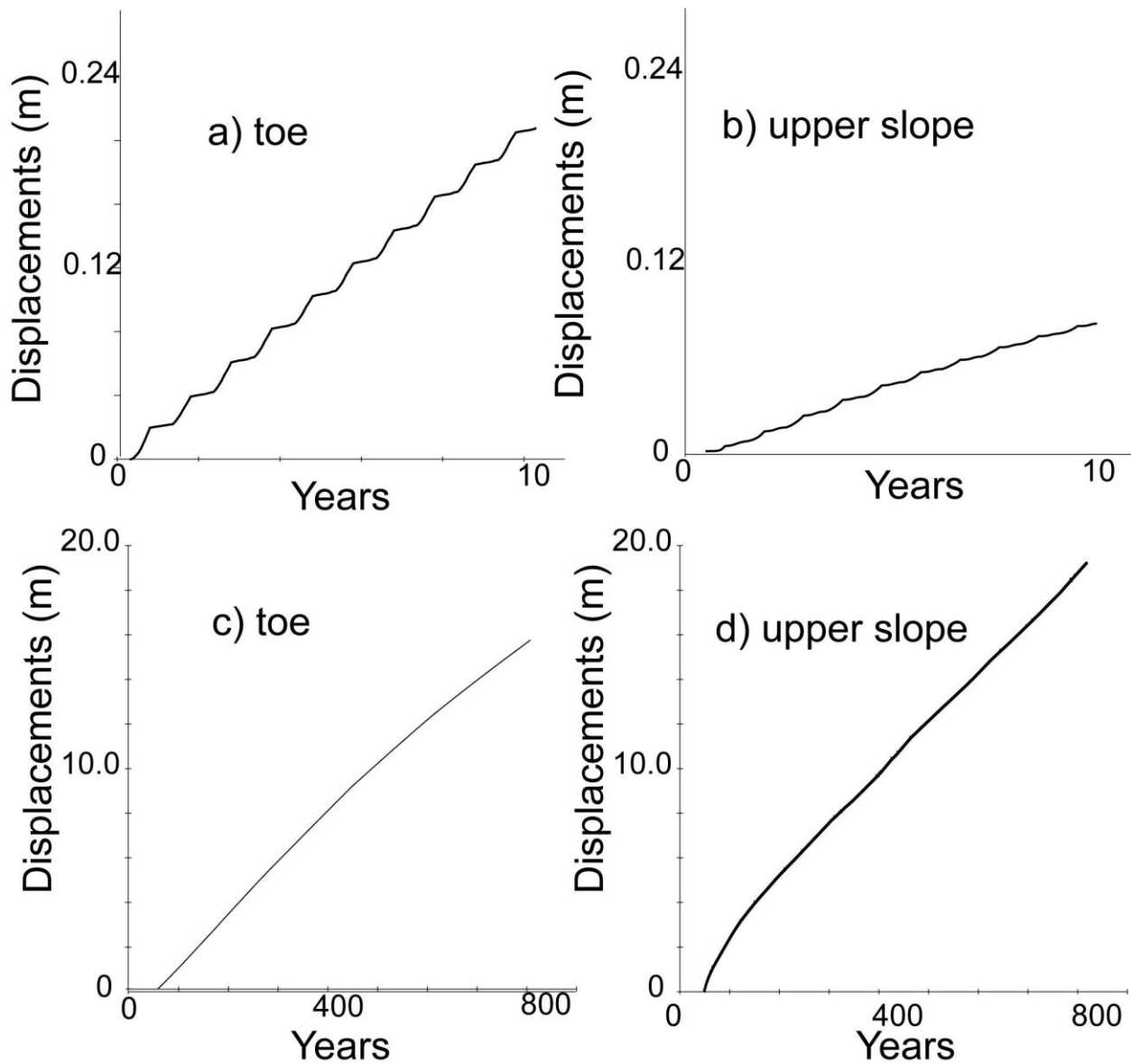


Figure 27: Displacement vs. modelled years: a) at the toe after 10 years; b) on surface behind the lower fault scarp after 10 years; c) at the toe after 800 years; and d) on surface behind the lower fault scarp 800 years at the surface.

These results may be compared to real monitoring data from the slide, as shown in Figure 29. Here it can be seen that the displacements (shown in blue) follow a similar intermittent, periodic trend to those seen in Figure 28 of the modelled data. The real data differs in that the wet and dry season are of different lengths, but the same general trend of intermittent movement behaviour is seen for each year. The other major difference is that in the real data, the peak velocities vary from year to year, while in the modelled data they don't. This is attributed to the fact that the water table was modelled with the same seasonal high and low values each dry and wet season, whereas in reality this varies from year to year introducing variation into the recorded data.

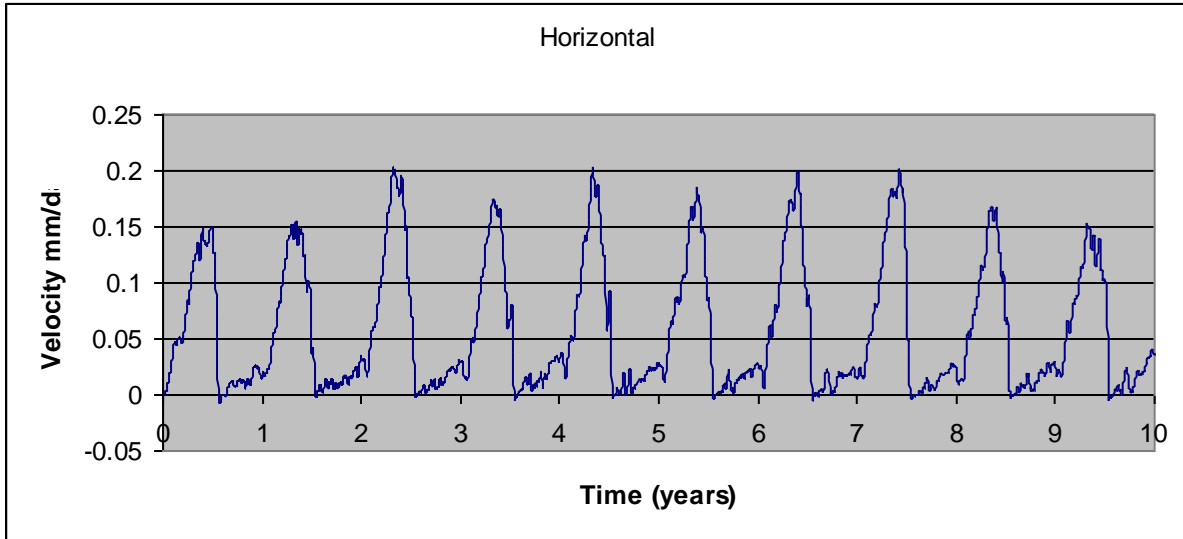


Figure 28: Horizontal velocities at the toe of the slope for the first 10 years.

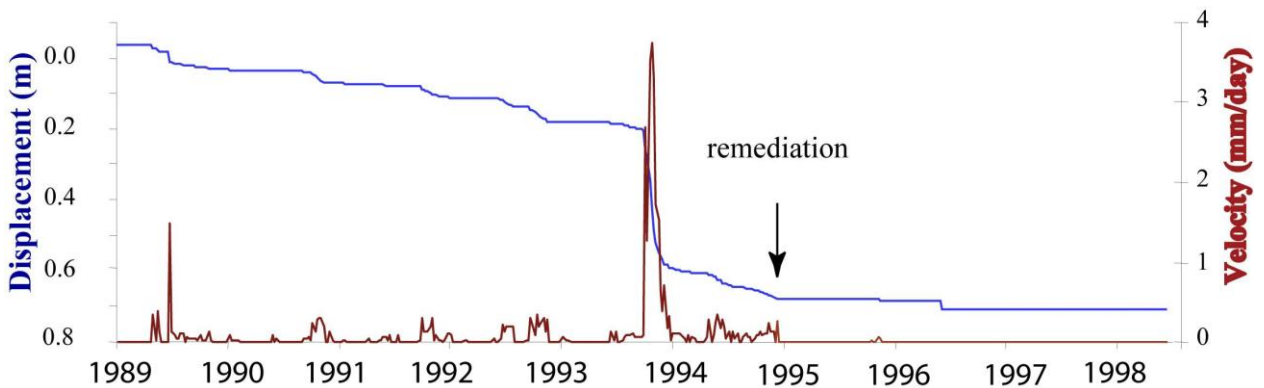


Figure 29: Displacement and velocity data from the Campo Vallemaggia landslide after Bonzanigo et al (2007)

It can be clearly seen that the displacements measured at the toe have a very regular pattern, while those in the upper part of the slide show more variation with each cycle. This is logical given that the toe is unconstrained and would be free to move in response to the changing effective stress conditions along the basal sliding surface. This difference illustrates why it is often difficult to interpret periodic accelerations in geodetic monitoring data. A perfectly placed measurement point may pick up the periodic stepped velocity pattern seen in the model results, and over time, the more generalized continuous behaviour (i.e. constant velocity) with repeated cycles. However, it is often the case that a measurement point depicts a more localized response of complex movements and is therefore not necessarily representative of the global landslide behaviour.

The presence of faults and internal shears may cause surface reflectors to not simply record the overall movement of the slide along the basal sliding surface, but to also record the internal deformations related to blocks shifting and rotating in place as well. Accordingly, the interpretation of geodetic

monitoring data and the development of an early warning alarm threshold should be based on several reflectors spatially distributed across the slope. An added value is that the presence of numerous reflectors also allows for the relative movements of the various blocks to be measured within the landslide as discussed by Bonzanigo et al. (2007).

Modelling results presented in this chapter have shown the development of fatigue effects in the Campo Vallemaggia slide, as well as continual intermittent movement. The development of fatigue was seen in the opening of the fault in the originally unfaulted version of the model. Changes can be seen in terms of opening of spaces between blocks, an increase and subsequent drop off in the number of yielded elements present in the model, and localization of high and low stresses behind the developing fault as it opens. This pattern of change is what would be expected for a fatigue based failure due to cyclic loading from a raised and lowered water table.

The overall slide does not have a similar fatigue effect, likely due to the relatively simple translational nature of the slide. Instead, a pattern of intermittent movement, dependent on the water table cycling, is seen to continue up to at least 3000 years. This movement consists of 2-3 cm of displacement during the wet season, and almost none during the dry.

5 The Little Chief Landslide

Building on the understanding gained through the conceptual modelling of fatigue effects for the Campo Vallemaggia landslide, further modelling was carried out for a more complex site: the Little Chief slide. Little Chief is a large slow moving rockslide being monitored by BC Hydro. Little Chief was considered to be a more complex case for a number of reasons: i) both the basal detachment and internal shear surfaces were not well understood, and ii) that a more complex toe shape is considered likely, making the question of toe release relevant to this slide. The modelling carried out for Little Chief involved three different sets of models. The first focussed on trying to model the initiation, localization and progressive development of the basal sliding surface. The second repeated the fatigue modelling applied to Campo Vallemaggia based on the basal slide surface inferred from borehole drilling. The third focussed on fatigue and reorganization of the internal rockmass using a combination of the previous two approaches.

5.1 Geology

The Little Chief Landslide is located in the Interior of British Columbia on the Columbia River upstream of Mica Dam. Its toe is submerged in the Mica Dam reservoir. This is a mountainous region characterized by metamorphic rocks, primarily gneisses and schists. As the name implies, the rock in the surrounding areas of Mica Dam, are quite rich in mica content.

Like the Campo Vallemaggia slide described in Chapter 4 (see Figure 8), the Little Chief Slide appears to be made up of two neighbouring bodies extending side-by-side from the top to bottom of the slope. Cross-sections have been drawn along two lines of drill holes, parallel to the general direction of movement, as well as one along the toe. From these it has not proved possible to project a sliding surface that is laterally consistent across the moving body. Instead, two different 2-D profiles can be generated for the northern and southern sets of exploratory boreholes, see Figure 30. The northern half of the slide has been chosen for the analysis in this thesis, as there was insufficient data to make an interpretation of the southern half.

5.2 Engineering Geology and Slide Features

The geology of the Little Chief Slide consists mainly of mica schist and mica gneiss interbedded irregularly to form one composite unit. The gneiss is comprised of quartz, feldspar and minor biotite while the schist contains significantly more mica in coarse muscovite selvages. Other variations in rock type including a hornblende gneiss and biotite schist are also found within the slide (Watson, 2006a). The slide exhibits an extensive headscarp and numerous linear troughs in the area above the scarp (Figures 30, 31), which are indicative of a significant amount of extension in this region. The side scarps are also prominent and clearly exposed, with the north side scarp running sub-parallel to the regional foliation. The surface of the slide is significantly depressed compared to the ridges on either side, and no clear stratigraphy can be seen in the rock layers. A large toe bulge is made obvious by the shape of the reservoir bank (Figure 32). All of these serve as indicators that the slope has experienced a long history of sliding and is likely to have a well defined detachment surface.

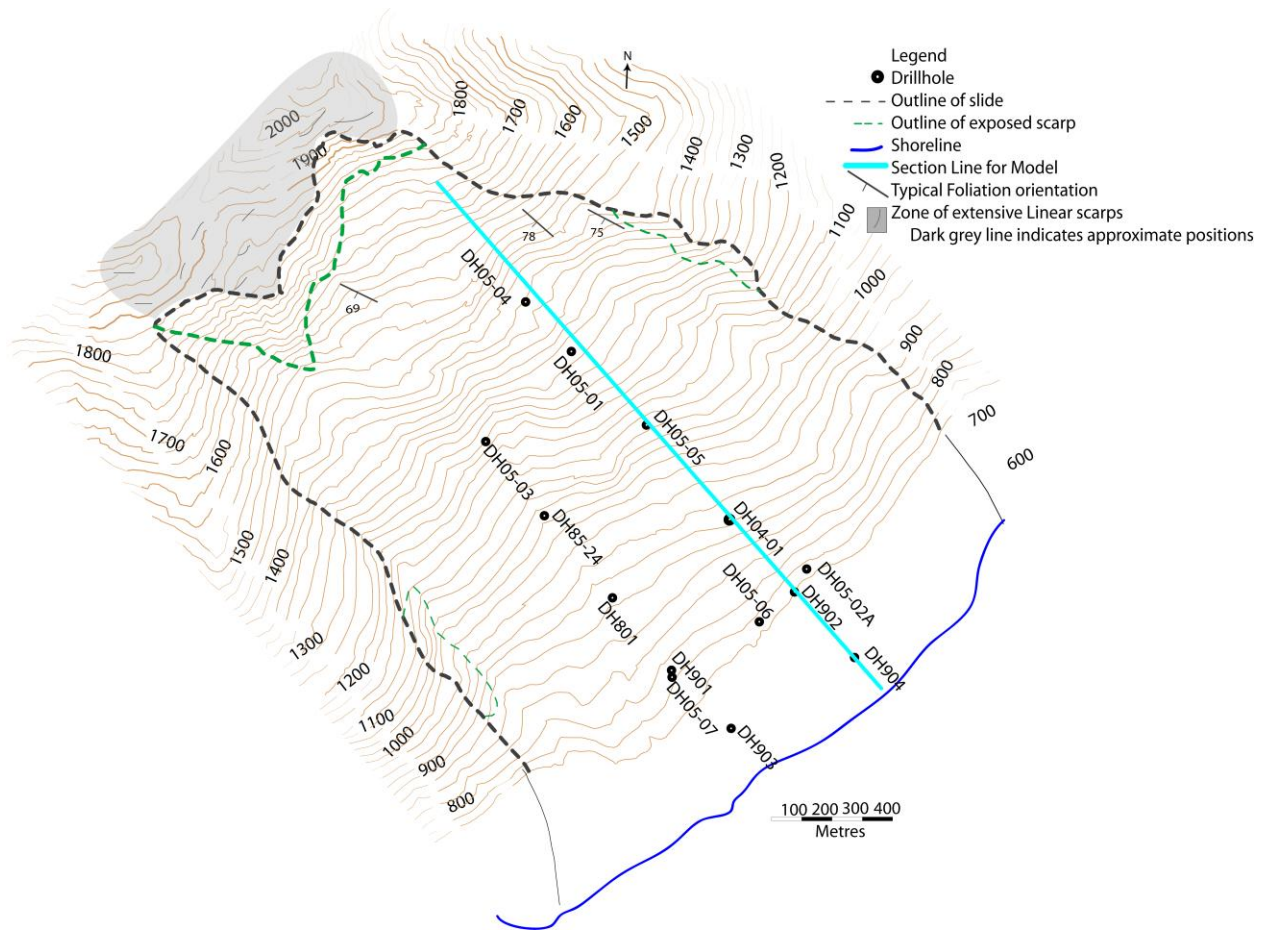


Figure 30: Plan view map of the Little Chief Slide showing slide boundaries and borehole locations, and areas of linear extension, as well as areas experiencing greater degrees of movement. (after Watson, 2006b)

A consistent foliation across the slide and surrounding rock is steeply dipping to the south east as observed at surface (Figure 304). Boreholes have shown this to be highly variable within the body of the Little Chief Slide however, especially at depths near and below the basal detachment (Watson, 2006a). As well, air photos of the area show the potential for some extensional features behind the scarp of the slide, as shown on Figure 33.

5.2.1 Basal Detachment

Extensive borehole drilling has been used to identify and delineate the basal detachment, i.e. sliding surface, below the mass of the Little Chief Slide. These show it to be reasonably well defined in the northern half of the slide based on inclinometer readings and abrupt changes in rock mass properties found in core material. The detachment is less defined in the southern portion of the slide. The material in the detachment zone has a high clay mineral content, is soft and gouge like, and typically includes many rock fragments (Watson, 2006a). Testing has been done on the gouge material from the detachment zone and a range of friction angles between 19 and 26 degrees was found, with samples from one borehole giving a value as low as 10 degrees (Watson, 2006c).



Figure 31: Disturbed rock near the top of the headscarp of the Little Chief Slide.



Figure 32: Toe bulge at base of the Little Chief Slide.

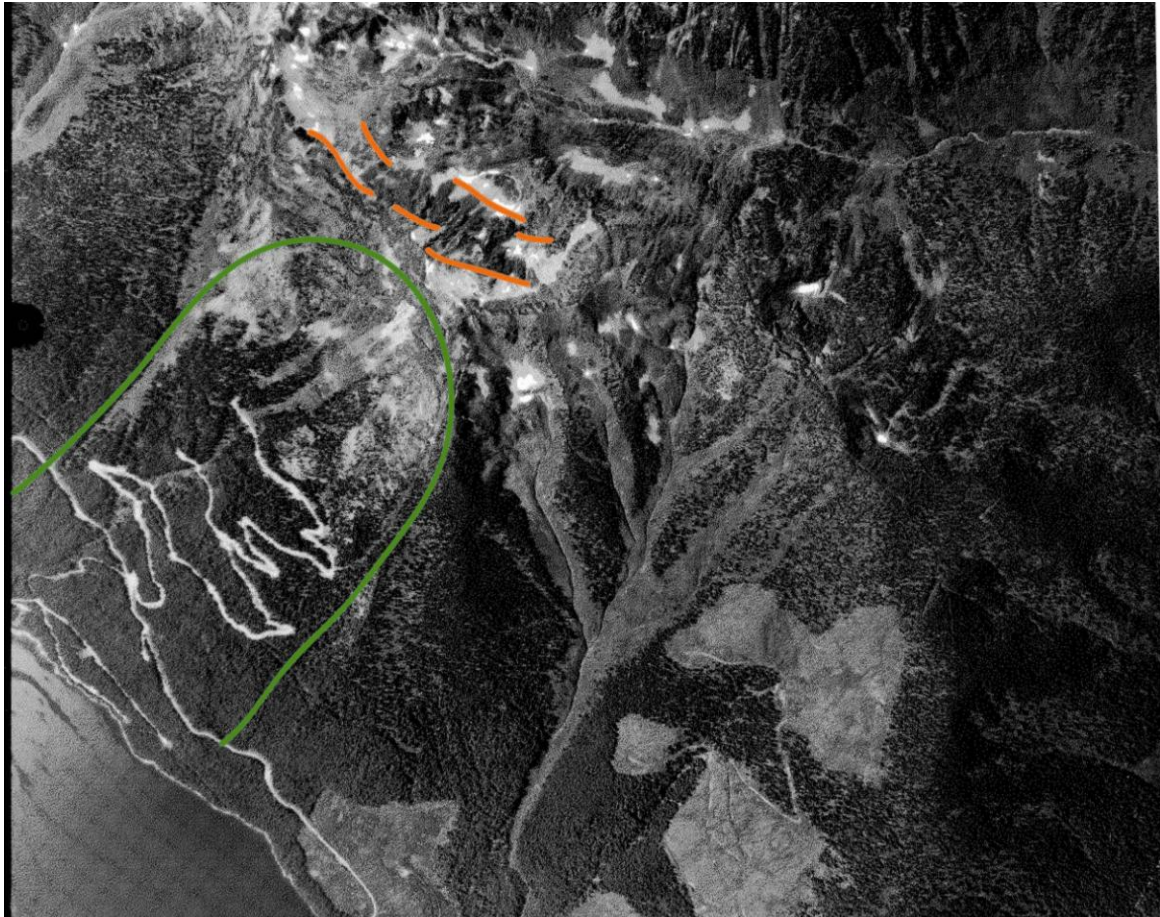


Figure 33: Air photo of the Little Chief Slide. The approximate slide boundaries are shown in green. The road up the slide is the distinct white feature present, and potential extensional features behind the slide are identified in orange.

Layers of till have been found in boreholes near the toe of the slide (Watson, 2006a). These are another indicator of extensive prehistoric sliding at the site as they suggest that in the past the slide mass has overridden surficial valley fill deposits on at least two occasions. An interpretation of the location of the sliding surfaces within the landslide is shown in Figure 34.

5.2.2 Rockmass Properties

The rockmass is broken and highly variable. The gneiss is generally blocky, whereas the schists tend to be more fragmented and disturbed. The jointing is quite planar, but the surfaces seen within the Dutchman's Ridge drainage adit nearby to the Little Chief Slide do not appear to be polished or altered significantly. This is consistent with outcrop observations of relatively fresh surfaces seen at ground surface. Figures 35 and 36 are photographs of surface outcrop of the rockmass, showing its blocky, broken nature and variable block size.

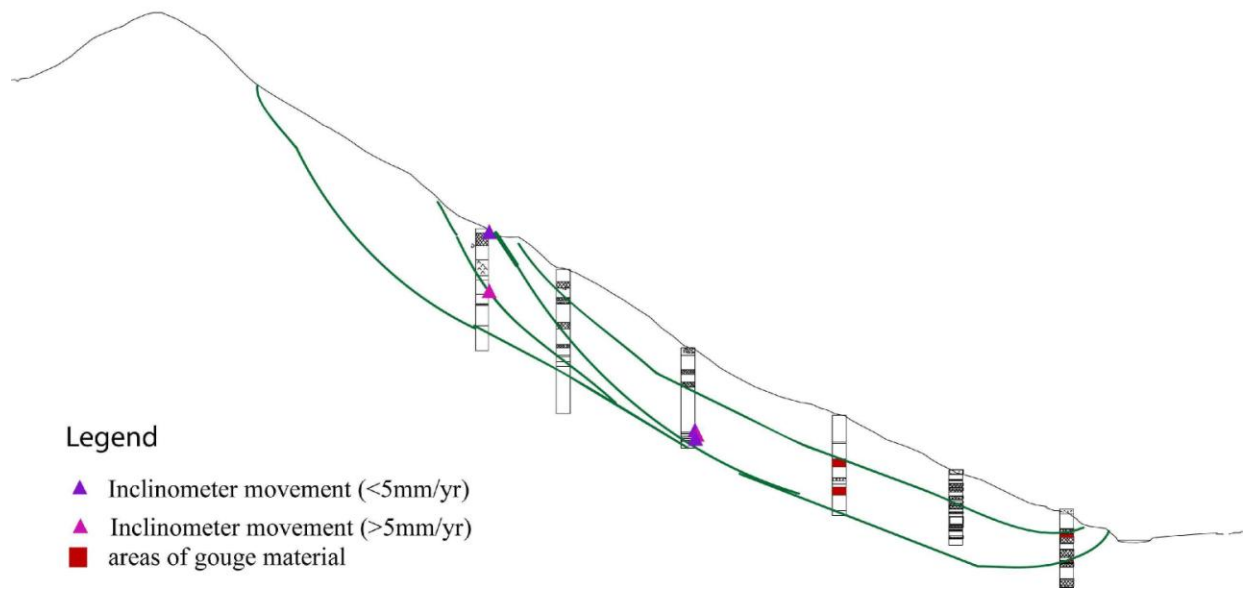


Figure 34: Sketch showing interpretation of internal sliding surfaces relative to the basal detachment and ground surface. Borehole profiles showing gouge zones and areas of movement detected by inclinometers are included.



Figure 35: Blocky rockmass outcrop near the top of the Little Chief Slide



Figure 36: Rockmass outcrop near the bottom of the Little Chief Slide

The Geological Strength Index (GSI; Marinos et al., 2005) of the rock was estimated separately for the schist and the gneiss. The schist has a very-blocky to slightly seamy structure and good to fair joint surface conditions giving a range of GSI values from approximately 40 to 55. The gneiss has a blocky to very blocky structure and generally good joint conditions for which a GSI range of 50 to 65 was selected. Because the interbedding of the schist and gneiss are irregular and difficult to represent as individual units in the numerical models developed, a GSI range of 50 to 55 was assumed for the slide body (Figure 37) as a homogeneous rock mass.

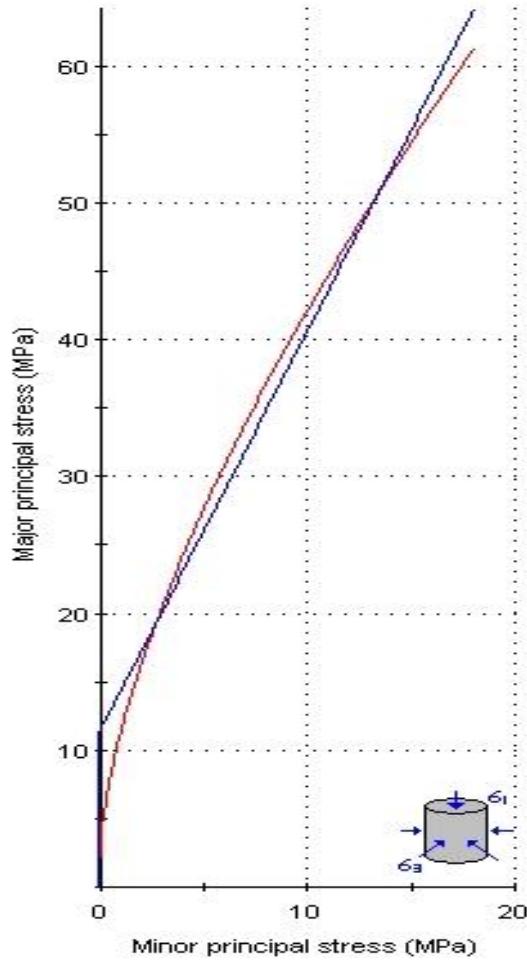


Figure 38: Comparison between non-linear Hoek-Brown failure envelope for the Little Chief mica schist (in red), and linear Mohr Coloumb envelope fit (in blue) through the stress range of interest.

Table 4 lists the different rockmass properties determined using the RocScience program RocLab (RocScience, 2007), as follows. A representative range of 100-250 MPa was chosen for the Uniaxial Compressive Strength (UCS) of the gneiss, and 50-100 MPa for the schist (RocScience, 2007). Similarly, an m_i value of 28 was assumed for the gneiss and 10 for the schist, based on those recommended in look-up tables in the RocLab software. From these, together with the estimated values for the GSI, the non-linear Hoek-Brown rock mass shear strength parameters were calculated within RocLab. Equivalent Mohr-Coulomb rock mass shear strength parameters were also estimated using RocLab by fitting the linear Mohr-Coulomb envelope along the non-linear Hoek-Brown envelope across the stress range of interest based on the minor principal stress, σ_3 . This relationship is demonstrated in Figure 38. This was calculated using the software assuming a 1000 m high slope.

Table 4: Summary of rockmass properties calculated broken down by individual rock units and combined homogeneous slide mass.

		Gneiss	Schist	Equivalent Homogeneous
Input:	GSI	50-65	40-55	50-55
	UCS (MPa)	100-250	50-100	100-120
	m_i	28	10	17
	Unit Weight, δ (MN/m ³)	0.027	0.027	0.027
Output	m_b	4.6-8.1	1.2-2.0	2.85-3.4
	s	0.0039-0.0205	0.0013-0.0067	0.0039-0.0067
(rock mass):	a	0.502-0.506	0.504-0.511	0.504-0.506
	c_{rm} (MPa)	5.7-10	2.6-4.3	4.9—5.7
	ϕ_{rm} (°)	41-52	25-34	37-40

It should be noted that because the conversion of Hoek-Brown to Mohr-Coulomb shear strength parameters is stress dependent, further adjustments of the Mohr-Coulomb rock mass properties were required. Initial values of rockmass cohesion were quite high and generated little yielding or movement when used in the UDEC models of Little Chief. As this does not agree with observations and instrumentation recordings from the site (Watson, 2006a; Watson, 2006c) the rock mass cohesion was lowered until a more appropriate behaviour was modelled.

5.2.3 Fracture Network and Discontinuity Properties

The fracture frequency on average in the rockmass is highly variable, ranging from the softer schistose rock where the foliation fractures occur every few cm or less, to the more blocky gneiss where blocks up to 0.5 m or larger are seen. An average spacing on the order of 10-30 cm was adopted here as being representative of the slide mass as a whole. A joint friction angle of 30 degrees and joint cohesion of zero was assessed for those fractures explicitly represented in the numerical models, based on the appearance of relatively fresh joint surfaces observed in the Dutchman's Ridge drainage adit.

5.2.4 Water Table

The level of the wet and dry season water tables were interpreted from piezometric data obtained from boreholes in the slope. The groundwater within the slope is complicated, with perched water tables and variable levels. This was simplified to two water tables, one for the wet season and one for the dry season, by taking the head in each borehole and connecting them. Any high pressure confined aquifers are thus treated as though the water table is at the level of the pressure head. Artesian pressures were not recorded for any holes along this profile. Figure 39 shows these water tables and the boreholes they were interpreted from. This was a conservative assumption as in some areas of the slope there are dry sections below perched water tables which have been modelled as wet. This simplification was necessary due to restrictions in groundwater modelling within UDEC.

Water Tables

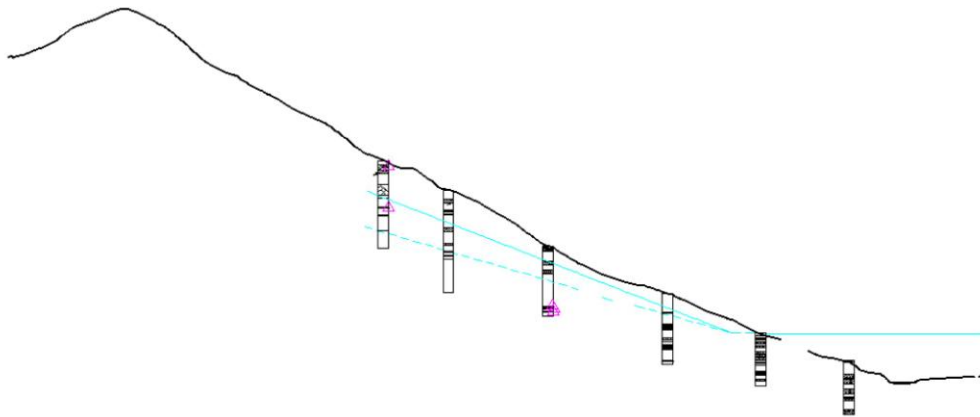


Figure 39: Water tables (shown in light blue) with the borehole profiles from which it was interpreted.

5.2.5 Assumptions and Implications

The following assumptions are those that were necessary in order to develop a computationally efficient model of the Little Chief Slide. Most relate to limitations in the modelling software and inherent uncertainties as to the state of the rockmass below the ground surface.

1. A representative set of equivalent rock mass properties was applied to the entire slide body as opposed to differentiating between the gneiss and schist units. A set of stronger rock mass properties was applied to the stable rock below the slide body in models where the slide surface was explicitly included. This rock was also treated as an elastic material to reduce calculation times. Using representative properties simplified the results and may not have given the full complexity desired. However, there was concern that the arbitrary placement of a distinction between poor and fair rock could influence where localization of yielding and movement occurred. This issue did not exist for the poor to good rock transition as movements were already mostly localized along the sliding surface when explicitly included in the model. It should be noted that by treating the rock mass outside of the slide boundaries as an elastic material, the models were unable to develop tensile and/or plastic shearing features such as the linear features seen above the headscarp at the site.
2. A detachment friction angle was chosen within the tested range (19-26 degrees) based on the ability to keep the slope in a sub-stable state under the assumed lower bound water table and in a moving state under the upper bound water table. The use of a single uniform friction angle for the entire basal slide surface is likely unrealistic, but it was assumed here for simplification purposes.
3. It was impossible to develop a practical model with jointing anywhere close to the actual spacing of that seen in the rock mass. Instead, an initial joint spacing on the order of 25m was used. Smaller spacings were also tested to determine whether any important kinematic effects would develop due to changes in the joint spacing. The rock mass between the modelled joints was

treated as an equivalent continuum rock mass with Mohr-Coulomb shear strength parameters as previously discussed. In this sense, the discontinuities present (1:1 scale) were accounted for in terms of their effect on the rock mass strength. Thus a balance was sought between representing the in-situ joint spacing and its effect on both the kinematic behaviour and strength of the rock mass, and achieving reasonable model run times. It is necessary to note that the results obtained are dependent on the density and locations of these joints; if they are shifted slightly, the localization and displacement pattern that develops could vary. Running multiple models using more than one potential fracture network allowed this uncertainty to be reduced.

5.3 Modelling of Initiation and Progressive Development of Failure Surface

In order to better understand the initiation and progressive development of the basal and internal shear surfaces, and their spatial characteristics (particularly that at the toe of the slope), modelling was carried out using a geometry without the projected slide surface (Figure 40).

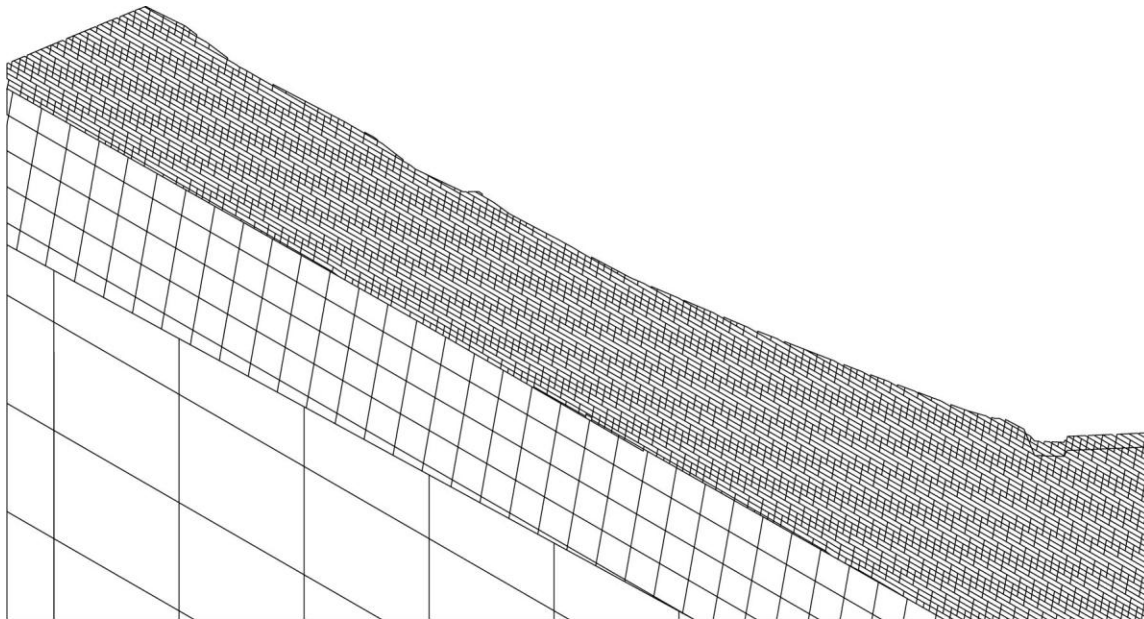


Figure 40: The starting model for the Little Chief Slide when no pre-existing surface is being used. This version is with the presence of valley fill.

5.3.1 Model Set-Up

5.3.1.1 Fracture Network

There are three distinct joint sets in addition to the persistent regional foliation present in the Little Chief Slide mass (Moore and Watson, 2007; Watson, 2006a). Two of these run approximately parallel to the plane of the section used for modelling, which coincides with the alignment of the drill holes. Therefore the 2-D section along the slide profile contains only the foliation joints and a set of cross-joints; the other two sets of cross joints serve as lateral release joints for the blocks.

The set of cross joints present in the modelled section were mapped and described in the site investigation reports as dipping steeply upslope. A repeating joint dipping at 80 degrees into the slope was used to represent this. The regional foliation dips steeply south-east at surface; however there is evidence that it shallows significantly with depth and likely contributed to the formation of the sliding

surface (Watson, 2006c). Therefore a persistent joint set dipping at 30 degrees, approximately parallel to the basal detachment was used to represent this joint set. These were spaced every 15 m and were continued well below the depth of the sliding surface. The full persistence of these foliation joints was implemented after numerous models failed to produce any significant movement. A close up of the joint network pattern is shown in Figure 41. The vertical joints were represented using an overlapping brick-like pattern generated by using two joint sets each with a 45 m spacing.

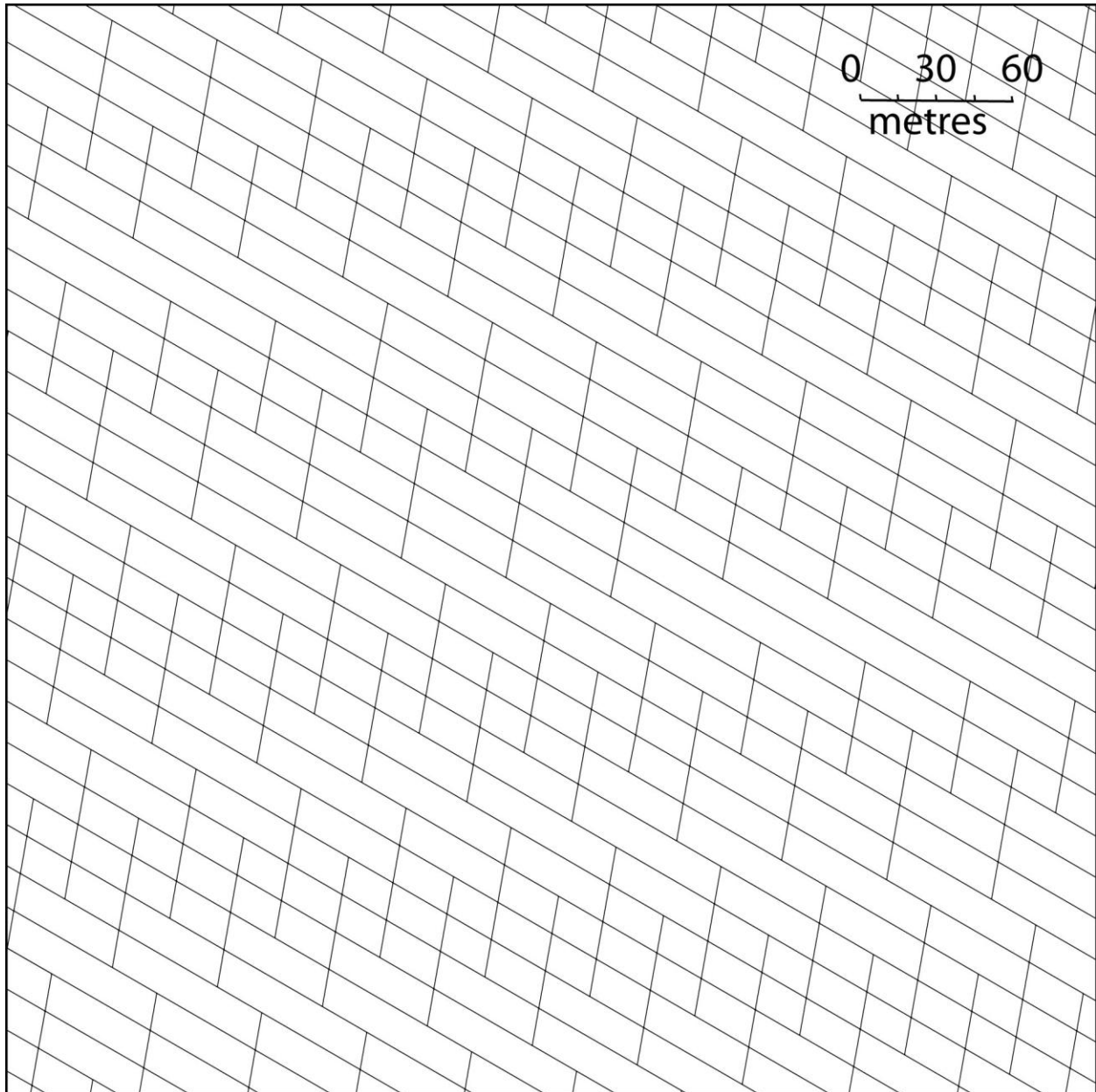


Figure 41: Joint pattern used in models generating sliding surface.

5.3.1.2 Water Table

Two varying water tables were used in this series of models to represent the dry and wet seasons. These are shown in Figure 42 in red and orange, and are based on measurements from the piezometers

and boreholes at the site. Although they do not perfectly represent the complex groundwater situation present at this location, which is dominated by compartmentalized fracture flow, they are believed to give a reasonable representation of the pore pressure at most locations. The site does exhibit a few perched water tables, which were not included, but simplified so that the top of the water table sits at the top of these perched tables. This is considered a conservative assumption when it comes to applying any results from this to the site, as this assumption will tend to somewhat raise pore pressures at a few locations.

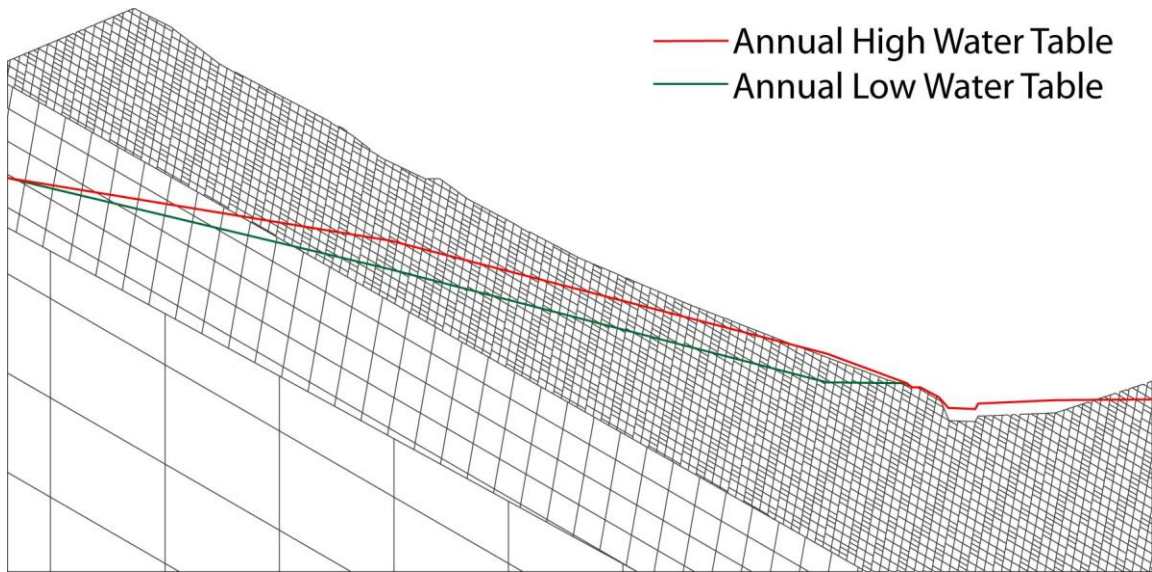


Figure 42: Model setup showing the different water tables used in the fatigue cycling of the Little Chief slide. Shown for the version of the model with no valley fill

5.3.2 Initial Results

Models were first solved assuming a standard Mohr-Coulomb elasto-plastic constitutive model. However, no meaningful results were obtained. An image of a typical Mohr-Coulomb model result is shown in Figure 43. No localization of failure along the sliding surface is seen in this model, indicating that under elasto-perfectly plastic like yield conditions, the model does not simulate the formation of the slide detachment surface. There is a large concentration of yielded elements in the upper corner of the model, but this may be a boundary effect. There is also some failure localization around the toe, but spreading along the surface in the opposite direction from that of the slide body. This may be related to surface instability at the valley bottom.

After the attempts at using the Mohr-Coulomb elasto-plastic constitutive model yielded unsatisfactory results, a strain softening model was applied. This constitutive model incorporates strain weakening of the material based on plastic strain thresholds set by the user. This weakening encourages the localization of failed zones. The residual values used for the strain softening models were determined as described in chapter 3. Both a gradual strain softening model, with the strength decreasing in multiple stages, and a more abrupt strain softening model with only one stage of weakening were used (the latter simulating a more brittle response). As very little difference was seen in the early results, the abrupt model was chosen for continued modelling. Figure 44 shows the pattern of strength decrease with strain

for both the cohesive and frictional strength within the blocks. Tensile strength was varied as a function of the cohesive strength.

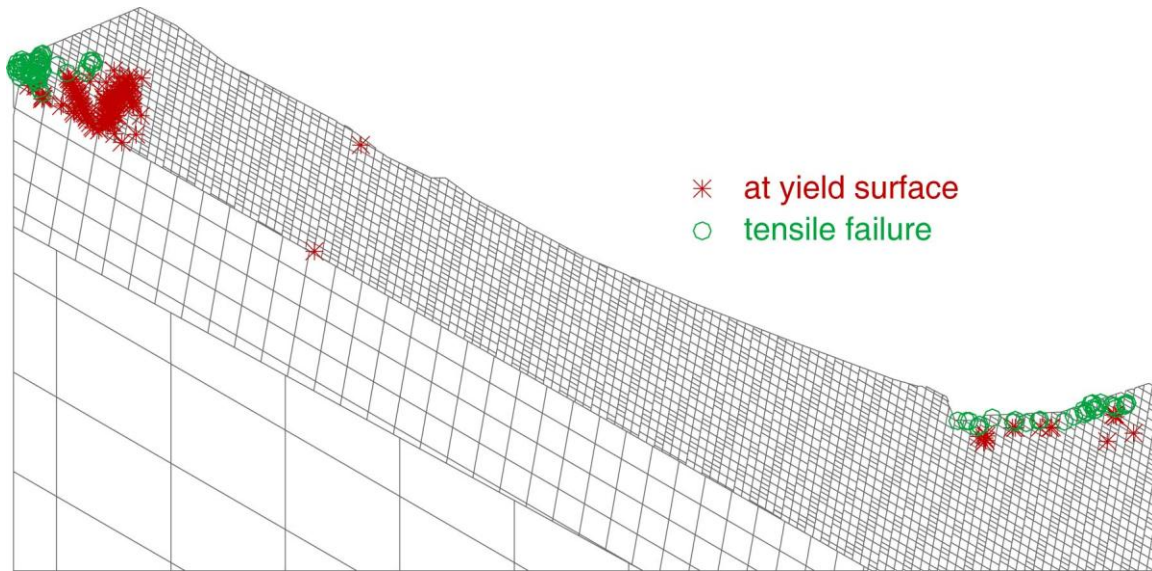


Figure 43: The Mohr-Coulomb model having been allowed to come to equilibrium with the low water table and then cycled for 30 years. This is just one typical example of Mohr Coulomb results that fail to show landslide initiation.

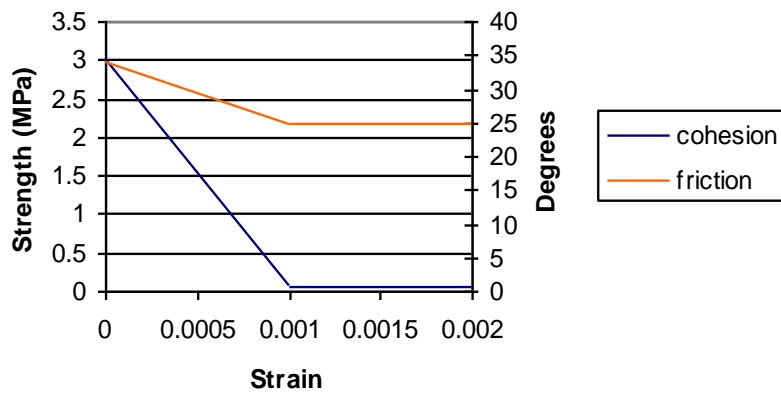


Figure 44: Chart showing strain softening rate for the abrupt strain softening.

Figure 45 shows the yield indicators of the strain softening model after initialization of the in-situ stress conditions and initial equilibrium and then cycled for 70 years of alternating between the low and high water tables. There is little change noted when cycled for longer than this, just rearrangement of yield in the same general areas. These models all show the formation of a surface closer to the top of the slope, which does not correlate with the upper limits mapped in the field. The absence of a key geological feature near the mapped scarp and/or assumption of homogeneous rock mass strength and joint spacing may be possible explanations for this discrepancy, as well as the simplified representation of the 3-D slide body into 2-D. For these models the valley fill, which is approximately 45 m deep (Moore and Watson, 2007), is not included in the model. This is because these models attempt to simulate the

creation of the basal sliding surface, which likely occurred when the valley was deeper (i.e. before glacial sediments were deposited).

Figure 46 shows the toe with and without valley fill, showing the change in localization seen for the same rock mass and joint properties. The version with fill shows a nice progression of failure into the toe, however this failure is much shallower than any expected to be present. Instead this surface matches nicely the internal surface thought to be present near the toe, potentially indicating that the formation of that sliding surface was influenced by partial infilling of the valley (either with pre-glacial fluvial sediments or perhaps receding glacial ice). The valley fill in these models was modelled as a compliant elastic material as yielding of the fill was not of interest. It was given a density of 1.9 g/cm^3 . Figure 46b without the fill shows less yielding than seen in the version with fill. However the yielding is somewhat deeper. This is logical as the surface topography is deeper in this model. This deeper yielding would be necessary in order for the steep toe release, as interpreted, to initiate and develop.

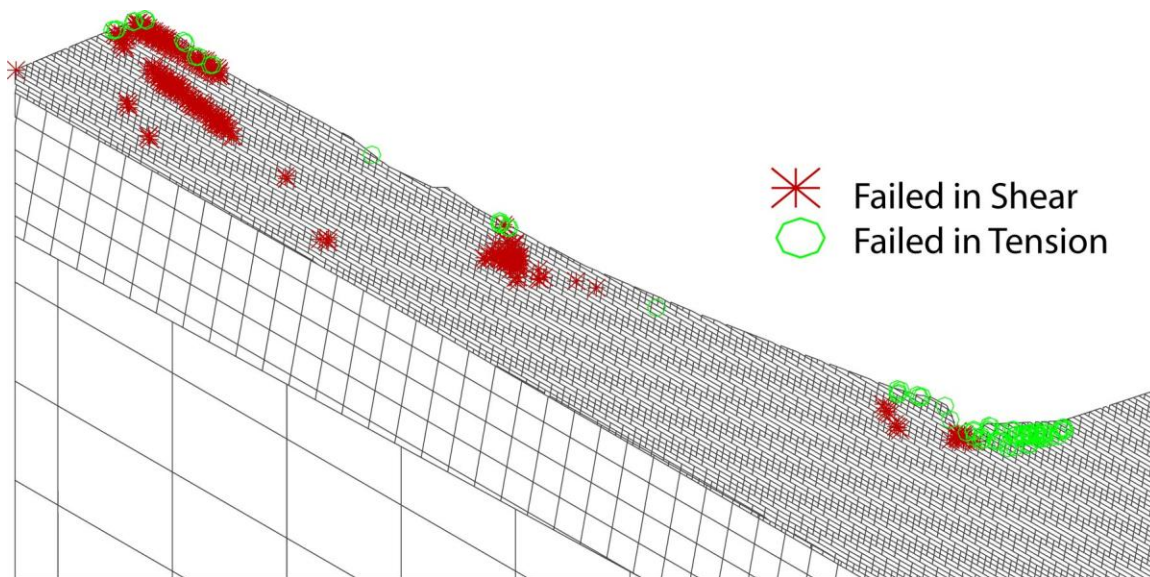


Figure 45: Development of toe, and upper part of slide in strain softening model, 70 year simulation

The results found in this first set of models performed for Little Chief, while they do not match what is predicted based on borehole drillings, do give a reasonable approximation of where initiation and localization of the basal slide surface might start, and certainly do not contradict anything interpreted from the site investigation data. Localization occurs at the landslide toe in the general area in which it is expected. There is also a localization of yield farther up the landslide at a location coinciding with a potential internal shear surface.

The inability to fully model the progressive development of the full length of the slide surface may be attributed to a number of factors as previously noted. Of these, the simplification of the 3-D structural geology into a 2-D representation is significant. It is likely that factors in the third dimension have contributed to the formation of the slide surface. As well, the landslide is a heterogeneous mass. There are possibly structures and weak areas within the rockmass that helped guide the formation of the sliding surface, which have not been included in the model.

In many of the model results obtained, a detachment occurs on the back side of the crest, as seen in Figure 45. While this has not been recorded in the site investigation reports, there is no indication that any detailed mapping has been carried out behind the crest. Therefore it is possible that there may be some extensional features present there. An examination of air photos covering this area shows the potential for these features to exist (see Figure 33).

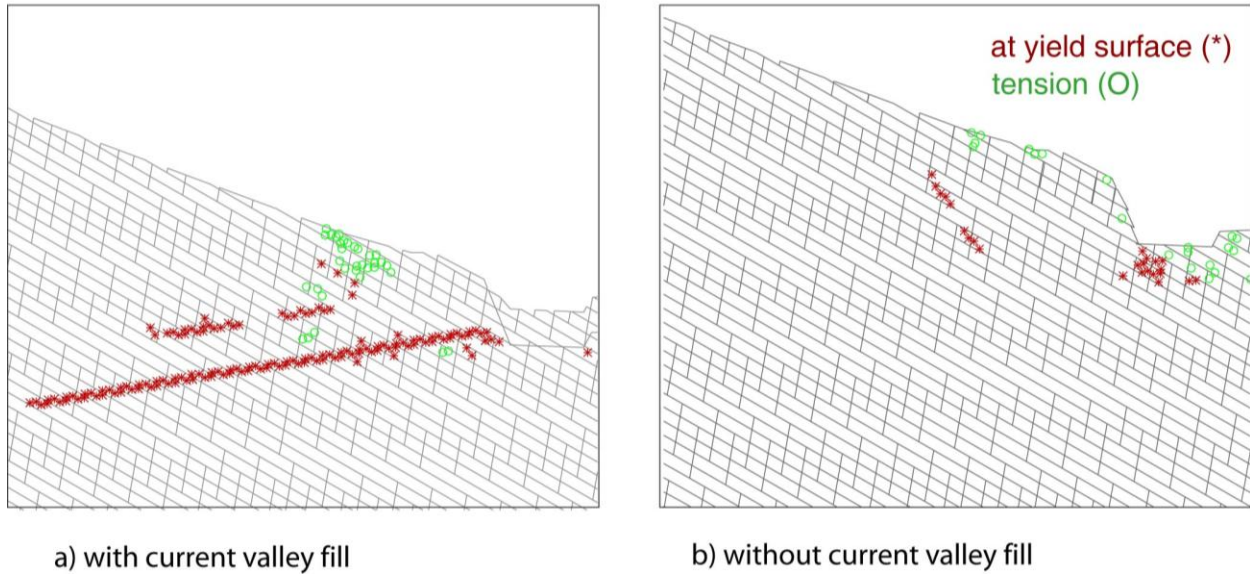


Figure 46: Comparison of landslide toe in strain-softening models with and without fill in the valley.

5.3.2.1 Lower Bound Properties

Given that the previous set of models based on the average estimated rock mass properties did not produce clear results showing the initiation, localization and formation of the Little Chief sliding surface, further modelling was carried out using lower bound properties. These properties are provided in Figure 47. As before, tension is one tenth of cohesion. No other properties were changed. The purpose of this assessment was to see whether there were conditions which could produce the surface seen, and to look at what might happen in a much weaker rock mass.

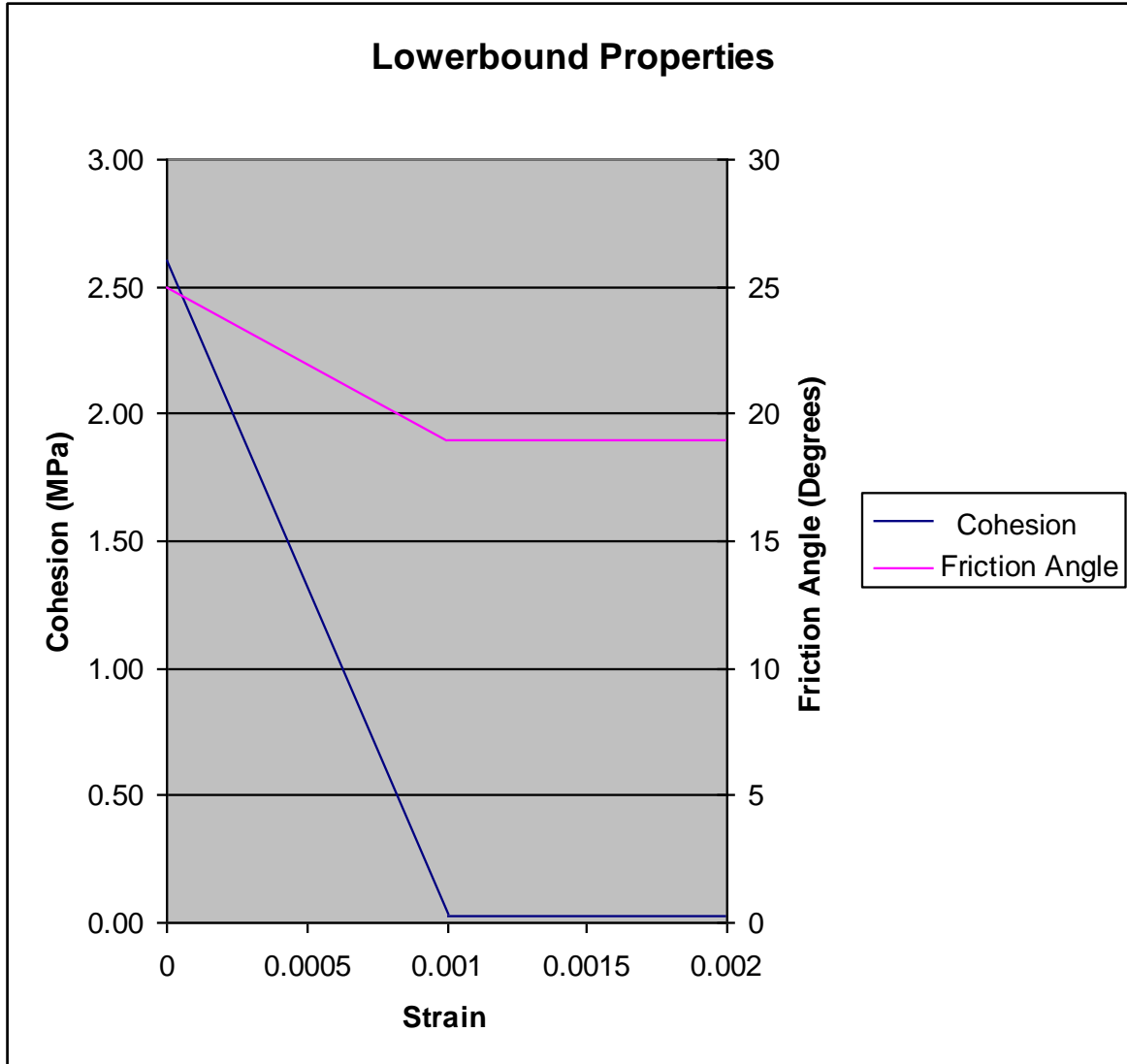


Figure 47: Chart showing the strain softening rate for the lower bound properties.

These results produced a more defined sliding surface. However, this is not taken to mean that the lower bound properties are representative of those at the site. More likely, some other limitation, or heterogeneity in the rock mass that is not considered in the model contributed to the formation of the sliding surface. For modelling purposes these lower values were required when using a rock mass with homogeneous properties (other than the valley fill) to get the same result.

The use of these lower bound properties for the rock mass was successful in producing a sliding surface which bears similarities to that seen at the slide. Figure 48 shows the yield patterns in the model without (a) and with (b) fill in the valley. The interpreted landslide surface is superimposed on these images for comparison. It can be seen that the presence of valley fill leads to a landslide much more similar to that interpreted than without fill. The slide surface that develops without valley fill matches nicely the expected location and formation of the toe release, although a bit deeper. However the upper part of the slide surface is completely different, in particular it is much deeper and appears to be a

separate circular failure, rather than a translational failure connected to the toe. This circular failure is constrained in its depth by the transition of the material to a coarsely jointed elastic material. As this transition location was placed significantly deeper than any recorded indication of movement or sliding, it was felt that this represented a problem in modelling accurately the surface, not in the depth of this transition. No through going failure surface occurs in this model. Sections 5.3.2.2 and 5.3.2.3 address this issue, as well as the question of why the upper slide surface develops up to the mountain peak.

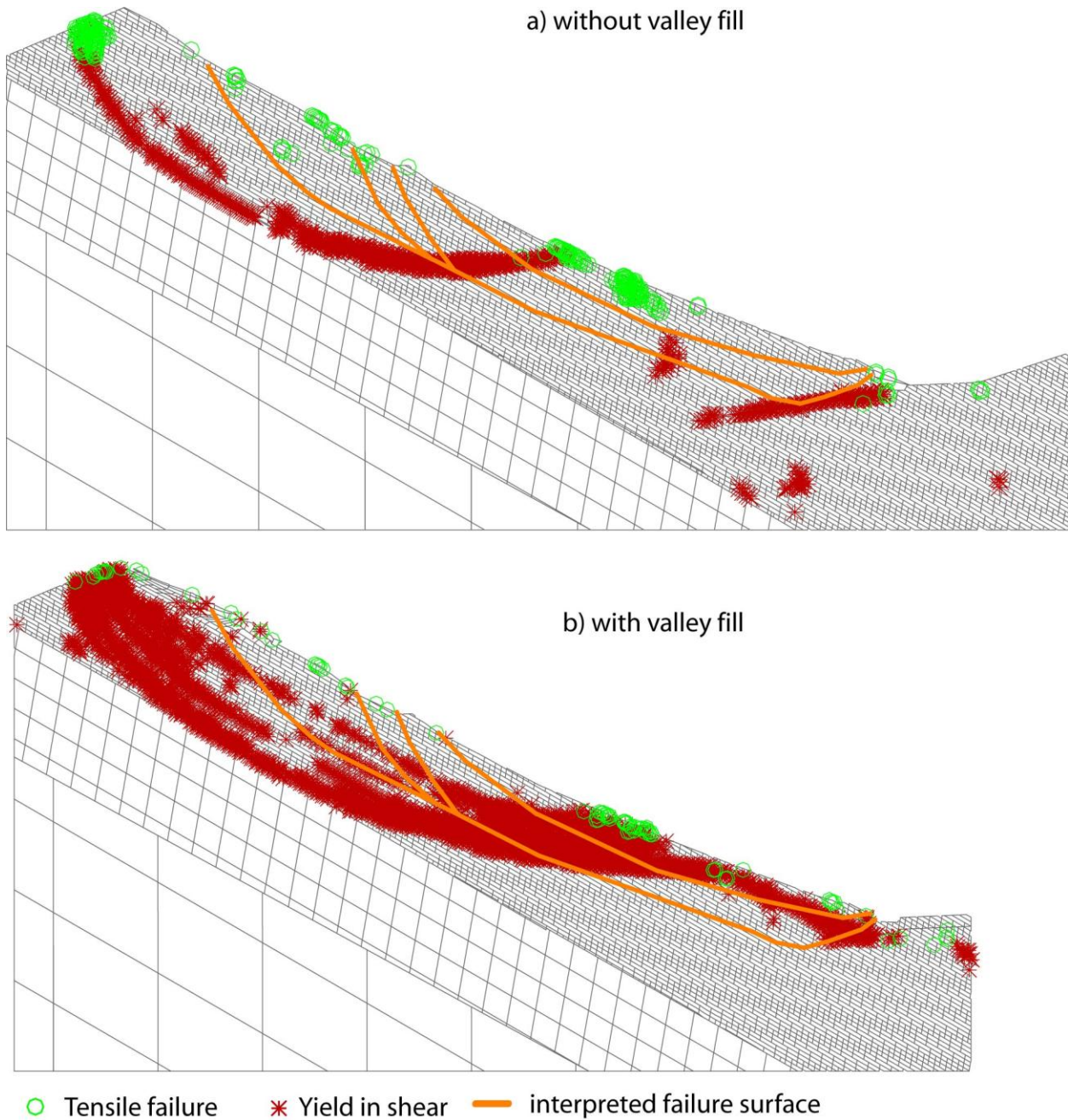
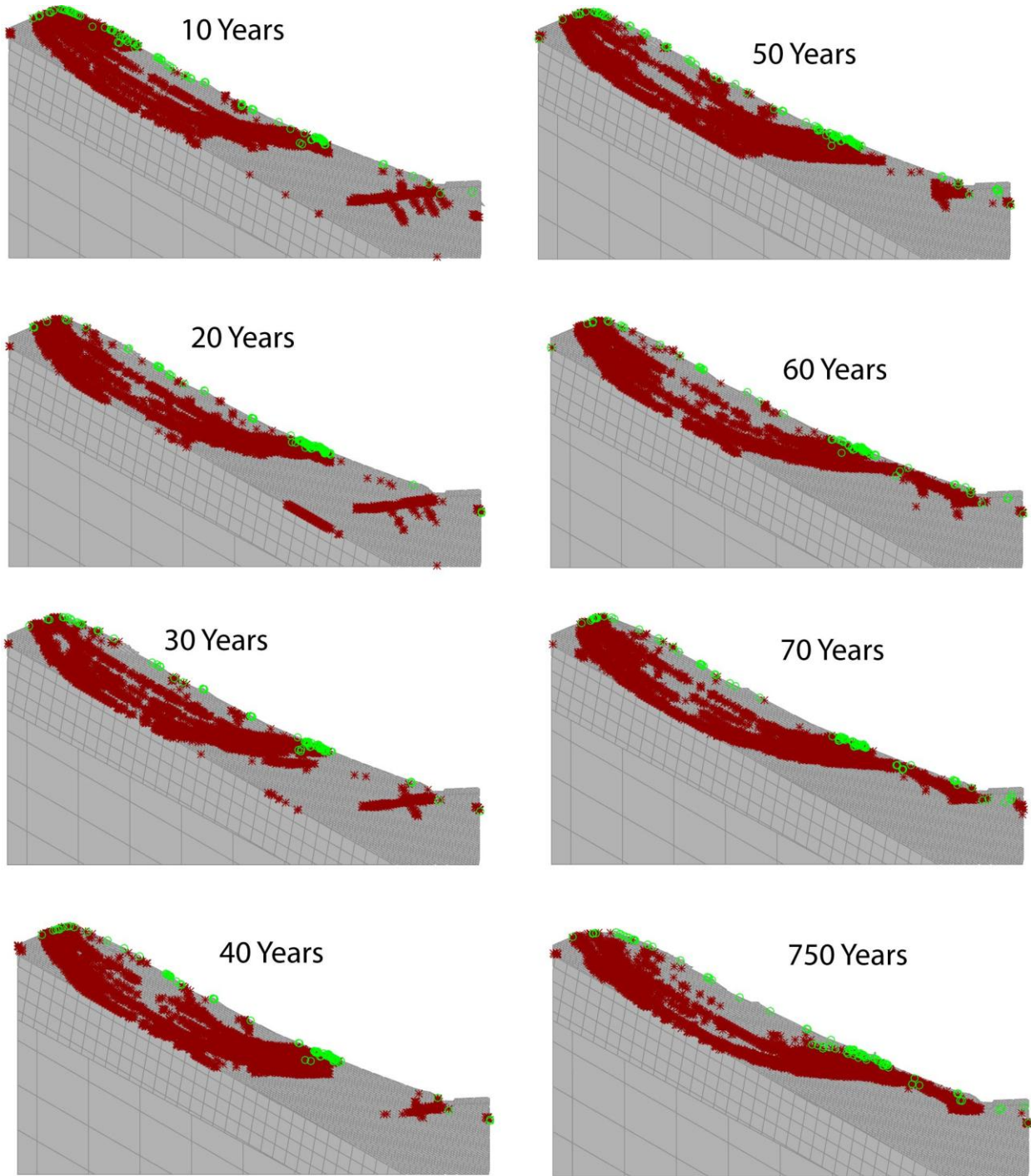


Figure 48: Strain softening models showing the development of a sliding surface in models with and without valley fill. In both cases this is compared to the sliding surfaces interpreted based on site investigation and monitoring data.



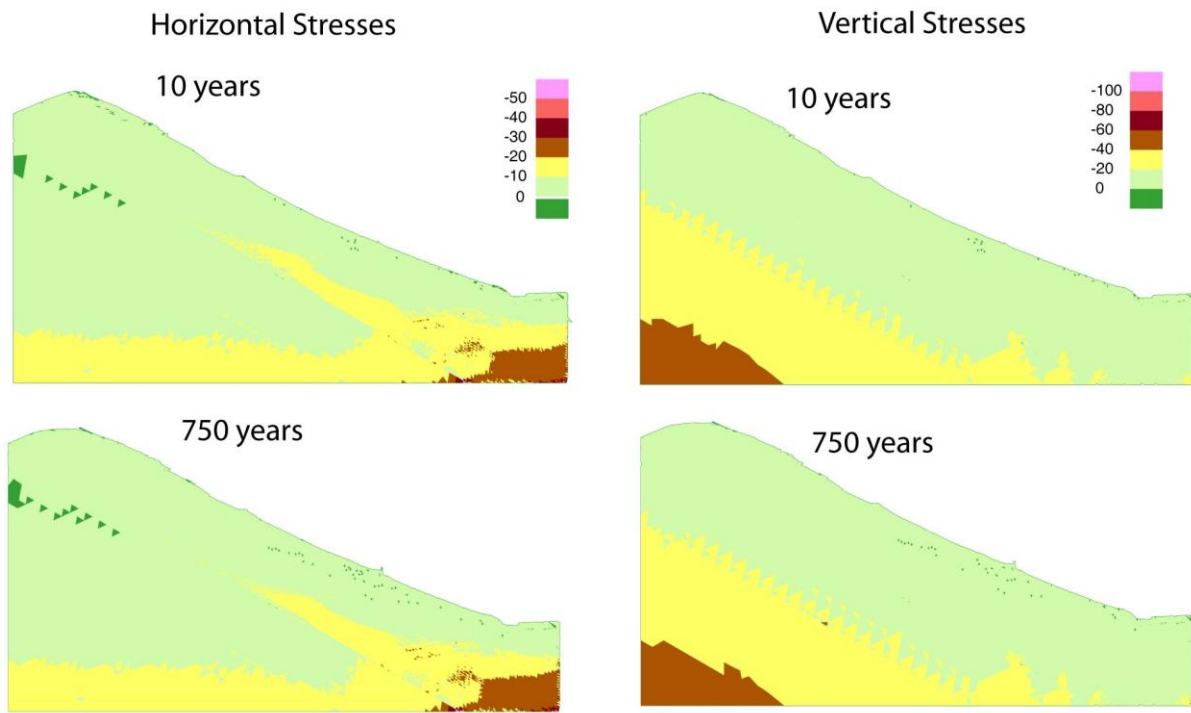


Figure 50: Horizontal and vertical stress distribution sin the whole model at 10 and 750 years, with valley fill. Stress contours are in MPa.

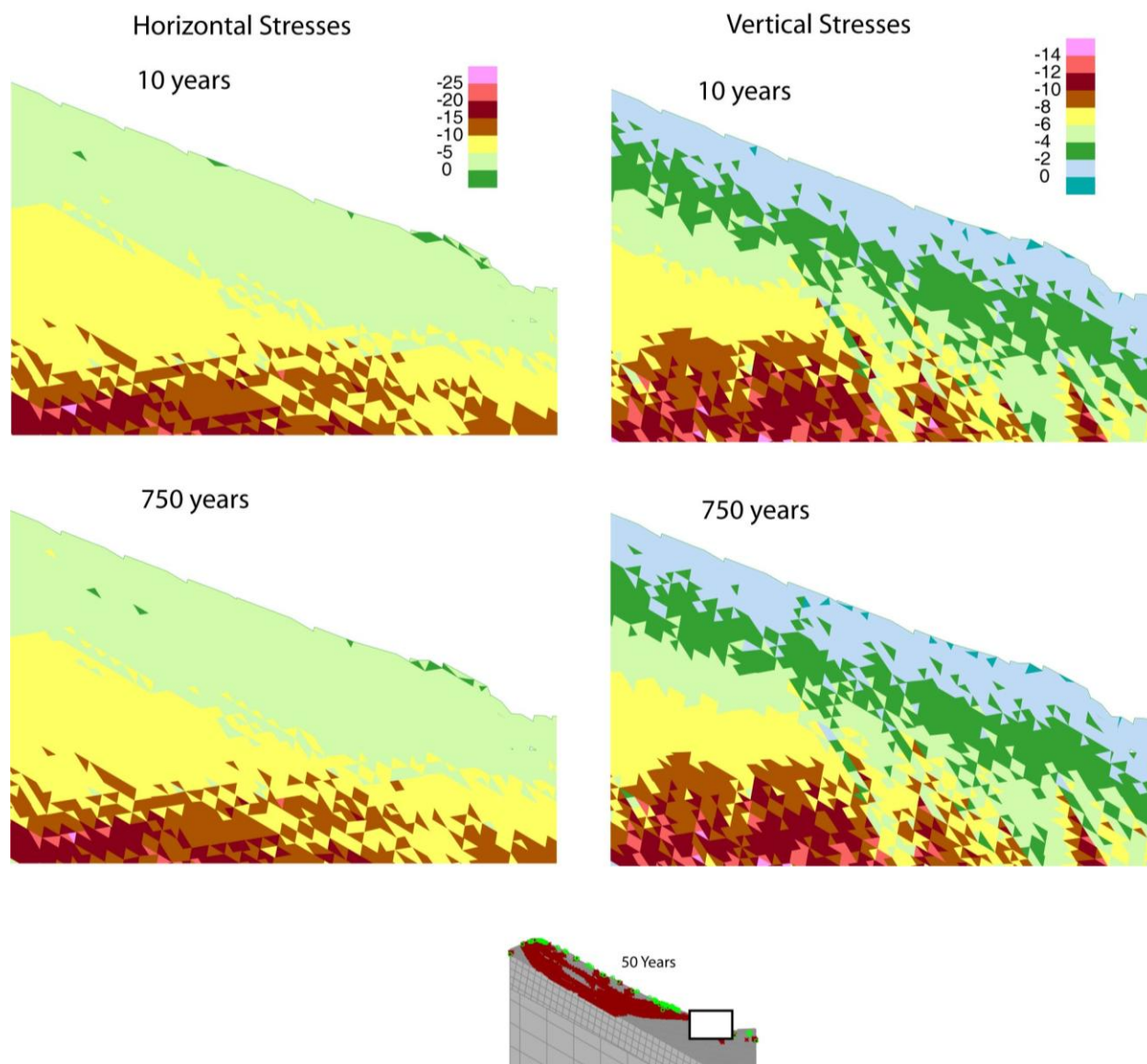


Figure 51: Horizontal and vertical stresses in the toe of the model at 10 and 750 years, with valley fill. Stress contours are in MPa.

Figure 49 shows the progressive formation of the landslide surface generated with fill in the valley with plots at 10 year intervals, up until the surface is fully formed at 70 years. The surface can be seen to develop gradually, with the toe becoming shallower as the landslide areas coalesce. It is likely that as yielding above allowed the landslide to begin to mobilize, this in turn drove the yielding that eventually joined the upper surface to the toe between 50 and 60 years. The 750 year image is included to demonstrate how little the slide surface changes once it is fully formed. Figure 50 shows the horizontal and vertical stresses in the whole model at 10 and 750 years, there is no significant change in the stress distributions in the model at this scale. Figure 51 shows the horizontal and vertical stresses at the model toe for 10 and 750 years, as before there is no great change in stress distributions. Significant yielding has already begun in the toe by 10 years and continues through all of the time modelled. These consistent stresses cause the toe to continue to yield and change shape with time, instead of the stresses changing. If

catastrophic failure were to occur at this site, significant changes in the stress state in the toe would be anticipated, however as this has not occurred, these results are unsurprising.

The velocity and displacements of the sliding surface at 70 and 750 years are shown in Figures 52 and 53, respectively. The velocities shown in Figure 53 are not true velocities based on real time. They are instead based on the calculation timestep. Therefore the velocity plots presented here are not meant to be interpreted as true velocities, but show the relative movement taking place incrementally within the model. These velocities show two areas that are moving actively compared to those around them, indicating that the sliding surface has not fully joined up and the slide mass is not moving as a unit at all. This is contrast to the displacement figures, which instead show the total absolute movements. Little change is seen between the two velocity figures at 70 and 750 years, indicating that even to this point the model has not really reached a non-moving equilibrium. If computing time allowed (potentially weeks required), continuing the model further to see if any fatigue results occurred would be of interest.

Figures 52 and 53 show that the majority of the movement is occurring in the upper part of the slide body. In fact, the surface does not appear to have fully mobilized in the lower part. As this does not agree with what has been observed at the site, it was determined that perhaps some factor or variation at the toe was missing from these models. See sections 5.3.2.2 and 5.3.2.3 for a discussion on changes made and considered.

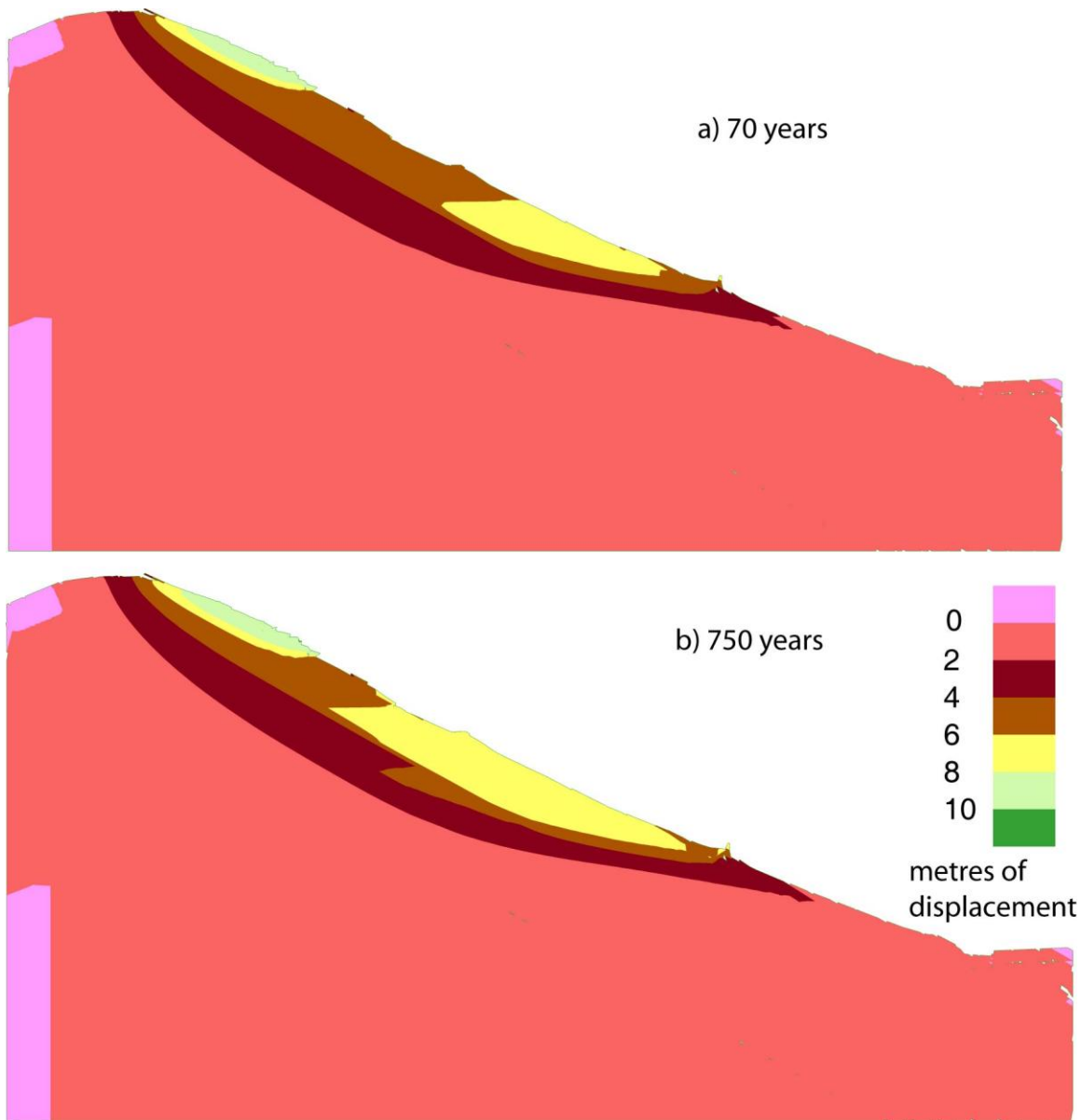


Figure 52: Horizontal displacements in the strain softening model at a) 70 and b) 750 years

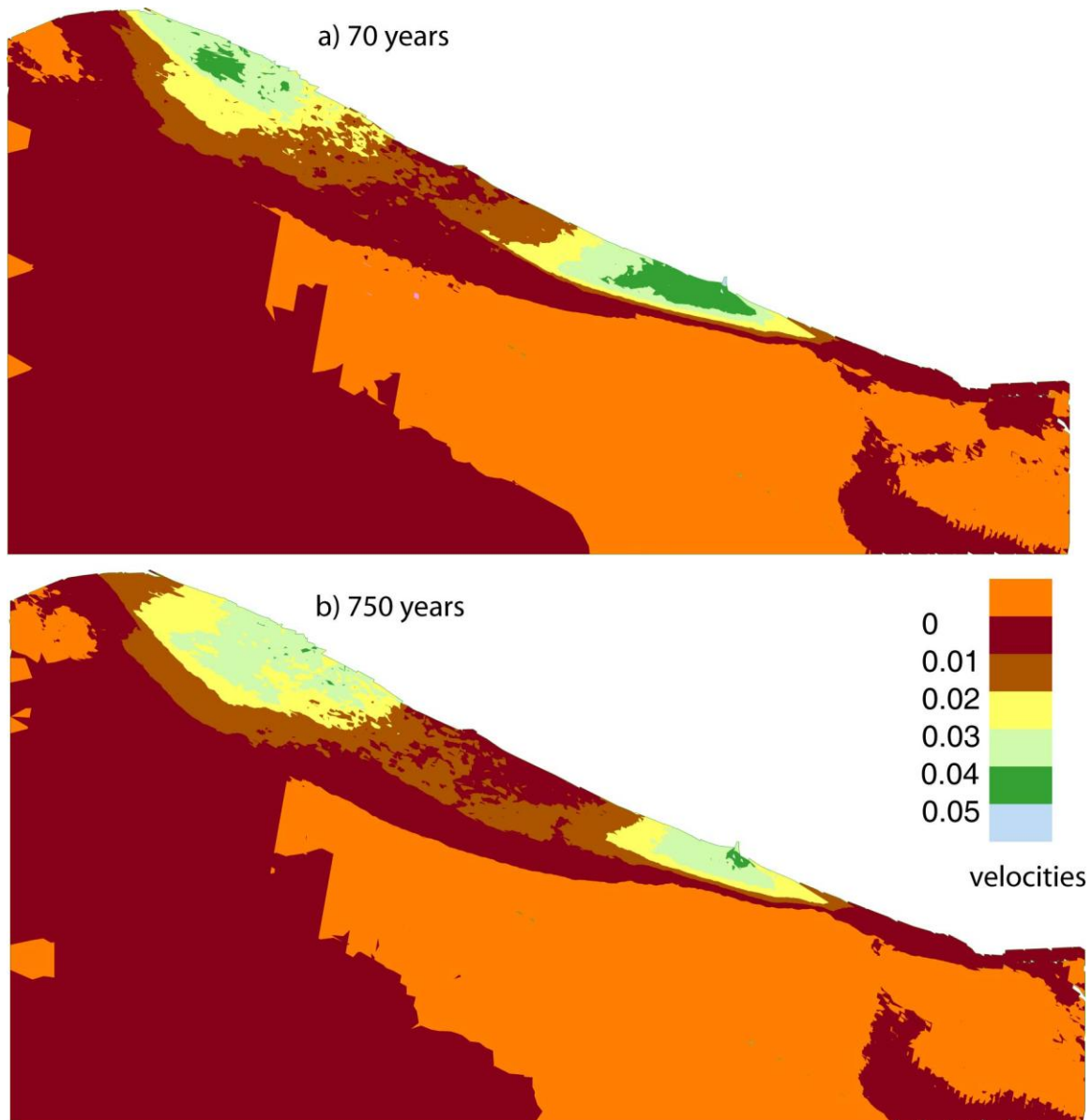


Figure 53: Velocities of the strain softening lower bound model at a) 70 and b) 750 years

5.3.2.2 Spatial Variation of Properties

Further modelling was carried out to achieve a better fit with the mapped and interpreted features at Little Chief by investigating the influence of spatially varying properties with depth. First, the strength of the rock mass was increased with depth. This was based on the assumption that weathering and the frequency of jointing decreases with depth. A similar assumption was made for UDEC modelling carried out by Zangerl et al. (2008), also for crystalline rock. There is no direct evidence that this is true at the Little Chief site, but an assessment of core logs shows a slight trend towards an increasing competency of the rock quality with depth. This effect was incorporated by means of the rock mass shear strength properties, rather than through a change in the spacing of the joints modelled. Three layers were used, with the upper layer being assigned the lower bound properties (see 5.3.2.1) and the lowest layer being

assigned the average expected properties. The intermediate layer was assigned rock mass values between these.

Figure 54 shows the layered model and results. No through going sliding surface is formed with the yielded elements. However, when looking at the horizontal displacements (Figure 54b), movement can be seen with differential displacements developing above and below the projected Little Chief sliding surface. This goes quite deep in the centre, but is well developed at the toe. This is very encouraging, and suggests that continued efforts to refine the increase in strength with depth to be more continuous rather than simply layered, may lead to an even better fit of the modelled and mapped sliding surfaces. However, due to time restrictions, further testing of the effects of heterogeneity was not continued beyond the results shown in Figure 54.

The other approach was to investigate the possibility of glacial damage (through unloading and relaxation) at the toe of the slide influencing the initiation, localization and development of the Little Chief sliding surface. To study this, a model was used in which the presence of a large glacier was included in the model, and then removed. The density of the glacial ice was set to 1.9 g/cm^3 and reached a maximum height of approximately 1000m. Any differences in the yield pattern between this, and the non-glaciated version, would be considered glacial damage. Significant glacial damage at the toe would serve as a justification to weaken the rockmass in this area, helping to deepen and rearrange the toe failure that develops in the model.

Figure 55 shows the yielded elements after the simulated removal of the valley glacier and the model has been cycled for 10 years. The glacier is included in the figure to show its relative size. The results show significantly more damage both along the surface and at the toe, compared to non-glaciated models. These results, and those involving the strength layering, provide a starting point for further study into the initiation and progressive development of the basal sliding surface. As previously noted, time restrictions and shifting focus back to the primary objectives of this thesis (influence of cyclic loading and fatigue), prevented further work on these models from being carried out. As is, no tested variants have produced better results than those shown in Figure 54 at the time of writing.

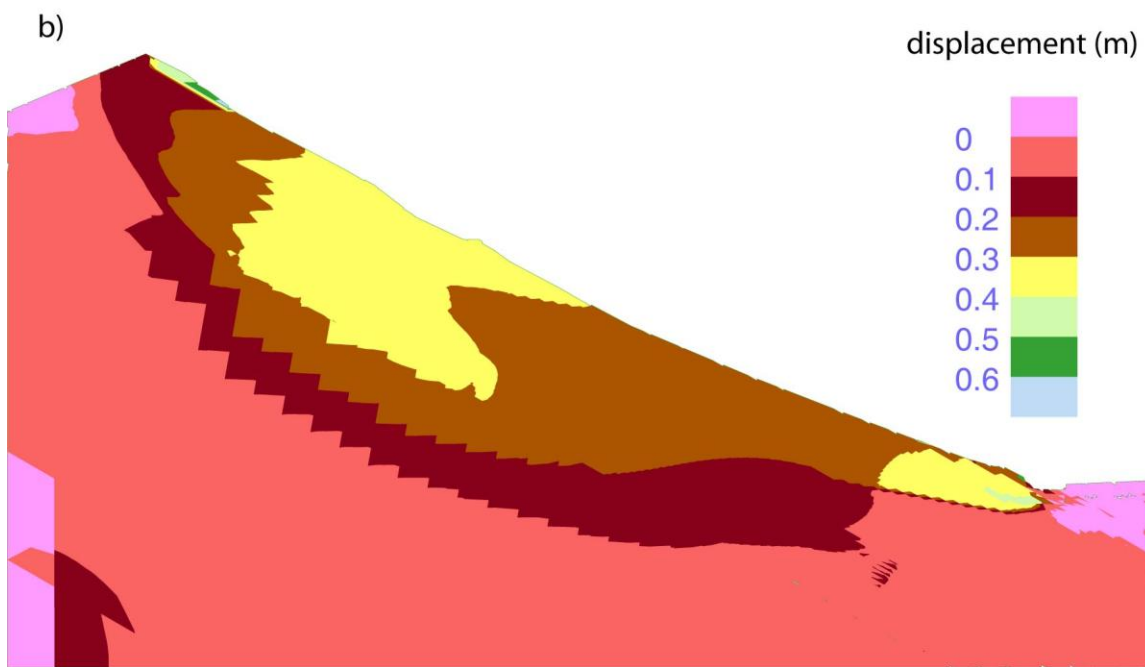
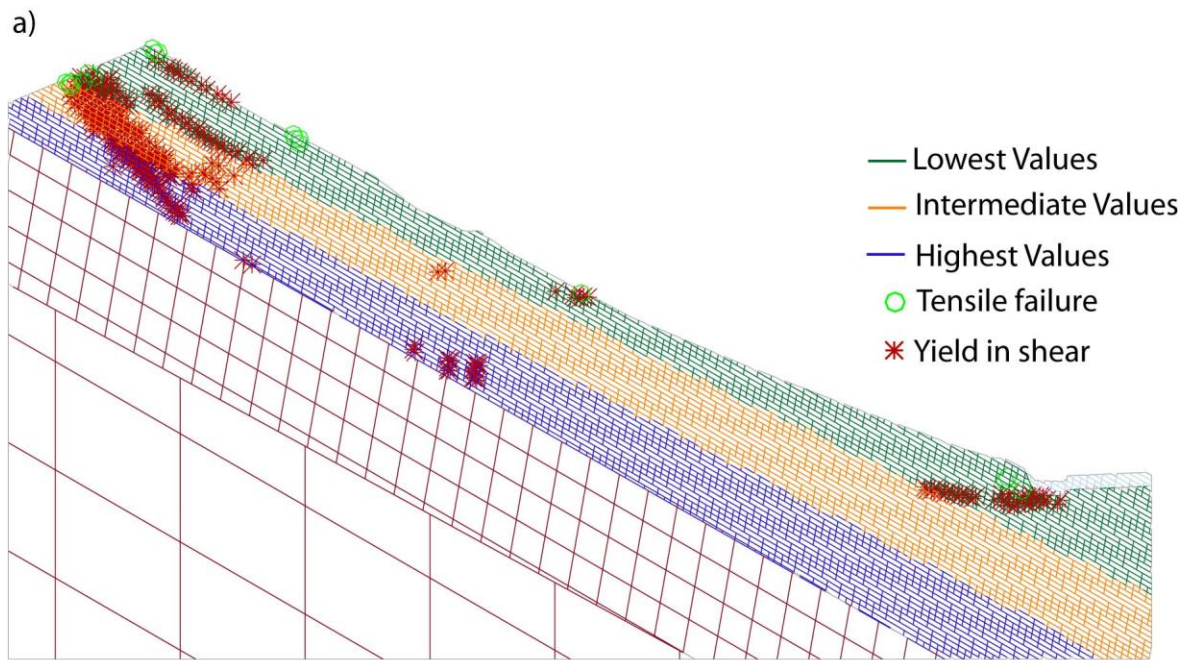


Figure 54: a) Layering and plasticity indicators, and b) horizontal displacements in the layered model after 30 years of cycling.

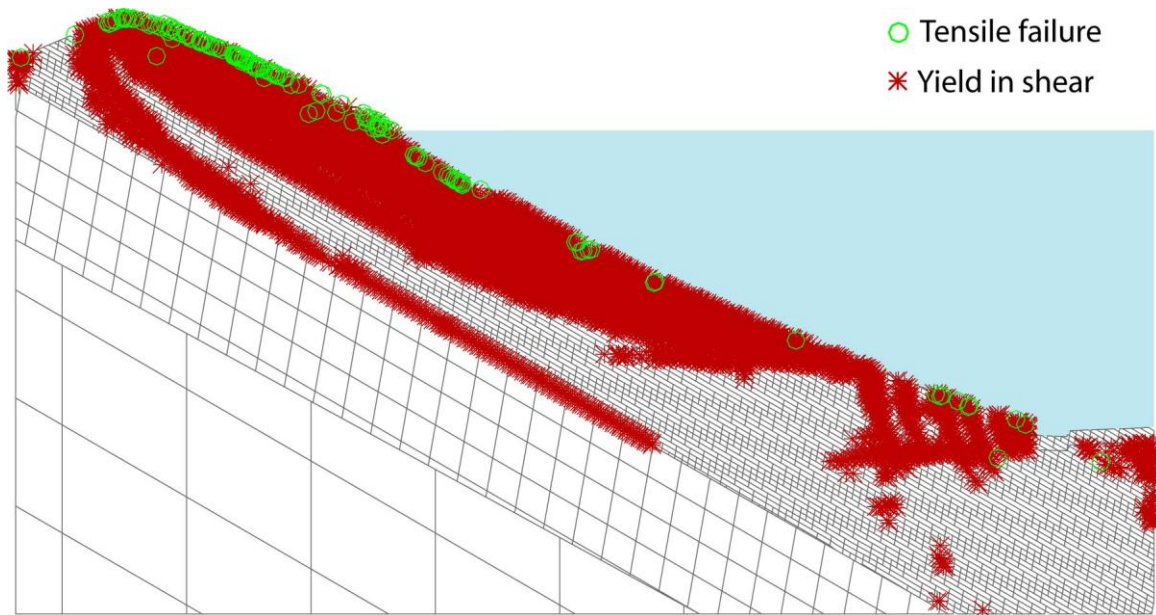


Figure 55: Plasticity indicators showing extra damage along the surface and at the toe ten years after the removal of the valley glacier. The glacier is shown in blue.

5.3.2.3 Reasons for imperfect fit

There are a number of likely reasons why the models of the Little Chief sliding surface were unable to produce an identical fit to the surface interpreted from borehole core logs. Some of these are related to model simplifications and the impossibility of perfect knowledge of the geology, while others are related to time limitations in carrying out this work and deficiencies in the software being used.

- 1) Variation of rockmass properties with depth: This has been addressed in section 5.3.2.2 to the extent that time and computing capabilities allowed. Little is known of the variation with depth of the rockmass, and even less can be said about the conditions before the sliding surface developed.
- 2) Homogeneous versus heterogeneous representation of the rock mass: Representative properties were used as the scale of variation within the rock mass is more defined than the scale of what is possible in the model. A high level of detail could not be readily captured in the model and still solved in a reasonable amount of time, even if the information available included more detail. As is, the geological details included were based on surface mapping and core logs from six boreholes, and this level of detail can be viewed as being reasonable when compared to the amount of detail typically available for such analyses.
- 3) Important geological structure(s) not identified may be present within the rock mass: Even the most detailed site investigation is not capable of imaging the entire subsurface of a large deep-seated rockslide. Interpretations must be made from the data collected, but it is always necessary to remember that a missed geological structure has the ability to influence the rockmass in question. As well, this rockmass has undergone significant deformation, it is possible that structures which contributed to the development of the sliding surface have

become incorporated into the surface, or disguised by it with time. Therefore without these unknown features in the model the surface is unlikely to develop exactly as it did in reality.

- 4) The influence of the third dimension is something that cannot be ignored: It is possible that lateral influences, or variations outside the 2-D cross-section plane adopted, may control the shape and depth of the sliding surface.

5.4 Fatigue Modelling Based on Interpreted Basal Sliding Surface

Using the results from the UDEC modelling investigating the development and location of the basal slide surface and toe release kinematics, as presented in the previous section, the interpreted internal shear surfaces were introduced into the model and cyclic loading applied to examine intermittent movement behaviour and fatigue. The same method as that used for Campo Vallemaggia was applied.

5.4.1 Model Setup

5.4.1.1 Basal Detachment

The Little Chief Slide has two very distinct north and south regions with different basal detachment surfaces. For this model, the north region was chosen, as it is reasonably well defined. The head of the slide in the model was based on the location of the head scarp mapped at the site. Most of the profile of the slide was extrapolated using information gained from inclinometers and core logging, which noted an abrupt improvement in the rockmass quality at depth in nearly all the drill holes, likely indicating the bottom of the mass which had experienced significant movement (Watson, 2006a; Watson, 2006b).

The exact placement of the slide toe is unknown as it is below the reservoir level. There is no record or indication to suggest that the slide surface daylight at the toe of the slope or on the far side of the valley beneath the reservoir. Its placement, however, has major implications for both the volume of the slide and its modelled kinematics; if the slide surface daylight in the valley floor on the opposite side of the valley, this would suggest that the slide body has already run up against the other side of the valley and is buttressed by it. Shallower slope movements would still be possible due to subsequent undercutting by the river. Borehole observations near the toe of the slope allow for an alternative interpretation in which the slide surface daylight on the same side of the valley. This latter location was adopted based on the modelling results from the previous section and the borehole core logs; in all models reported in section 5.3, development of a toe breakout structure occurred on the same side of the valley as the slide body. The resulting fatigue model used, showing the internal sliding surfaces, is illustrated in Figure 56.

5.4.1.2 Fracture Network

A different fracture network was used in these models than in the landslide initiation models (as described in section 5.3.1.1). For the fatigue models, the foliation jointing was not designated as being fully persistent for the length of the model. This was deemed to be a better representation of the actual joint conditions and was implemented as such.

The modelled fracture network was initially set to have a joint spacing of 100m for the subvertical joints and a spacing of 25m for the sub horizontal joints. These spacings were decreased in later versions in order to test the difference of a smaller spacing. This testing resulted in a spacing of 30m for the vertical joints and 20m for the horizontal joints, with the latter represented through two joint sets

spaced in an overlapping brick-like pattern. Where the sets overlapped, these joints had a spacing of 10m. See Figure 57 for the fracture network pattern used.

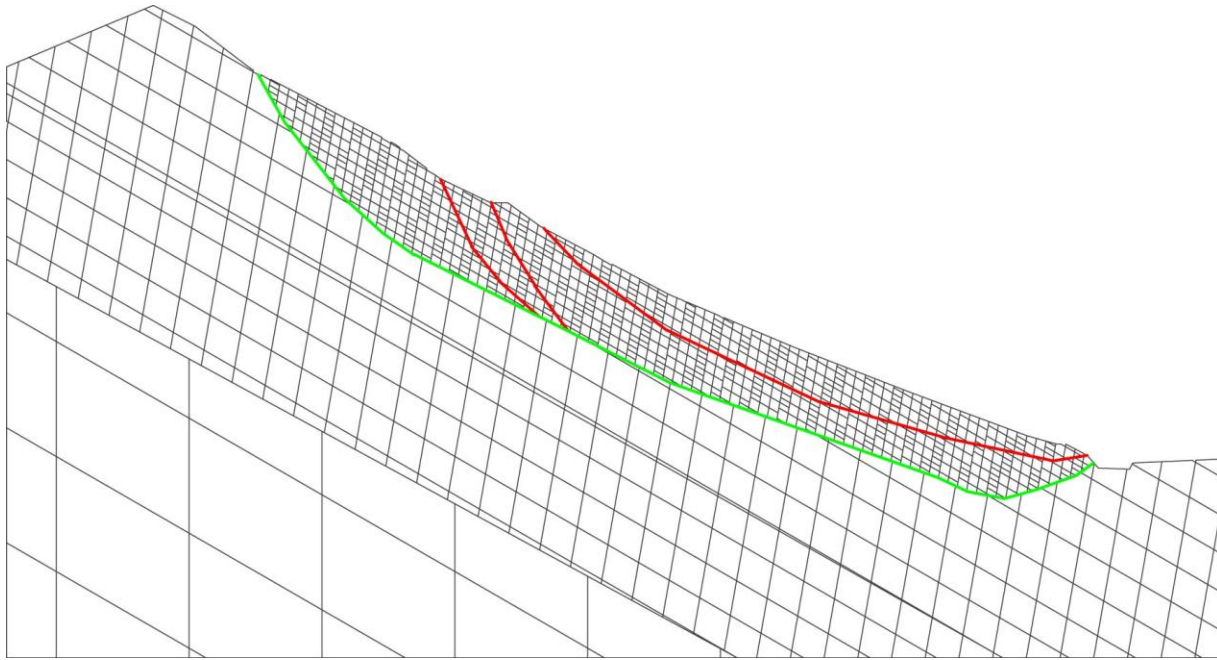


Figure 56: The Little Chief model used to test the effects of fatigue. The basal sliding surface is shown in green, and the internal sliding surfaces are shown in red.

5.4.1.3 Water Tables

In the initial versions of the fatigue model, the same two water tables described in section 5.3.1.2 were used. In later versions, two variants of the high water table were added in response to the intermittent slope velocities seen in the initial results for Little Chief, as was seen for Campo Vallemaggia. These include those representing a 10-year repeat storm event (i.e. an above average higher water table every 10 years) and a 100 year repeat storm event (i.e. an exceptionally high water table every 100 years). These are shown in Figure 58 as green and blue. Note that these two water tables are not directly based on data from the site, but are an upward extrapolation of the average high water table.

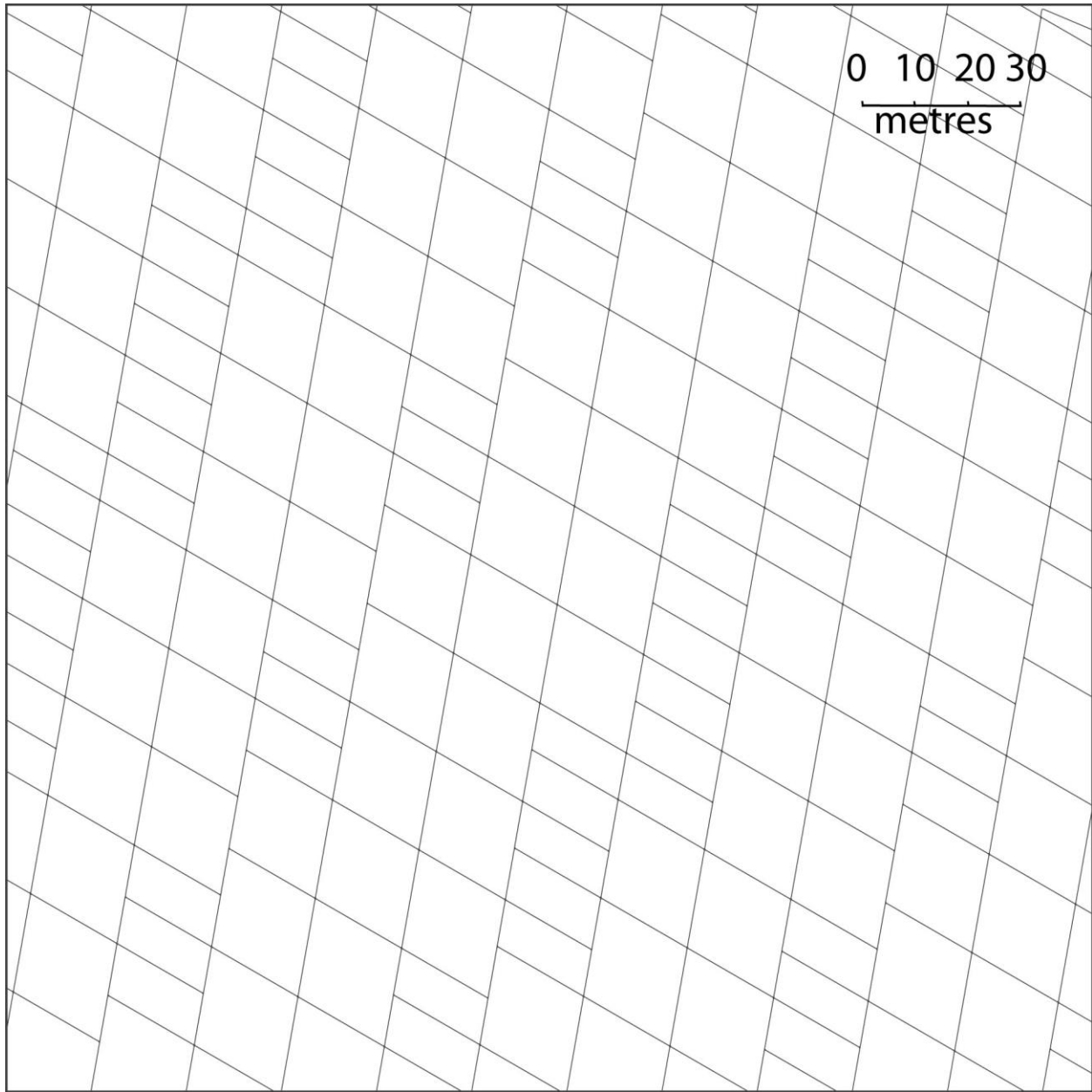


Figure 57: Close up view of the brick pattern of joint spacings used in the slide body in the Little Chief slide model.

5.4.2 Intermittent Displacement Behaviour

When the cyclic loading of the alternating water tables was applied for multiple years, patterns of periodic intermittent movement with larger displacements occurring during the wet season were observed. Little to no displacement was seen during the dry seasons. The first series of results produced a perfectly uniform stick slip pattern with approximately the same amount of movement every year. This does not count the first few years in which greater movement was seen in the wet season due to initialization and consolidation effects in the model. If the model is run only with the higher water table, then a decelerating pattern transitioning into a steady state behaviour is seen, similar to that idealized in creep curves as described in Chapter 2 (e.g. Figure 1).

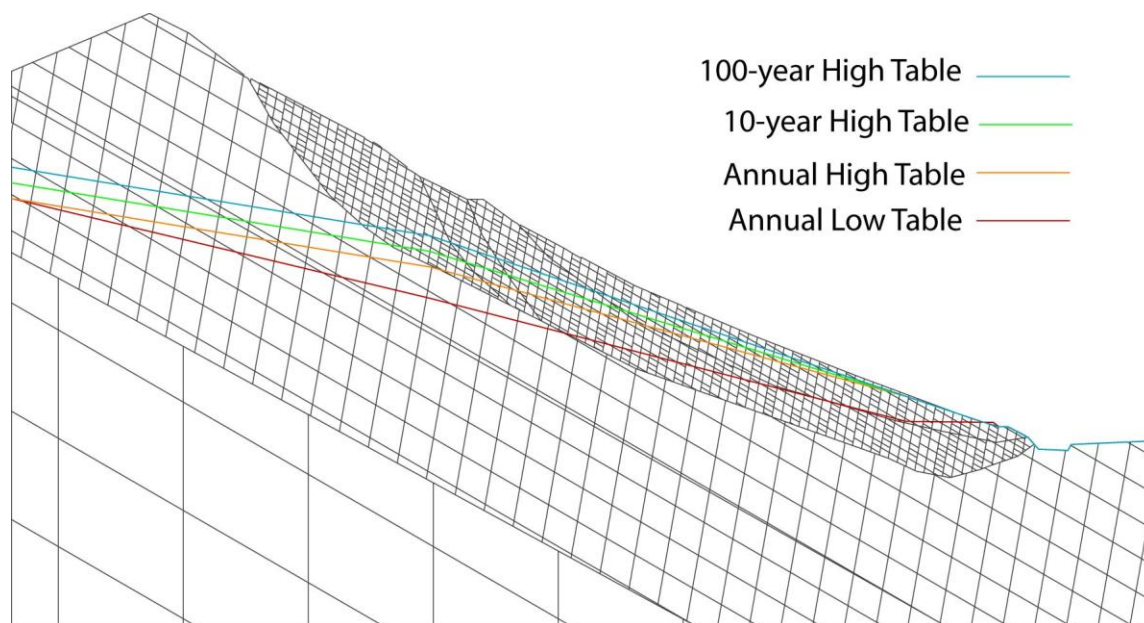


Figure 58: Model setup showing the different water tables used in the fatigue cycling of the Little Chief slide

Later versions of the models incorporated the large storm events described in section 5.4.1.3. This introduced a different shape to the displacement time results, although they still maintain the same overall stick slip pattern. Up to 1000 years, while this greatly increases the total amount of displacement seen (note that these displacements are significantly larger than those actually seen at the site) it does not appear to have any effect on the rate of movement seen when the lower water table is being used. That is, the differences occur only during the years when the storm events are taking place. The 10, 1000 and 3000 year displacement models for the lower middle part of the slide are shown in Figures 59 a-f. Figure 60 shows the location of the monitoring points used in all displacement and velocity history plots, for reference.

In both cases, with and without high precipitation/snow melt storm events, the ideal version of the movement is seen in the lower slope below the internal shear surfaces. The monitoring points higher up the slide show a more irregular movement, due to damping of the movement by the lower slope. The toe pattern in this case is actually somewhat different from that of the rest of the slide. This is due to the shape of the sliding surface, where loading of the passive block at the toe up against the toe release surface results in its upward movement in response to the down slope movement of the upper active slide body. This deformation mechanism is aided by elasto-plastic yielding of the rock mass at the toe. A comparison of the horizontal and vertical displacement histories near the top, upper middle, lower middle and toe of the slide at 10 and 3000 years are shown in Figures 61 and 62, respectively.

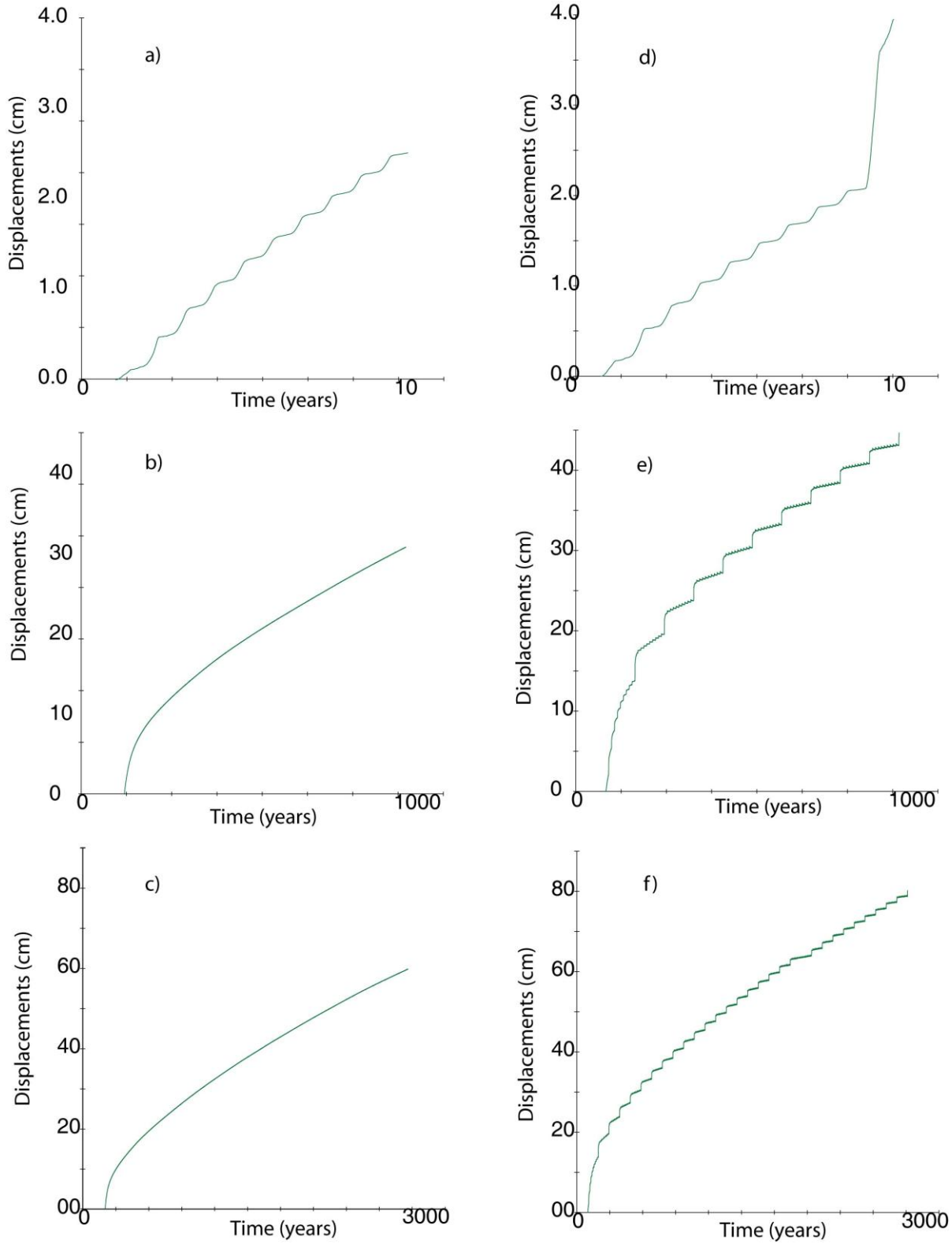


Figure 59: Displacements at the toe at: a) 10 years, b) 1000 years, c) 3000 years, d) 10 years with one peak 10 year event, e) 1000 years with 10 and 100 year peak events, and f) 3000 years with 10 and 100 year peak events.

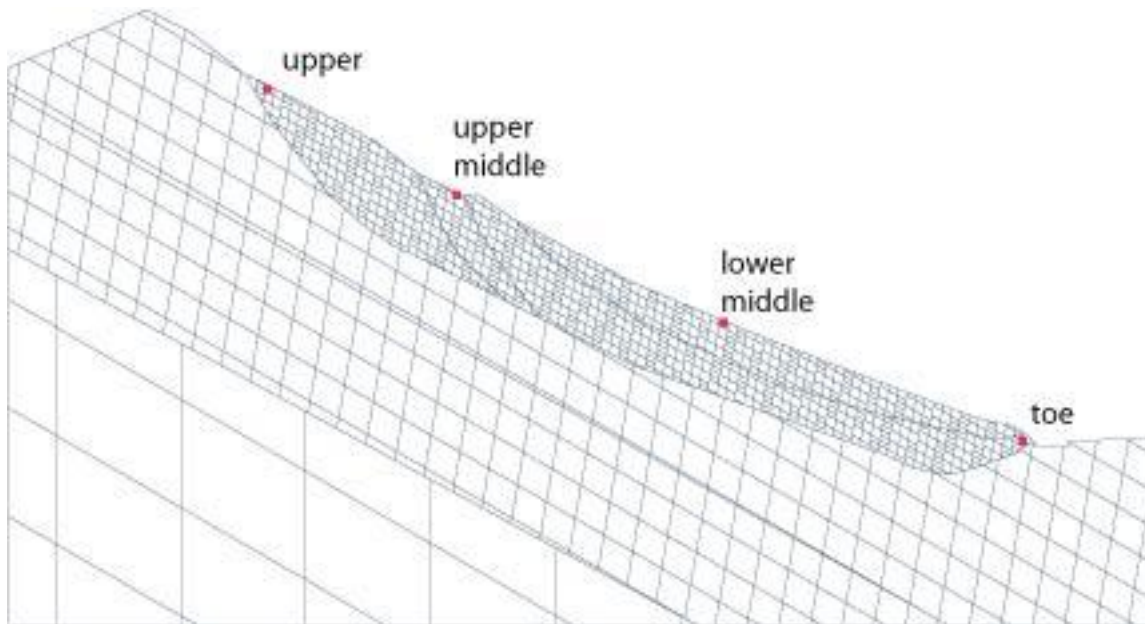


Figure 60: UDEC slide model showing location of history monitoring points used to track intermittent displacements and velocities.

Finally, Figure 63 shows the horizontal velocities at these same 4 locations for 10 years. Only ten years are included here for comparison. These velocities were calculated using the same method as those for Campo Vallemaggia (see section 4.3.2).

The resulting intermittent displacement response shows no sign of fatigue when using a Mohr-Coulomb elasto-plastic constitutive model. There is no noticeable increase in the displacements with time (i.e. accelerating behaviour). Instead, the velocity trends generally show a slight decrease over time. All of the results point to a continued expected behaviour of slow downslope movements with no major/catastrophic accelerating events triggered by water table changes or the cyclic loading thereof. Toe release is discussed further in section 5.5.3.

The horizontal velocities show a steady repetition with little variation from about 4 years on. All of the velocities peak together during the wet season, and drop very low during the dry season. This is exactly what is expected to be seen from this model.

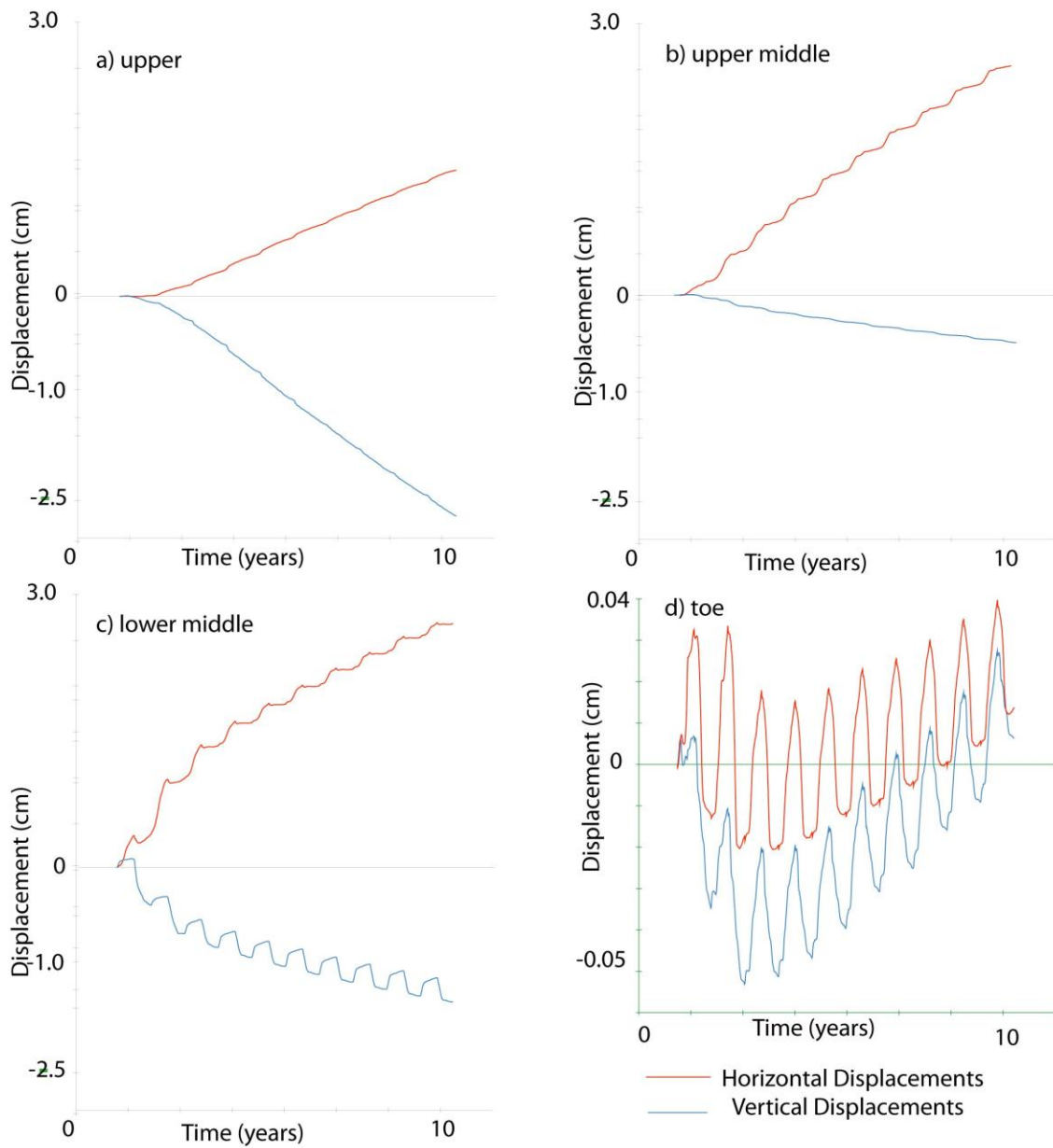


Figure 61: Horizontal and vertical displacements as they vary across the slide surface at 10 years. Note that negative vertical values indicate downward movement.

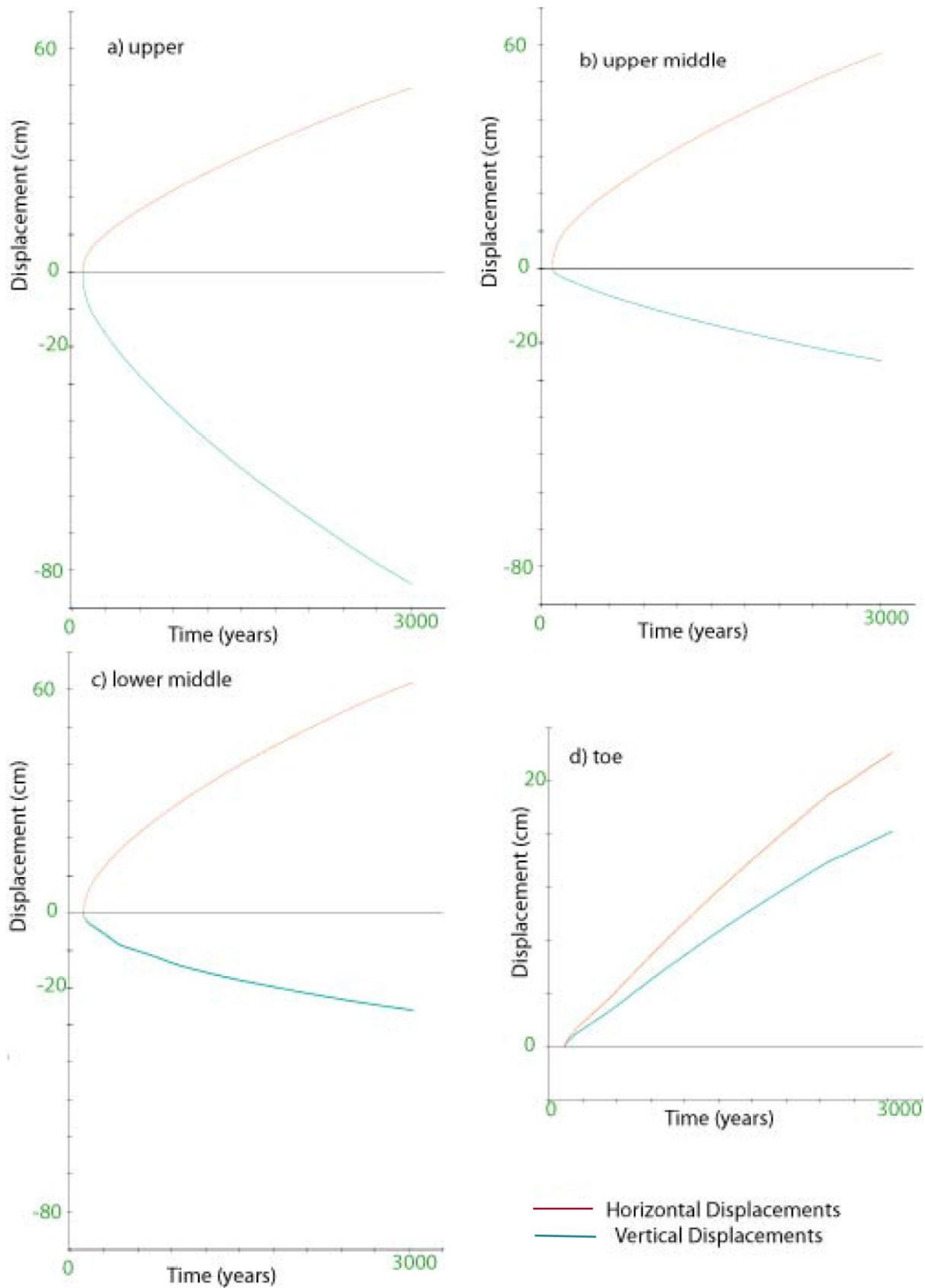


Figure 62: Horizontal and vertical displacements as they vary across the slide surface at 3000 years. Note that negative vertical values indicate downward movement.

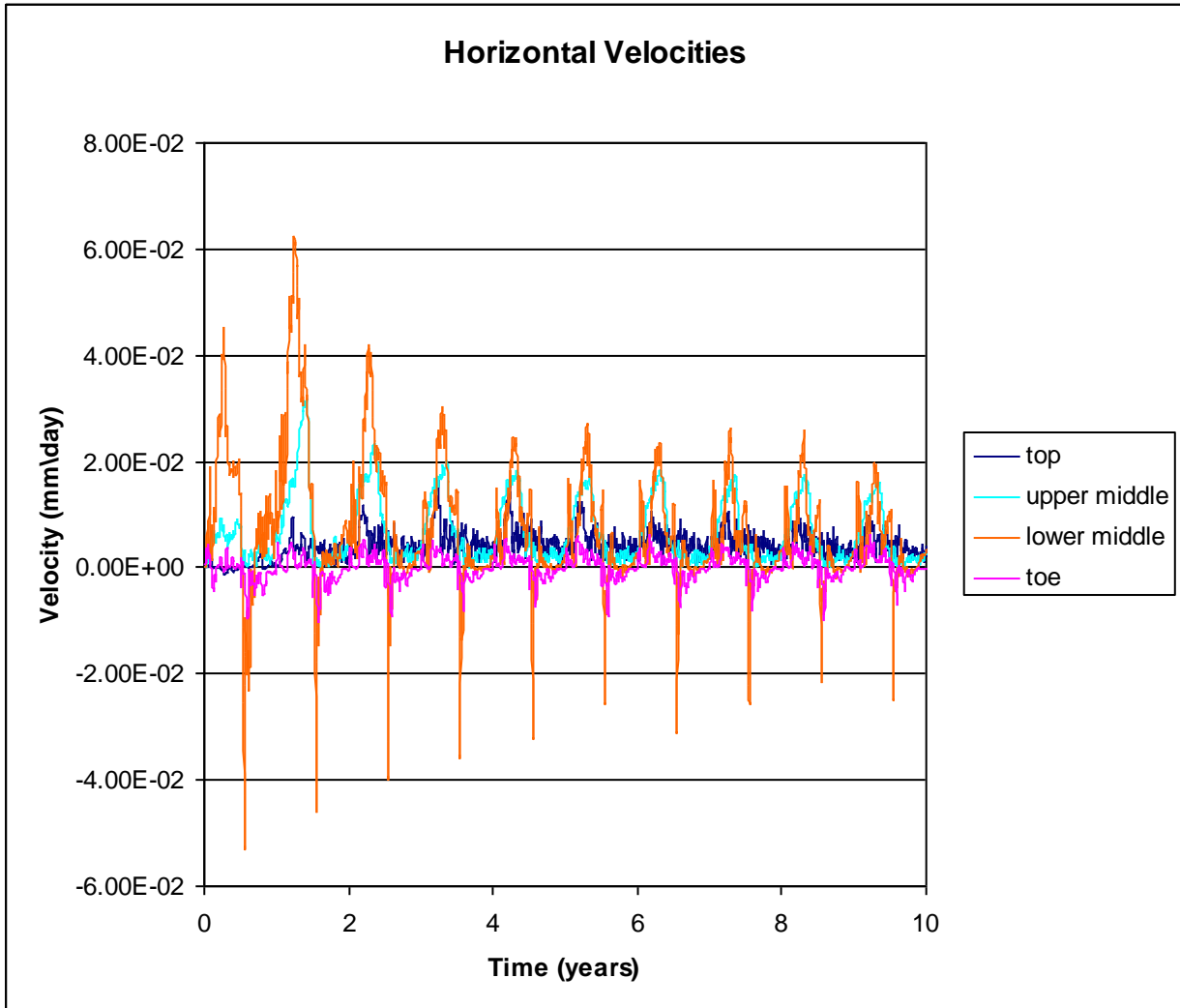


Figure 63: Horizontal velocities as the different history points along the slide surface at 10 years.

Figure 64 shows the displacement vectors in the slide at 10 and 3000 years, giving an indication of the variations in movement over the slide surface. Note that the vectors are at different scales in the two halves of the figure. Both show significantly more movement above the internal surface seen in the downslope half of the model. However at 3000 years, significant displacement is also seen below this surface, until the scoop of the toe, beyond that point displacements become much smaller, logical given that material in this location must be pushed up in order for movement to occur.

Figures 65 and 66 show the horizontal and vertical stresses in the model at the same two times. Very little change is seen in the overall distribution between the two times. This is expected as in the model the basal surface is already in place, and so no major areas of weakness or stress concentration need form for movement, except if movement takes place in the toe. However as Figure 64 shows, movement in the toe is minimal in this model.

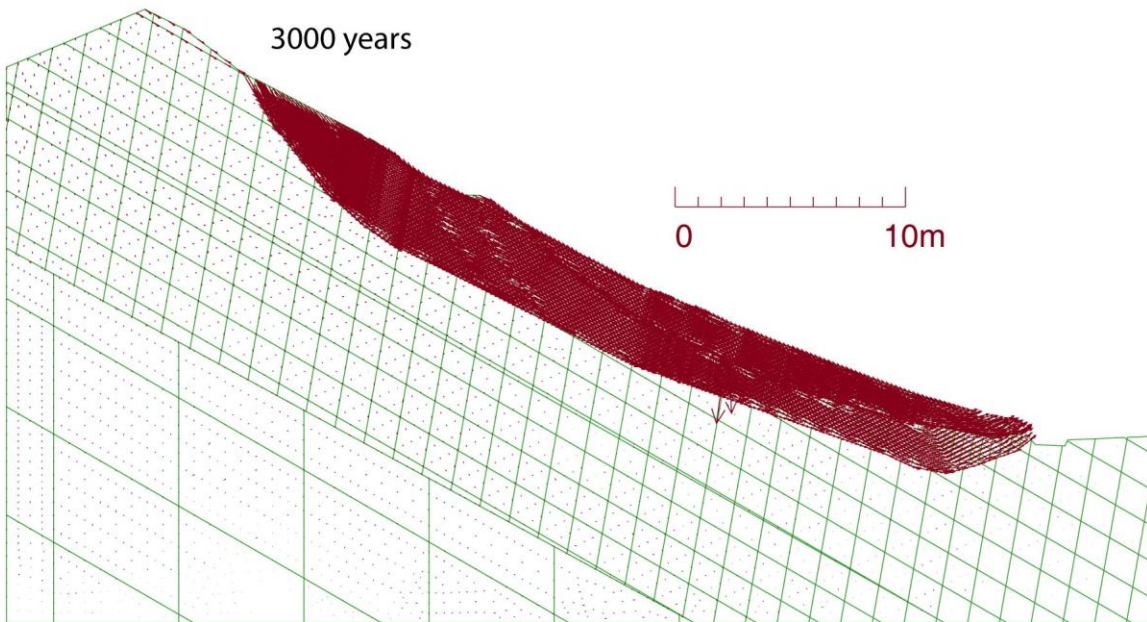
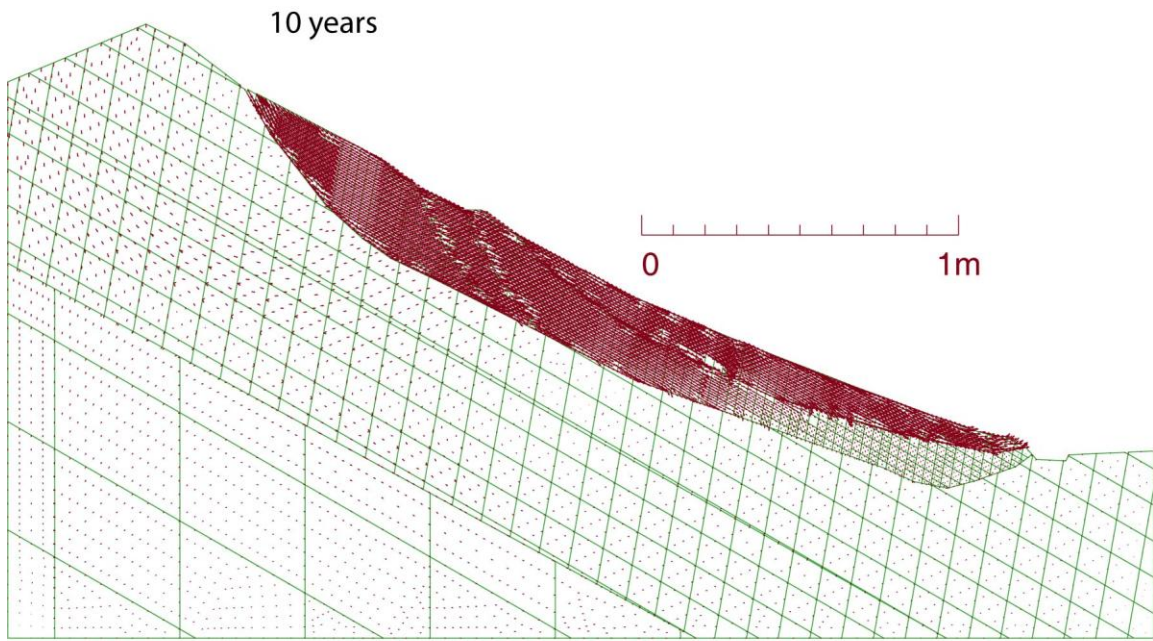


Figure 64: Displacement vectors (in red) showing movement direction and magnitude. Note that the two parts have different scales for the vectors so that both are visible

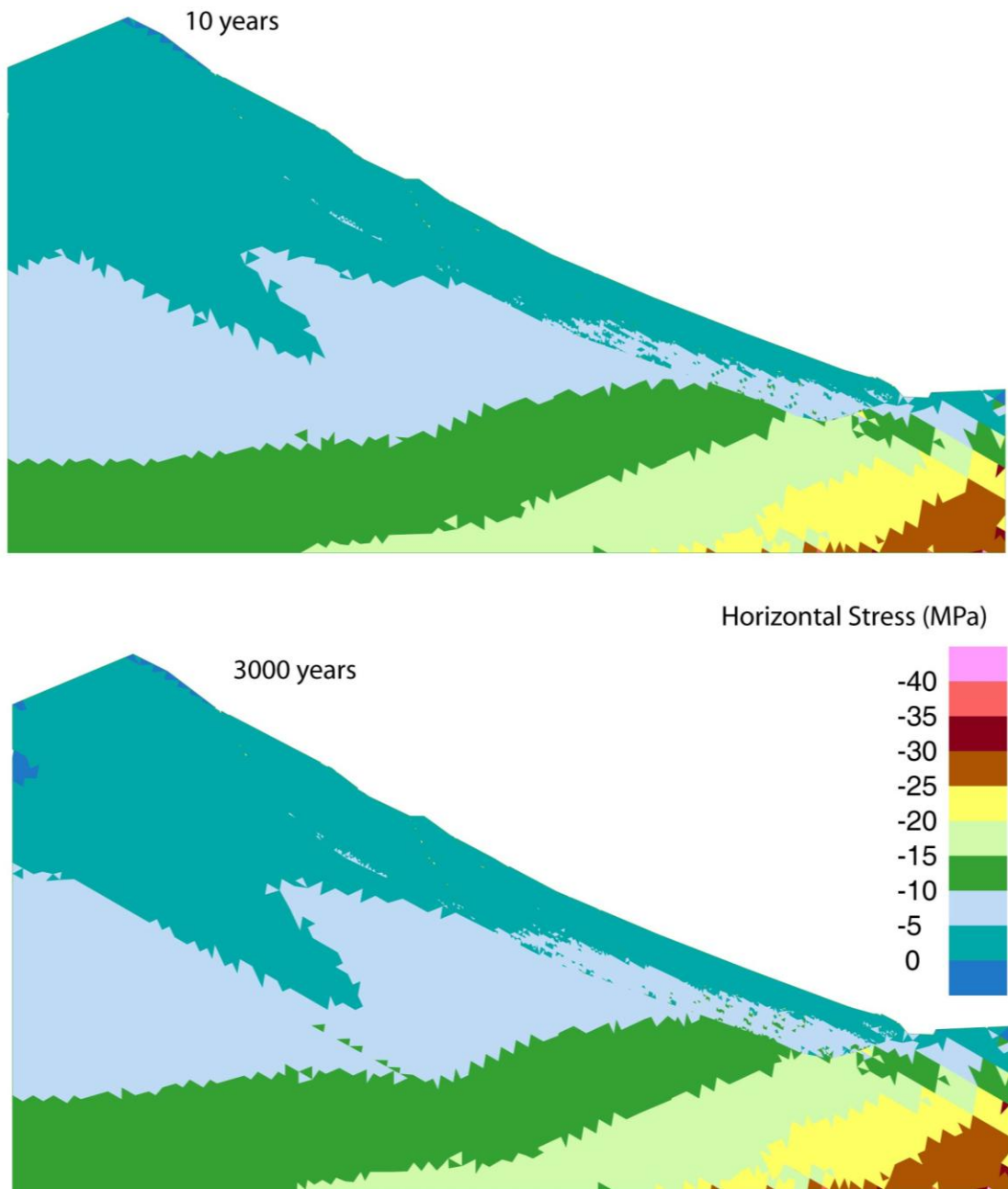


Figure 65: Horizontal stresses in the model at 10 and 3000 years

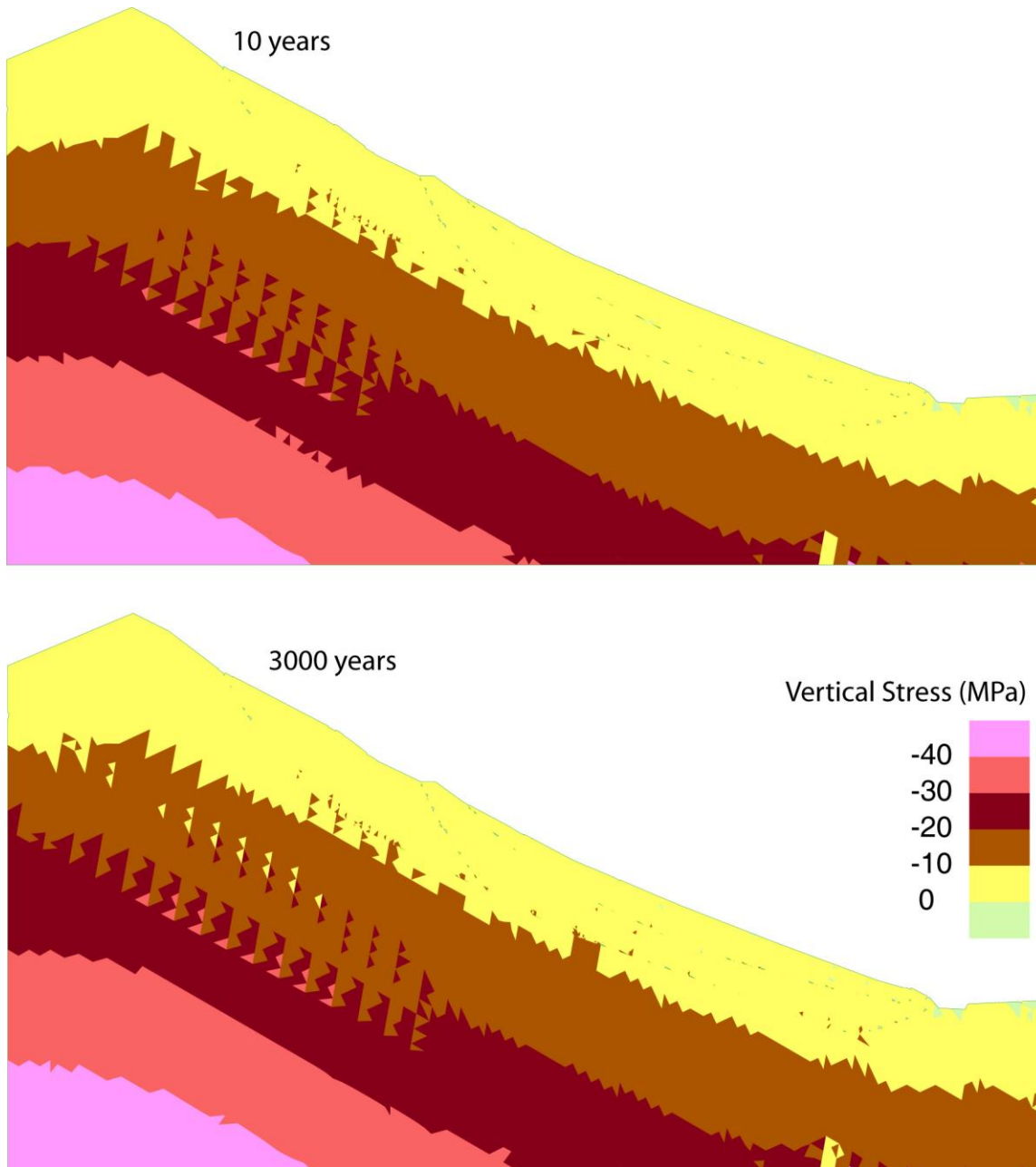


Figure 66: Vertical stresses in the model at 10 and 3000 years

5.5 Internal Deformation Modelling

After the fatigue modelling was completed, another set of models was run without the presence of internal shear surfaces to consider the effects of internal deformation of the rock mass as done with the Campo Vallemaggia landslide. These models were run as a hybrid of the landslide initiation and fatigue models.

5.5.1 The Model

The UDEC model used assumed a fracture network similar to that in the fatigue models described in section 5.4.1.2. Only the lower and normal upper water tables were used in these models. Both Mohr-

Coulomb elasto-perfectly plastic and strain softening models were applied, with the same properties used in the fatigue and initiation models described in sections 5.3 and 5.4, respectively.

5.5.2 Internal Deformation Results

Figure 67a, b shows the landslide at 300 years with no internal faults, assuming an elasto-plastic and strain softening constitutive model, respectively. Although the agreement is less distinct in this case than for Campo Vallemaggia (described in Chapter 4), localization of shear indicators can be seen in the strain softening model at the base of the slide surface where one of the mapped internal faults can be observed (Figure 67b). Still, there are no clear indicators on which to draw conclusions with any degree of certainty.

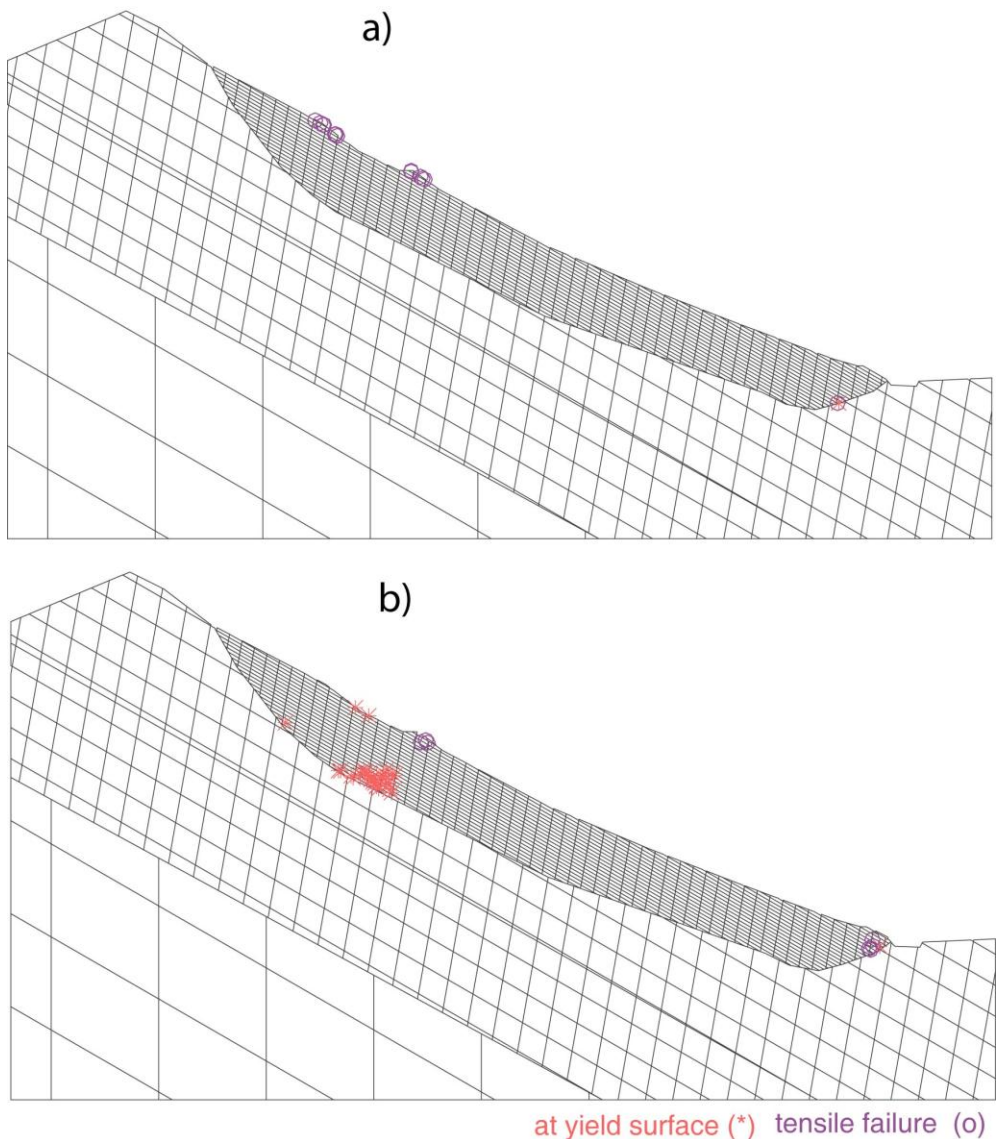


Figure 67: Yielding as an indicator of the development of internal faults assuming: a) an elasto-perfectly plastic, and b) strain softening constitutive model.

The next series of models examined reducing the rock mass properties from those deemed most likely to be present to the lower bound properties (see Figure 47). This was considered to be an unlikely condition/scenario, but was tested to examine the effects of a weaker rock mass and increased yielding and fatigue on the development of the rockslide. The results show that a significantly larger amount of internal yielding and shearing develops (Figure 68). Although localization never really occurs to the point that it exactly matches the mapped surface scarps (interpreted as internal shear zones at depth), there is some general agreement.

In addition, this model shows significant downslope movement and a large amount of yielding in the toe. Section 5.5.3 discusses toe release in more detail, but this yielding is expected as a required precursor to any increased acceleration of the slide mass. That is, the kinematics of the slide body is such that the toe of the slide is constrained at the valley bottom requiring shearing and release at the toe before any larger rockslide movements can follow. For the given conditions, catastrophic failure of the slope does not develop in the model, at least up to the fatigue state reached (1100 years), which in turn was limited by the computing time available (see Appendix A for computing times).

For both the expected and lower bound properties, the evolution of fatigue was based on the changing number of yielded elements, as was performed in Chapter 4 for the Campo Vallemaggia slide. The analysis included a survey of the entire slide as well as a windowed area encompassing the toe. The results are shown in Figures 69 to 72.

Assuming the expected rock mass shear strength values, the number of yielded elements present in the model was minimal limiting the conclusions that can be drawn. However, it can be noted that the number of yielded elements decreases slightly with time, both for the entire slide body, Figure 69 and for the toe (Figure 70). Of the yielded elements present in the slide, the percentage that occur in the toe increases with time to nearly 100 percent by 1000 years. This indicates that rearrangement of yielded rock blocks within the toe, as hypothesized and discussed in section 5.5.3, is likely an important and necessary step toward development of greater movement within the model. This also indicates that at properties similar to those estimated on site, it is likely that the slide body is not in a highly evolved unstable state, reasonable given that estimated properties were for the rockmass in general, not specifically the weakest parts thereof.

With the lower bound values, there is significantly more yielding (by orders of magnitude of the number of yielded elements). As with the models with no sliding surface, an anomalous, fast moving surface near the top of the slope develops, which does not appear to agree with observations at the site. The development of a distinct fatigue pattern is not seen up to 1000 years. There is a slight decrease in the amount of yield in the overall model after approximately 500 years, but it is very little. However, there is a marked increase in the number of yielded elements present in the toe after 850 years. It is considered possible that these are the start of internal shearing and rock mass rearrangement that could, with continued cycling, lead to fatigue failure of the toe. This is discussed further in section 5.4.4.

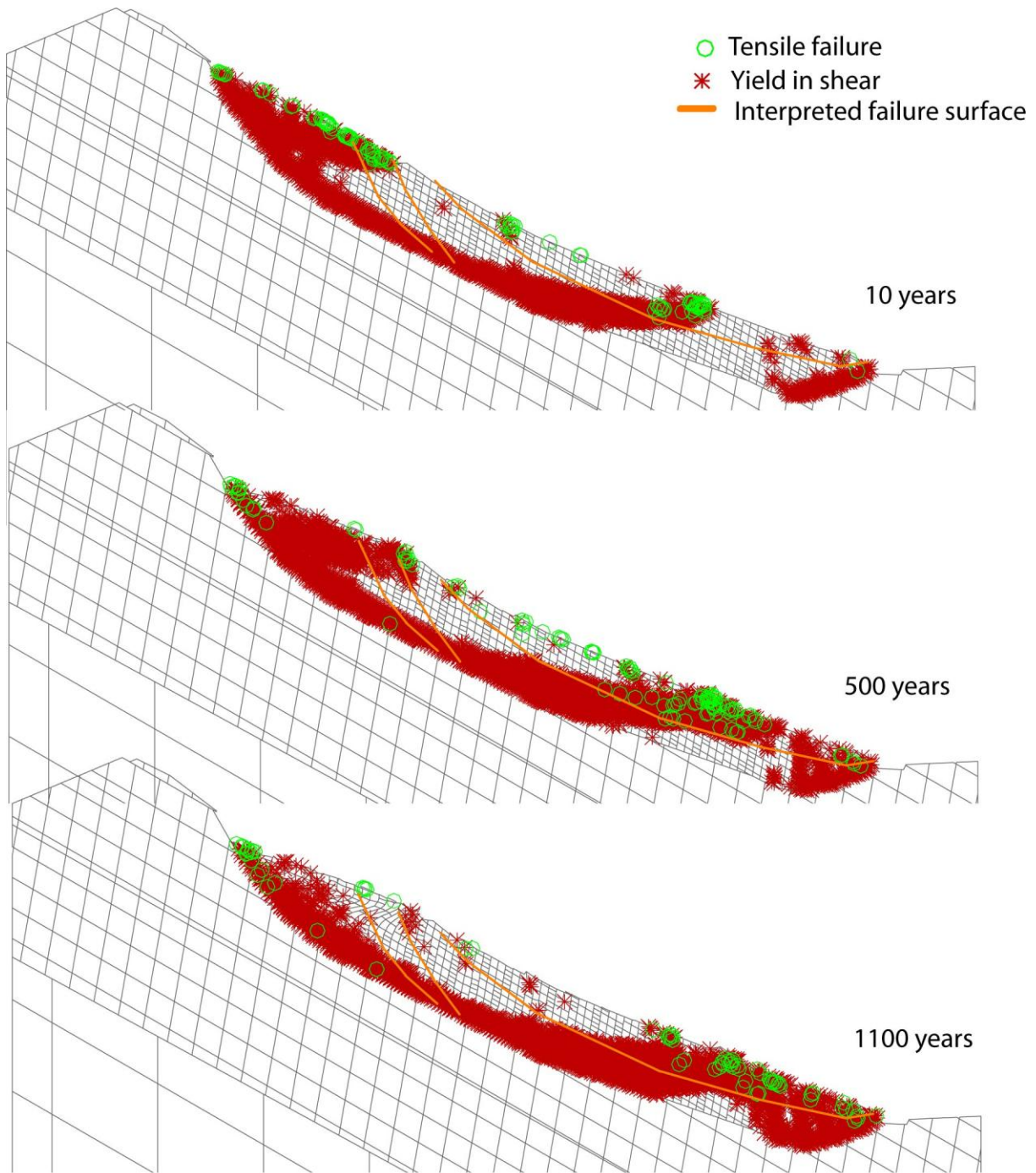


Figure 68: Strain softening model assuming lowerbound properties with the basal sliding surface included, but with no interior sliding surfaces.

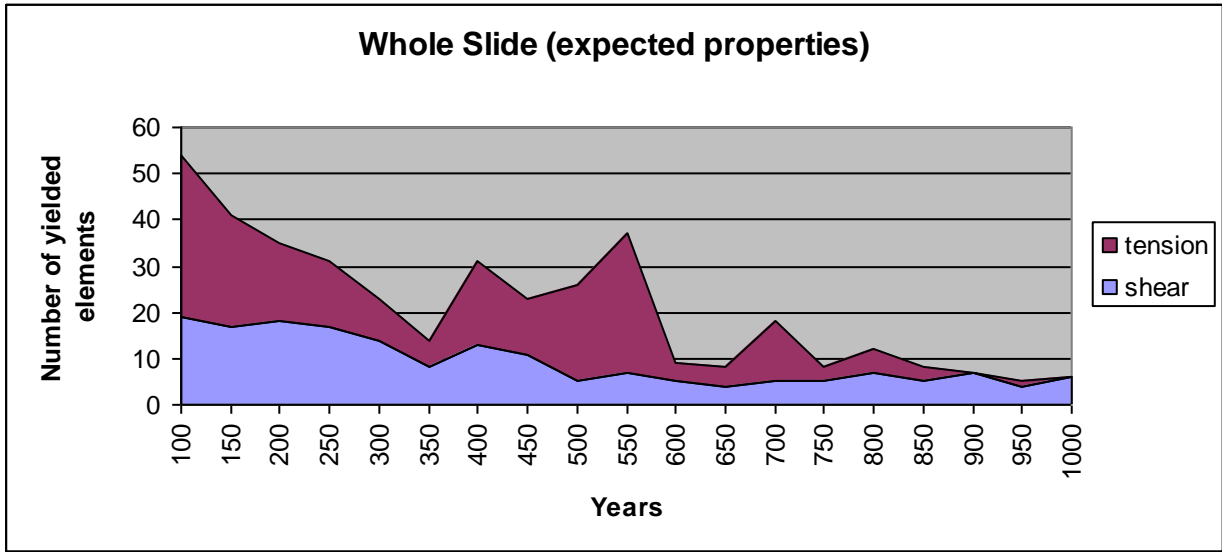


Figure 69: Change in the number of yielded elements present in the slide body with cyclic loading up to 1000 years, assuming expected rock mass properties for a strain softening constitutive model.

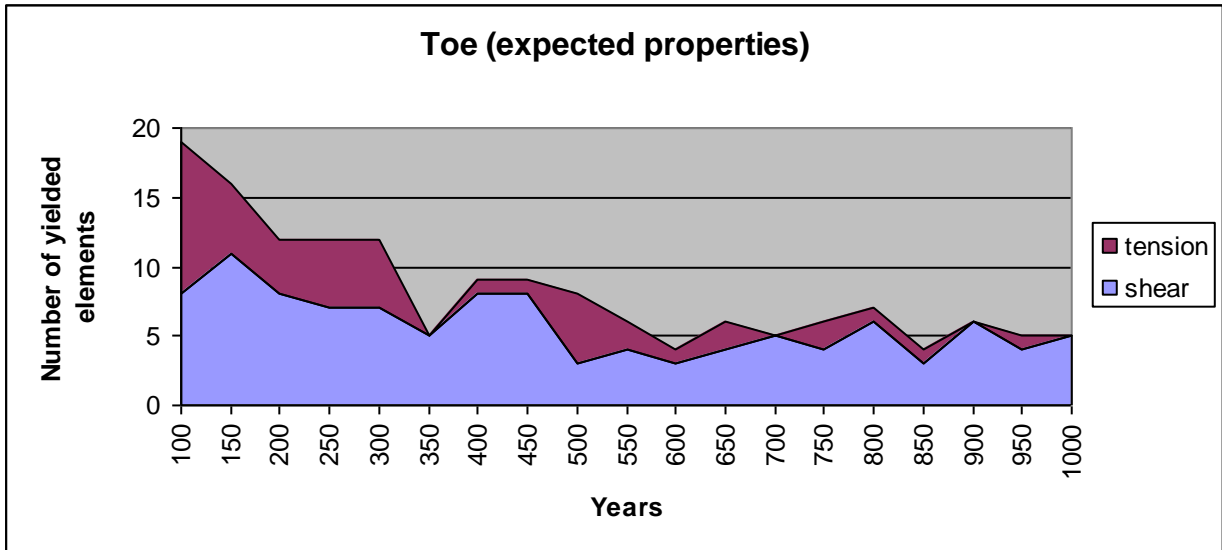


Figure 70: Change in the number of yielded elements present in the toe with cyclic loading up to 1000 years, assuming expected rock mass properties for a strain softening constitutive model.

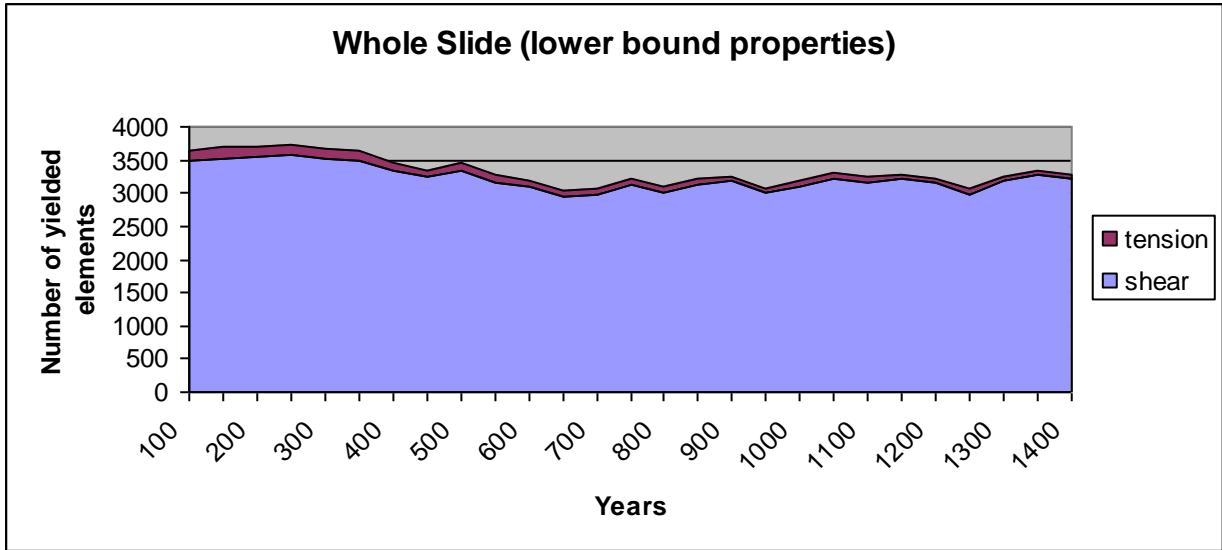


Figure 71: Change in the number of yielded elements present in the slide body with cyclic loading up to 1400 years, assuming the lower bound rock mass properties for a strain softening constitutive model.

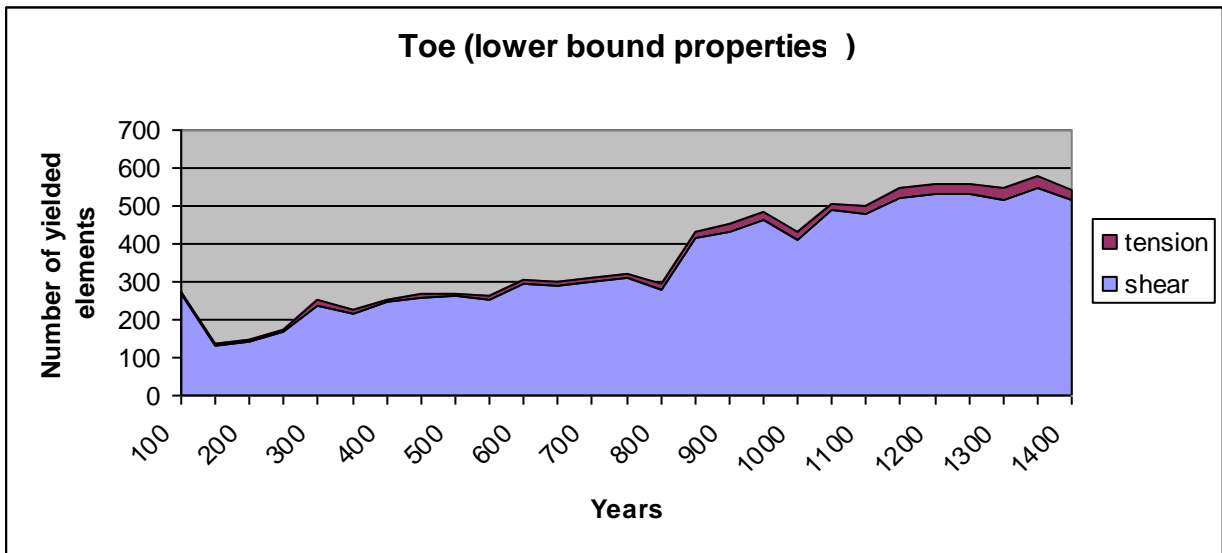


Figure 72: Change in the number of yielded elements present in the toe with cyclic loading up to 1400 years, showing a marked increase after 850 years, assuming the lower bound rock mass properties for a strain softening constitutive model.

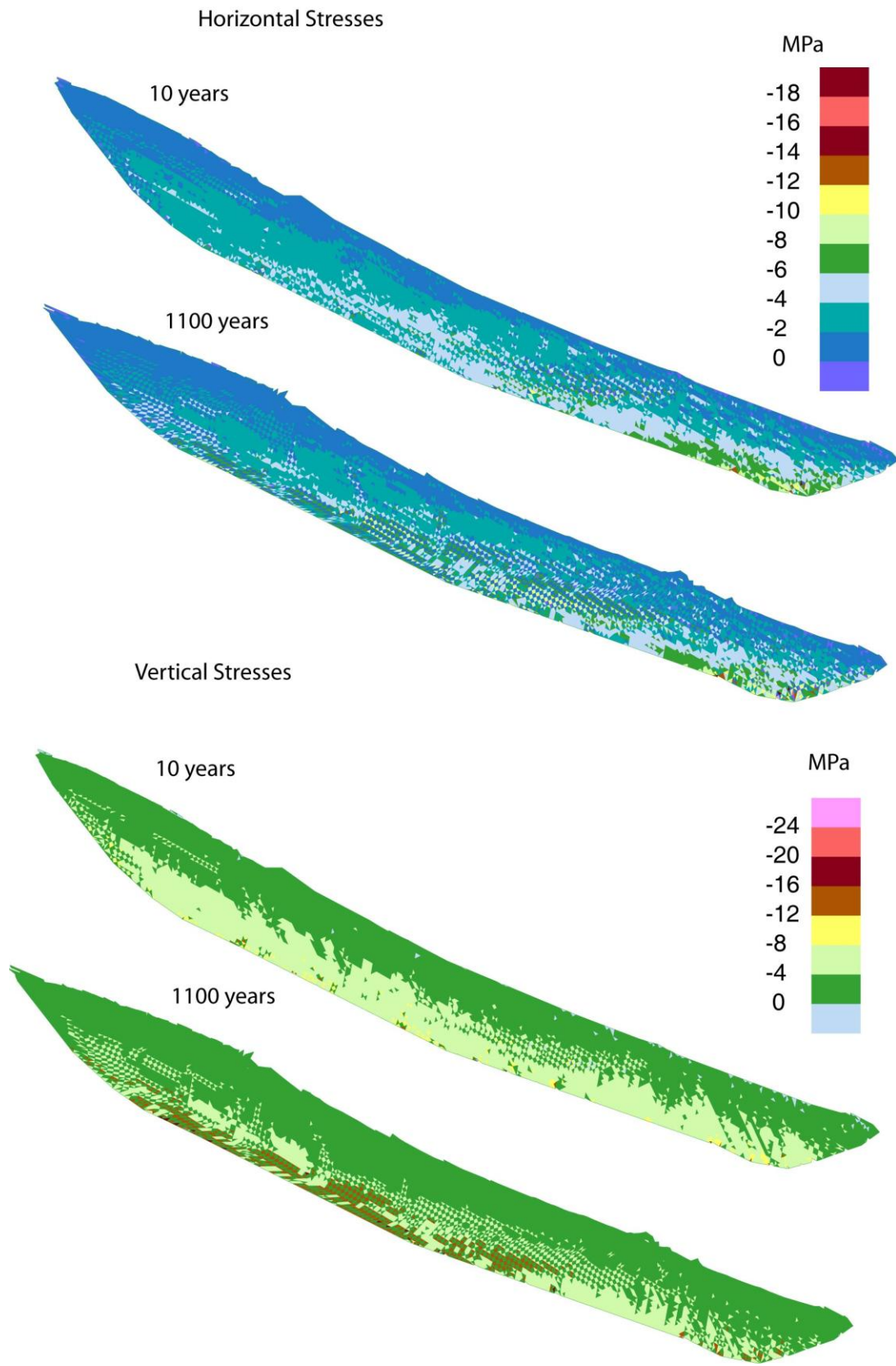


Figure 73: Horizontal and vertical stresses above the basal detachment surface and 10 and 1100 years

Figure 73 shows the horizontal and vertical stresses above the basal detachment surface at 10 and 1100 years. The horizontal stresses show little variation, although at ten years the stresses in the bottom of the toe are a bit higher than those seen at 1100. This is logical as movement and rearrangement of the toe between these times could have contributed to reducing these stresses. The vertical stresses at 1100 years are quite different than those at 10 years. There are higher vertical stresses near the detachment surface and the bottom of the toe in the 1100 year model, and they transition more quickly toward the lowest values seen at the top of the slide. Again, this is interpreted to be due to the fact that these stresses drive movement that in turn allows for the relief and reduction of stresses, while the movement can drive an increase in stresses at other areas.

5.5.3 Movement Patterns and Toe Release

Figure 74 shows the distribution of horizontal movement within the slide body at 3500 years assuming the presence of several interpreted internal shear surfaces shown in earlier figures. It can be seen that there is little difference in the amount of movement seen throughout the slide body, except that the very top is not moving as much as the areas down slope. This is consistent with geodetic data recorded at the site, which shows little variation across the surface, with slightly more movement near the toe. In the lower half of the slide, much of the movement is taken up along the upper internal sliding surface, and significantly less movement is seen in the deep toe, indicating that the upper sliding surface is the preferential one for movement.

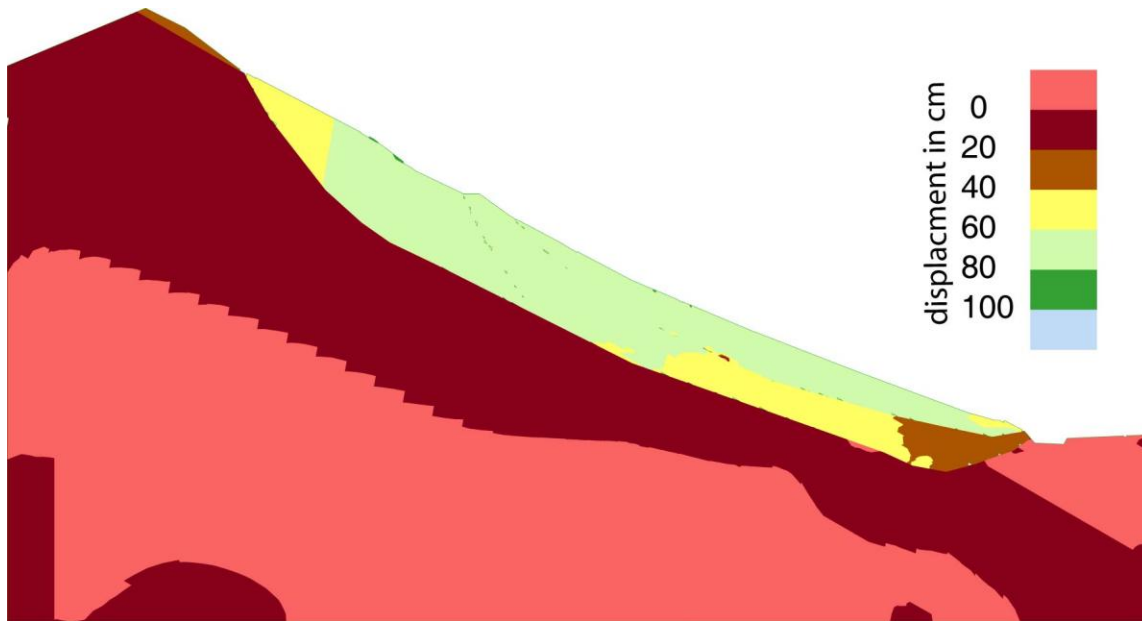


Figure 74: Distribution of horizontal displacement in the down slope direction.

Of interest in studying the distribution of movement and internal shearing within the slide body is consideration of the toe release mechanism. Studies of internal shearing and the development of a

transition zone between active and passive blocks of a slide body have been discussed in depth by Kvapil and Clews (1971; 1979) and (Fisher, 2009). This was not a major consideration in the Campo Vallemaggia slide due to the fact that the sliding surface daylighted into the valley in an unconfined manner and was relatively linear in shape. In contrast, the toe of the slide for Little Chief is confined. This would suggest that the toe represents both a passive wedge and transition zone, sometimes called a Prandtl wedge, being incrementally loaded through down slope movements of the upper active wedge. This coinciding transition zone and passive wedge would be expected to experience a significant amount of internal deformation and shearing, which in turn would allow down slope movement of the landslide.

Figure 68 provides an example of the extensive number of yielding elements that develop in the toe of the slide through a progression of 10, 500 and 1000 years. Shortly after modelling and initiation of yielding begins, the number of yielded elements in the fatigue models shows a significant increase in the toe area (Figures 69-72).

Figure 75 shows the resulting kinematics in terms of displacement vectors and movement of the slide mass within the toe. An upward rotational movement can be seen controlled by the toe release feature at the bottom of the slope. The confinement provided here is likely a key controlling factor in the limited movement of the slide body, which is on the scale of only a few millimetres per year. As well, it is likely that this necessity for toe release, combined with the valley fill cover, have contributed to the development of the secondary internal sliding surface present in the lower half of the slide. This surface does not have the same toe release requirements, and so can take up more movement of the upper half of the slide in a translational manner without the necessity of driving the toe upward.

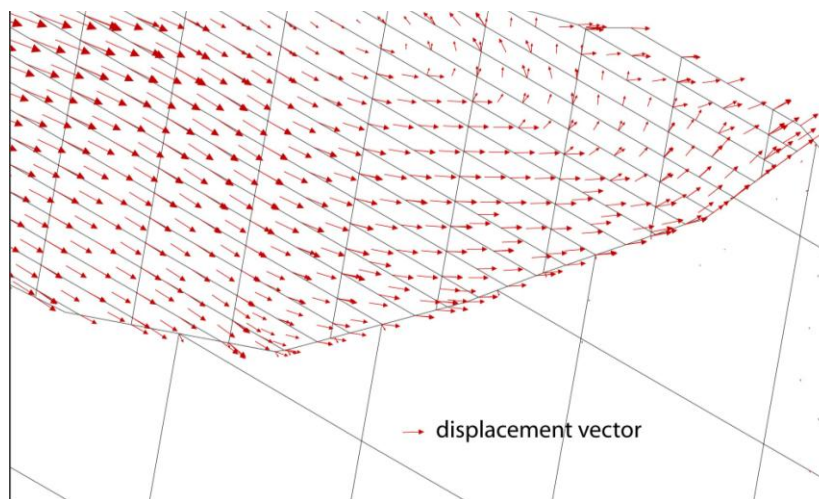


Figure 75: Toe of the landslide showing rotational movement necessary to release and allow movement higher up the slide.

Figure 76 shows the yielded elements, horizontal stresses and vertical stresses in the model at 1100 years. Marked on these is an area of relatively low stresses with very few yielded elements, which appears to be similar to a Prandtl wedge, as described above.

Three versions of the Little Chief model were run and the results presented in this chapter. The first version, aimed at developing a basal detachment surface was partially successful. Toe initiation, the most important point for further modelling, was achieved on the near side of the valley. A through going surface of yielded elements, and variable displacements was seen, however the surface was far deeper than site observations suggest. A full description of potential reasons for this discrepancy is included in section 5.3.2.3. Models of the movement patterns of the slide produce a continual intermittent motion based on water table cycling. Over 3000 years the slide continues to move downhill in the wet season, and stop in the dry. Finally internal deformation modelling produced evidence of the beginning of a fatigue effect in the landslide toe. The number of yielded elements increased with time and cycles. There was no final “breaking” and drop off in yielded elements as was seen at Campo Vallemaggia; however this may have been due to time restrictions that did not allow the model to be run beyond approximately 1400 years. This set of models also produced evidence of a Prandtl wedge forming in the toe, indicating that earlier discussion about the necessity of toe rearrangement for movement to occur was correct.

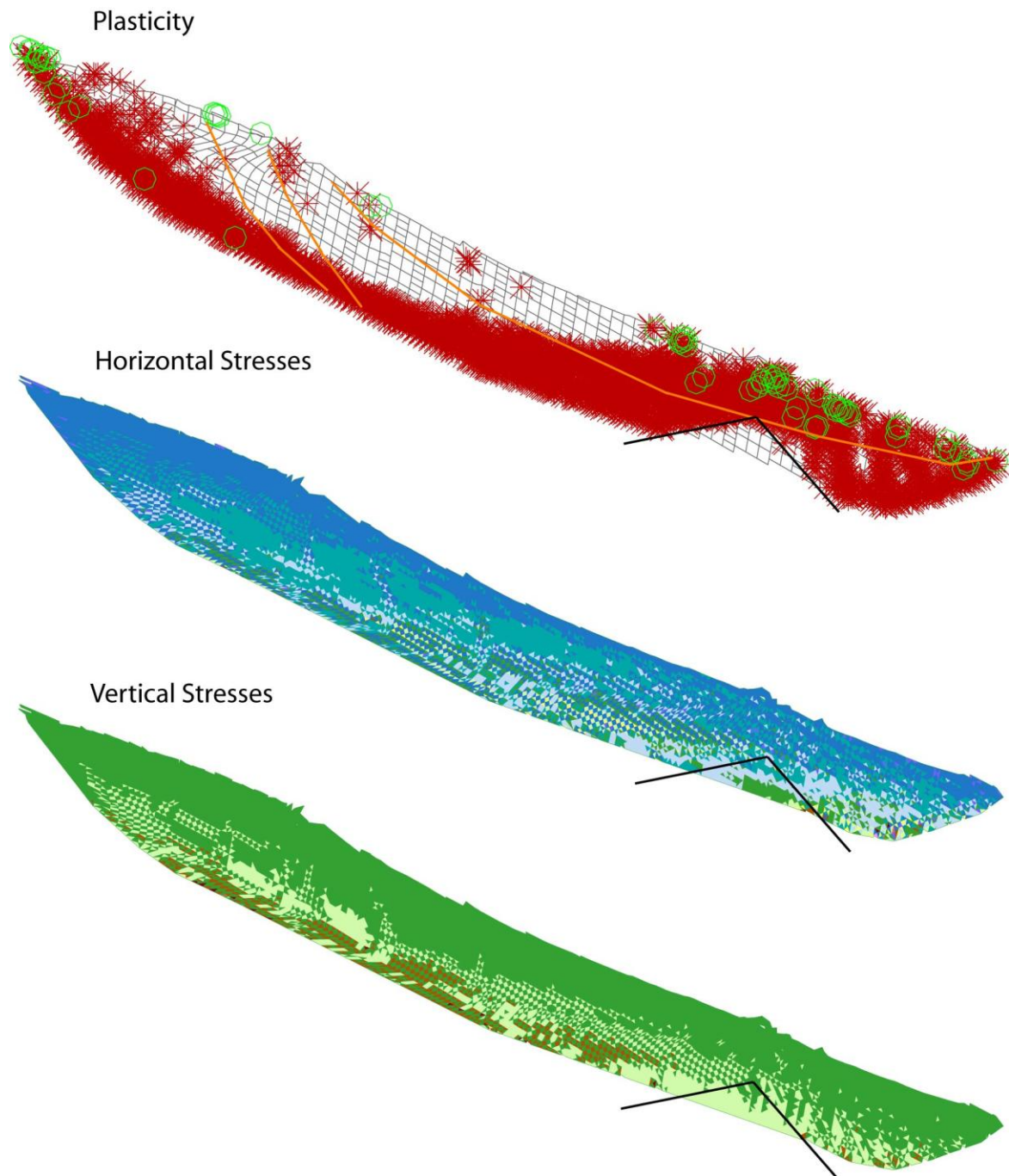


Figure 76: The Prandtl wedge, identified in the yielded elements, horizontal stresses and vertical stresses in the model

6 Conclusions

The primary objective of this thesis was to investigate the integration of time dependency and fatigue in the numerical modelling of deep-seated rockslide movements by treating time implicitly through the cyclic loading of high and low water tables. This was carried out using the distinct-element program UDEC.

The methodology developed involves bringing an elasto-plastic model to equilibrium, and then alternating a high and low water table, representing wet and dry seasons, to introduce cyclic fatigue loading. One high-low cycle was considered to represent one year. The only limitations on the number of years to be modelled were those of time and computing availability. Variations were used wherein different upper bound water tables were periodically introduced to represent storm events.

This methodology was applied to two case studies involving deep-seated rockslides in crystalline rock, Campo Vallemaggia and Little Chief, but for which the kinematics and sliding mechanisms differ. Modelling attempted to reproduce displacement rates and geological features mapped on site. The general pattern of movements seen as the water table is raised and lowered follows that which is expected based on previous behaviour of the slides (i.e. intermittent movements). A total annual displacement value that correlates with that measured on site was reproduced for each slide. These results validate the use of this methodology for including fatigue damage in rockslide models.

A secondary objective involved the determination of the degree of complexity required to apply this method. For these cases, in which the primary factor contributing to movement is the presence of water in the slope, it was verified that varying only the water table provided sufficient movement and no further complexity was required.. Future work, as described below, should be carried out for cases where the slope movements depend on more than one factor (e.g. temperature and water table fluctuations). It is expected that by incrementally increasing the complexity in such models, increased understanding can be gained as to the complex behaviour of deep-seated rockslides.

The rockslide fatigue modelling method investigated here is easily integrated with field monitoring data, and provides a means to better understand and interpret measured displacement *vs.* time and rockslide behaviour trends. At the same time, a comparison of modelled *vs.* real behaviour allows for deficiencies in the model to be corrected and the model to be calibrated as new data becomes available. Thus, the procedure can be dynamic, involving continual updating to incrementally increase and improve understanding of the model results and that of the rockslide behaviour.

6.1 Fatigue and Internal Shearing for an Unconfined Translational Slide Surface

The rockslide fatigue modelling method was able to reproduce both the stick slip behaviour and the location of internal shear surfaces that had developed in the Campo Vallemaggia slide. This case represents a deep-seated translational slide in crystalline rock with an unconfined toe. The slide body is interpreted to move on a relatively shallow sliding surface (approx. 20°) that daylight at the base of the slope. Continued stick slip movements found through modelling matched what has been recorded by

geodetic monitoring. For this type of simple translational movement, a Mohr-Coulomb plasticity model was sufficient to reproduce key characteristics of the actual slide movement and internal deformation.

Fatigue effects, produced through cyclic loading, were seen in the Campo Vallemaggia slide models. A sharp decrease in the number of yielding elements present in the slide was seen after 1300 cycles (or years), at which point significant dilation between blocks occurs in the model suggesting the localization and opening of an internal shear within the slide body. This development occurs as the result of accumulated brittle fatigue damage that reaches a threshold enabling localization and mobilization. It should be noted though, that this development does not lead to catastrophic failure of the rockslide, but leads to the opening of an internal fault, which subsequently accommodates differential movements in the upper and lower sections of the slide body. This modelled fault occurred at the same approximate location as that of a major fault feature mapped on the slide surface. Although influenced by the shape of failure surface, this provides a certain degree of validation to this method and demonstrates the importance of such internal shear surfaces in the evolution of deep-seated rockslides.

Furthermore, a very large number of fatigue cycles were required before the internal shear developed, indicating that in this situation, it is not a simple or sudden process, but instead one that incrementally develops over long periods of time.

6.2 Fatigue and Internal Shearing for a Confined Translational Slide Surface

Fatigue effects were considered for a second deep-seated slide in crystalline rock, the Little Chief slide, but where the sliding surface is interpreted as being confined at the slope toe. Kinematically, this requires a more complex toe break out mechanism for release than Campo Vallemaggia. Modelling focussed on scenarios with and without the sliding surface explicitly included, and use of a strain softening constitutive model to examine fatigue damage at the toe of the slide. In these cases it was an increase in yielded elements with continued cyclic loading that is interpreted as representing the early stages of fatigue.

Results showed an increase in the number of yielded elements at around 800 years at the earliest, although slow increases are seen before and after. These results combined with those from Campo Vallemaggia indicate that the fatigue and rockslide evolution process is a long one involving many cycles. Both of these slides only begin to show fatigue effects at cycling on the order of 1000 years. Many other models simply could not be cycled for this long due to computing constraints, and it may be speculated as to how many cycles would be required for accelerating behaviour of the entire slide body as opposed to localized accelerations.

The goal of validating the interpretation of the surface of the Little Chief slide was best achieved through strain-softening modelling. A full sliding surface was developed through yielded elements in the homogeneous lower bound model. When a layered model was tested, incorporating increasing rock mass strength and improved rock mass conditions as a function of depth, a similar surface could be interpreted in the horizontal displacement output. Specifically with regards to the toe, the models were very consistent with the location at which breakout occurred, providing validation for the assumption that the slide surface more likely daylight on the near side of the valley. Further refinement of this model could potentially improve this fit even further.

Overall, the results consistently agree with interpretations of the basal sliding surface made based on the exploratory boreholes drilled in the lower sections of the slide. All models run either show no localization and breakout of the toe, or localization on the near side of the valley. Again, this validates the interpretation that the slide surface daylight in the near side of the valley. Near the top of the slide, where field data is more limited, the model results point to the possibility of extensional features existing near or behind the peak of the slope. No direct field data was available to support or oppose this interpretation, however such an occurrence is compatible with other recent studies of other large rockslides in crystalline rock (Zangerl et al., 2010). Linear features seen in air photos of the backside of the mountain near the crest may be an indicator of the existence of an extended slide surface in the upper slope.

For the type of confined movement seen at the Little Chief slide, and the necessary rearrangement and yielding of the toe for any progression of the slide, a Mohr-Coulomb plasticity model was sufficient to reproduce the intermittent, periodic displacement behaviour of the slide. However, in order to obtain meaningful results relating to internal deformation and fatigue, a more complex strain-softening plasticity model was required. The confinement of the toe prevented the kinematic freedom required to enable mobilization of the slide to develop when using a Mohr-Coulomb elasto-plastic model to simulate the progressive weakening and fatigue of the rock mass. In contrast, the strain softening model produced these effects nicely, allowing increased deformations to develop at the toe, which in turn made further movement of the upper slide possible.

6.3 Recommendations for Future Work

A key direction for further work on fatigue and progressive failure of deep-seated rockslide systems is the expansion of this work into three dimensions. Modelling in 3-D using 3DEC or another 3-D numerical modelling program would allow for the better representation of 3-D spatial and kinematic effects. In turn, this would allow the models to more accurately represent reality, especially with respect to the complexity of the sliding surfaces which are highly variable across their width. A single 2-D cross section through the slide significantly simplifies the kinematic controls acting on the slide. As well, a 3-D treatment of the problem would allow for the incorporation of lateral constraint as a consideration in the modelling. This would likely require significantly more field data in order to be treated with any degree of confidence.

As well, this work may be expanded to consider other potential causes for apparent time-dependent movement, such as were discussed in Chapter 2. Narrowing of the subject scope for this study and focussing solely on large natural rockslides, has limited the treatment of the fatigue source to that of a varying water table. Open pit mine excavation sequencing (i.e. benching), incremental erosion, varying temperature and changing vegetation and land use, among others, could be considered in the same manner in which water table changes have been used as a representation of time within this thesis.

Expanding upon the idea of incorporating other types of apparent time dependence, it would be of interest to apply this method to a more complex landslide, where more than one factor drives the apparent time-dependent movement. For both of the slides considered in this study, the variation of the water table was sufficient to reproduce the movement seen at the site. However there are many landslides and rockslides that are controlled by very complex combinations of kinematics and rock mass deformation

and yield mechanisms. It would be of particular interest to see this method applied to a slide where the factors are not coupled with respect to time, such as a large open pit mine undergoing continuing excavation, which is also sensitive to groundwater levels or to thermal effects. This would be a significantly more computationally extensive problem than the ones considered in this study.

Preliminary work was carried out in Chapter 5 to incorporate spatial variation of rock mass properties into the model. However, this was largely limited by time restrictions. Only a very simple layered approach of varying the properties with depth was applied here. A more involved approach would be to more accurately assess the change in rock properties at the site and apply these in a more continuous fashion in the model. The viability of this approach is greatly dependent on the degree of variation at the site and the ability to characterize it. A discussion of several factors contributing to an imperfect fit between modelled and observed behaviour was included in section 5.4.1.3. Along with spatial variation and the 3-D effects, the presence of unknown geological structures (undetected in surface mapping or borehole data) is also very significant. Continued updating of models with the acquisition of new site investigation data is essential to improve the work, even if the updated data only affirm the results found to date.

Bibliography

- Angeli, M.-G., Pasuto, A., and Silvano, S. 2000. A critical review of landslide monitoring experiences. *Engineering Geology*, 55(3): 133-147.
- Bagde, M.N., and Petros, V. 2005a. Fatigue properties of intact sandstone samples subjected to dynamic uniaxial cyclical loading. *International Journal of Rock Mechanics and Mining Sciences*, 42(2): 237-250.
- Bagde, M.N., and Petros, V. 2005b. Fatigue properties of intact sandstone samples subjected to dynamic uniaxial cyclical loading. *International Journal of Rock Mechanics and Mining Sciences*, 42: 237-250.
- Bhandari, R. 1988. Special Lecture: Some practical lessons in the investigation and field monitoring of landslides. *Fifth International Symposium on Landslides*. A. A. Balkama, Lausanne, 1435-1457.
- Bonzanigo, L., Eberhardt, E., and Loew, S. 2007. Long-term investigation of a deep-seated creeping landslide in crystalline rock; Part I, Geological and hydromechanical factors controlling the Campo Vallemaggia landslide. *Canadian Geotechnical Journal*, 44(10): 1157.
- Corominas, J., Moya, J., Lloret, A., Gili, J.A., Angeli, M.-G., Pasuto, A., and Silvano, S. 2000. Measurement of landslide displacements using a wire extensometer. *Engineering Geology*, 55(3): 149-166.
- Cristescu, N.D., Cazacu, O., and Cristescu, C. 2002. A model for slow motion of natural slopes. *Canadian Geotechnical Journal*, 39(4): 924-937.
- Desai, C.S., Samtani, N.C., and Vulliet, L. 1995. Constitutive modeling and analysis of creeping slopes. *Journal of Geotechnical Engineering*, 121(1): 43-56.
- Eberhardt, E. 2008. Twenty-ninth Canadian Geotechnical Colloquium: The role of advanced numerical methods and geotechnical field measurements in understanding complex deep-seated rock slope failure mechanisms. *Canadian Geotechnical Journal*, 45(4): 484.
- Eberhardt, E., Stead, D., and Stimpson, B. 1999. Quantifying progressive pre-peak brittle fracture damage in rock during uniaxial compression. *International Journal of Rock Mechanics and Mining Sciences & Geomechanics Abstracts*, 36(3): 361-380.
- Eberhardt, E., Bonzanigo, L., and Loew, S. 2007. Long-term investigation of a deep-seated creeping landslide in crystalline rock; Part II, Mitigation measures and numerical modelling of deep drainage at Campo Vallemaggia. *Canadian Geotechnical Journal*, 44(10): 1181-1199.
- Federico, A., Fielibus, C., and Intero, G. 2002. The Prediction of Landslide Time to Failure - A state of the art. *Landslides, slope stability and the safety of infra-structures*, Singapore, 167-180.
- Fisher, B.R. 2009. Improved characterization and analysis of bi-planar dip slope failures to limit model and parameter uncertainty in the determination of setback distances, University of British Columbia, Vancouver.
- Font, M., Lagarde, J.L., Amorese, D., Coutard, J.P., Dubois, A., Guillemet, G., Ozouf, J.C., and Vedie, E. 2006. Physical modelling of fault scarp degradation under freeze-thaw cycles. *Earth Surface Processes and Landforms*, 31(14): 1731-1745.
- Franklin, J. 1990. *Mine Monitoring Manual*. Harpell's Press Cooperative, Ste-Anne-de-Bellevue.
- Fukuzono, T. 1985. A new method for predicting failure time of a slope. *IVth International Conference Field Workshop on Landslides*, Tokyo, Japan. 1, 145-150.
- Furuya, G., Sassa, K., Hiura, H., and Fukuoka, H. 1999. Mechanism of creep movement caused by landslide activity and underground erosion in crystalline schist, Shikoku Island, southwestern Japan. *Engineering Geology*, 53: 3-4.
- Gili, J.A., Corominas, J., and Rius, J. 2000. Using Global Positioning System techniques in landslide monitoring. *Engineering Geology*, 55(3): 167-192.

- Glawe, U., and Lotter, M. 1996. Time prediction of rock slope failures based on monitoring results. *Seventh International Symposium on Landslides*, Trondheim, Balkema. 3, 1551-1555.
- Goodman, R.E. 1980. *Introduction to rock mechanics*. John Wiley and Sons, New York.
- Goodman, R.E. 1993. *Engineering geology; rock in engineering construction*. John C. Wiley and Sons, New York.
- Gunzburger, Y., Merrien-Soukatchoff, V., and Guglielmi, Y. 1997. Influence of daily surface temperature fluctuations on rock slope stability; case study of the Rochers de Valabres slope (France). *International Journal of Rock Mechanics and Mining Sciences*, 42(3): 331-349.
- Hajiabdolmajid, V., Kaiser, P.K., and Martin, C.D. 2002. Modelling brittle failure of rock. *International Journal of Rock Mechanics and Mining Sciences*, 39(6): 731-741.
- Hajiabdolmajid, V., Kaiser, P., and Martin, C.D. 2003. Mobilised strength components in brittle failure of rock. *Geotechnique*, 53(3): 327-336.
- Hall, K. 1999. The role of thermal stress fatigue in the breakdown of rock in cold regions. *Geomorphology*, 31(1-4): 47-63.
- Halsey, D.P., Mitchell, D.J., Dews, S.J., and Anonymous 1998. Influence of climatically induced cycles in physical weathering. *Engineering Geology*, 31(4): 359-367.
- Hammah, R.E., Yacoub, T.E., Corkum, B., and Curran, J.H. 2005. A comparison of finite element slope stability analysis with conventional limit-equilibrium investigation. *Proceedings of the 58th Canadian Geotechnical and 6th Joint IAHCNC and CGS Groundwater Specialty Conferences – GeoSask 2005*, Saskatoon, Canada.
- Hart, R.D. 1993. *An introduction to distinct element modeling for rock engineering*. Pergamon Press, Oxford, United Kingdom.
- Itasca 2009. UDEC 4.0.
- Jaeger, J.C. 1979. *Fundamentals of rock mechanics*. Fletcher and Son Ltd., Norwich.
- Jin, F., Zhang, C., Wang, G., and Wang, G. 2003. Creep modeling in excavation analysis of a high rock slope. *Journal of Geotechnical and Geoenvironmental Engineering*, 129(9): 849-857.
- Kvapil, R., and Clews, K. 1971. An examination of the Prandtl mechanism in large dimension slope failures. *Transactions of the Institution of Mining & Metallurgy, Section A(A1-A5.)*.
- Kvapil, R., and Clews, K. 1979. An examination of the Prandtl mechanism in large slope failures. *Transactions of the Institution of Mining & Metallurgy, Section A*, 88: 1-5.
- Lajtai, E.Z. 1969. Strength of discontinuous rocks in direct shear. *Geotechnique; with French abs.*, 19(2): 218-233.
- Lee, Y.-K., and Pietruszczak, S. 2008. A new numerical procedure for elasto-plastic analysis of a circular opening excavated in a strain-softening rock mass. *Tunnelling and Underground Space Technology*, 23(5): 588-599.
- Leroueil, S., Vaunat, J., Picarelli, L., Locat, J., Lee, H.J., and Faure, R.M. 1996. Geotechnical characterization of slope movements. *Proceedings of the International Symposium on Landslides*, 7(1): 53-74.
- Marinos, V., Marinos, P., and Hoek, E. 2005. The geological strength index: applications and limitations. *Bulletin of Engineering Geology and the Environment.*, 64(1): 55-65.
- Martin, C. 1997. Seventeenth Canadian geotechnical colloquium: the effect of cohesion loss and stress path on brittle rock strength. *Canadian Geotechnical Journal*, 28(2): 698-725.
- Mikkelsen, P.E. 2003. Advances in inclinometer data analysis. *6th International Symposium on Field Measurements in Geomechanics*. Swets & Zellinger, Oslo, Norway, 555-567.
- Moore, D.P., and Watson, A.D. 2007. Mica Dam - Little Chief Slide Deficiency Investigation report B. Hydro. E521
- Moore, R., Lee, E.M., and Noton, N.H. 1991. Strategies for managing the landslide complex at Ventnor, Isle of Wight. *Proceedings of the international conference on Slope stability organized by the*

- Institution of Civil Engineers; slope stability engineering, developments and applications*. Thomas Telford, United Kingdom, Isle of Wight, United Kingdom, 225-230.
- Newmark, N.M. 1965. Effects of earthquakes on dams and embankments. *Geotechnique*, 15(2): 139-159.
- Perzyna, P. 1966. Fundamental problems in viscoplasticity. *Advances in Applied Mechanics*, 9: 243-377.
- Pichler, B., Hellmich, C., and Mang, H.A. 2007. A combined fracture-micromechanics model for tensile strain-softening in brittle materials, based on propagation of interacting microcracks. *International Journal for Numerical and Analytical Methods in Geomechanics*, 31: 112-132.
- Priest, S. 1993. *Discontinuity analysis for rock engineering*. Chapman & Hall, USA.
- RocScience 2003. Slide 5.0.
- RocScience 2007. RocLab.
- Rose, N.D., and Hungr, O. 2007. Forecasting potential rock slope failure in open pit mines using the inverse-velocity method. *International Journal of Rock Mechanics and Mining Sciences*, 44(2): 308-320.
- Saito, M. 1965. Forecasting the time of occurrence of a slope failure. *6th International Conference on Soil Mechanics and Foundation Engineering*. University of Toronto Press, Montreal, Canada. 2, 537-541.
- Salt, G. 1988. Landslide mobility and remedial measures. *Proceedings of the International Symposium on Landslides = Comptes Rendus du Symposium International sur les Glissements de Terrain*, 5: 575-762.
- Samtani, N.C., Desai, C.S., and Vulliet, L. 1996. An interface model to describe viscoplastic behaviour. *International Journal for Numerical and Analytical Methods in Geomechanics*, 20(4): 231-252.
- Smithyman, M., Eberhardt, E., and Hungr, O. 2009. Characterization and numerical analysis of intermittent slope displacements and fatigue in deep-seated fractured crystalline rock slopes. *Proceedings of the 62nd Annual Canadian Geotechnical Conference*, Halifax.
- Vitale, S., and Mazzoli, S. 2008. Heterogeneous shear zone evolution; the role of shear strain hardening/softening. *Journal of Structural Geology*, 30(11): 1383-1395.
- Watson, A.D. 2006a. Mica Dam - Little Chief Slide 2005 Field Investigation Report B. Hydro. E434 v2
- Watson, A.D. 2006b. Mica Dam - Little Chief Slide 2005 Field Investigation Report B. Hydro. E434 v3
- Watson, A.D. 2006c. Mica Dam - Little Chief Slide 2005 Field Investigation Report B. Hydro. E434 v1
- Watson, A.D., Moore, D.P., and W., S.T. 2004. Temperature Influence on Rock Slope Movements at the checkerboard Creek. *9th JSL.A. A. Bellarma*, Rio de Janeiro, Brazil.
- Watson, A.D., Martin, C.D., Moore, D.P., Stewart, T.W.G., and Lorig, L.J. 2006. Integration of geology, monitoring and modelling to assess rockslide risk. *Felsbau*, 24(3): 50-58.
- Willenberg, H., Evans, K.F., Eberhardt, E., Spillmann, T., and Loew, S. 2008a. Internal structure and deformation of an unstable crystalline rock mass above Randa (Switzerland); Part II, Three-dimensional deformation patterns. *Engineering Geology*, 101(1-2): 15-32.
- Willenberg, H., Loew, S., Eberhardt, E., Evans, K.F., Spillmann, T., Heincke, B., Maurer, H., and Green, A.G. 2008b. Internal structure and deformation of an unstable crystalline rock mass above Randa (Switzerland); Part I, Internal structure from integrated geological and geophysical investigations. *Engineering Geology*, 101(1-2): 1-14.
- Zangerl, C., Eberhardt, E., and Perzmaier, S. 2010. Kinematic behaviour and velocity characteristics of a complex deep-seated crystalline rockslide system in relation to its interaction with a dam reservoir. *Engineering Geology*, 112(1-4): 53-67.
- Zangerl, C., Evans, K.F., Eberhardt, E., and Loew, S. 2008. Consolidation settlements above deep tunnels in fractured crystalline rock: Part I - Investigations above the Gotthard highway tunnel. *International Journal of Rock Mechanics and Mining Sciences*, 45(8): 1195-1210.

Zhang, P., Li, N., Li, X., and Nordlund, E. 2009. Compressive failure model for brittle rocks by shear faulting and its evolution of strength components. *International Journal of Rock Mechanics and Mining Sciences*, 46(5): 830-841.

Appendix A - Time and Computing Requirements

Table A1: Computing time requirements for variations of the models

Intel Pentium 4 3.2 GHz. 2 GB RAM	
Campo Vallemaggia - 10years	10.5 hours
Intel Pentium 4 3.2 GHz. 4 GB RAM	
Campo Vallemaggia - 10 years	4.5 hours
Little Chief - 10 years (Mohr Coulomb)	2.5 hours
Intel Quad Core 2.46 GHz, 4 GB RAM	
Little Chief - 10 years (Mohr Coulomb)	1.75 hours
Little Chief – 3000 years (Mohr Coulomb)	525 hours
Little Chief - 10 years (Strain Softening)	4.5 hours
Little Chief - bring strain softening to equilibrium	26 hours

Table A1 gives the time requirements (approximate) for various common tasks on the available computers. Note that all of the times given are valid only when only one model is running at a time. Running multiple models on the same computer in parallel increases run times.

Appendix B - Modelling Code

B.1 Annual Cycling – Fish Code

This code, when applied to a landslide model at equilibrium, will cycle through two annual water tables. Present in the code presented here are the high and low table values for the Little Chief Slide with no 10 or 100 year events.

```
; low water table
table 1 0,1373 1339,1054 2864,660 3143,657 3161,643 3189,643 3254,609 3288,571 3382,567 3392,586
3663,598
;high water table
table 2 0,1373 1339,1154 2864,760 3143,657 3161,643 3189,643 3254,609 3288,571 3382,567 3392,586
3663,598

;fish loop to cycle water table 10 times (10 years)
def wtableloop
loop n (1,10)

command
insitu yw table 2
cycle 1000
end_command
command
insitu yw table 1
cycle 1000
end_command
endloop
end
```

B.2 Campo Vallemaggia Geometry

This code creates the basic Campo Vallemaggia model and brings it to equilibrium before water or plasticity are applied

```
round 0.5
block 1355,500 1355,2100 4120,2100 4120,500

; topography geometry
crack 1355,2100 1575,1935
crack 1575,1935 1620,1920
crack 1620,1920 1914,1825
crack 1914,1825 2337,1687
crack 2337,1687 3734,1060
crack 3734,1060 4120,960

; slide surface geometry
crack 1620,1920 1629,1881
```

crack 1629,1881 1656,1832
crack 1656,1832 1696,1779
crack 1696,1779 1734,1736
crack 1734,1736 1774,1702
crack 1774,1702 1823,1674
crack 1823,1674 2030,1620
crack 2030,1620 2056,1591
crack 2056,1591 2388,1495
crack 2388,1495 2431,1456
crack 2431,1456 2710,1374
crack 2710,1374 2964,1269
crack 2964,1269 3116,1229
crack 3116,1229 3271,1164
crack 3271,1164 3442,1115
crack 3442,1115 3490,1106
crack 3490,1106 3734,1060

; fault geometry

crack 1914,1825 1914,1794
crack 1914,1794 1920,1764
crack 1920,1764 1937,1734
crack 1937,1734 1951,1716
crack 1951,1716 2030,1620

; define blocks through material numbers

change mat=1 range block 202
change mat=2 range block 4155
change mat=2 range block 1990

; define joint material numbers

change jmat=1 range block 202
change jmat=2 range block 4155
change jmat=2 range block 1990

; delete overburden

delete block 541

; sub-vertical jointing in base

jset -75,0 1000,0 0,0 100,0 3335,1100 range mat 1
jdelete

; foliation/jointing of unstable mass

jset -5,0 450,0 0,0 5,0 1620,1920 range mat 2
jdelete

; sub-horizontal jointing for flow connectivity in base

jset -20,0 5000,0 0,0 50,0 3335,1100 range mat 1

```
; sub-vertical jointing for partial connectivity in unstable mass
jset -75,0 7,0 5,0 15,0 1620,1920 range mat 2
jdelete
```

```
; sub-vertical jointing for partial connectivity in unstable mass
jset -75,0 7,0 5,0 15,0 1610,1910 range mat 2
jdelete
```

```
; sub-vertical jointing for partial connectivity in unstable mass
jset -75,0 7,0 5,0 15,0 1620,1980 range mat 2
jdelete
```

```
; sub-vertical jointing for partial connectivity in unstable mass
jset -75,0 7,0 5,0 15,0 1610,1970 range mat 2
jdelete
```

```
; delete small blocks and tunnel
delete range area 100
```

```
; delete toe material
crack 3588,1129 3610,1082
jdelete
delete range 3589.5 3732 1069.5 1126
```

```
; mesh generation
gen quad 10 range mat 3
gen edge 10 range mat 3
gen edge 20
```

```
; material properties (base)
; granitic gneiss - E=30 GPa v=0.25
prop mat=1 dens=2600 k=20e9 g=12e9
prop jmat=1 jkn=1e10 jks=1e9 jfric=45.0
```

```
; material properties (slide block)
; weathered gneiss - E=10 GPa v=0.35
prop mat=2 dens=2600 k=11e9 g=3.7e9
prop jmat=2 jkn=1e10 jks=1e9 jfric=45.0
```

```
; define shear surface
change jmat=3 range mi 1 2
prop jmat=3 jkn=1e10 jks=1e9 jfric=45.0
```

```
; boundary conditions
bound xvel=0 range 1354 1356 499 2101
bound xvel=0 range 4119 4121 499 2101
```

```

bound yvel=0 range 1354 4121 499 501

; in situ stress conditions (gravitational loading)
insitu str -27.3e6 0 -54.6e6 ygrad 0.013e6 0 0.026e6 &
      szz -27.3e6 zgrad 0 0.026e6
grav 0 -10

; histories
hist unbal
hist xdis 3325,1180 ; (toe)
hist ydis 3325,1180 ; (toe)
solve
save iss.sav

```

B.3 Little Chief Geometry

This code creates the basic Little Chief model and brings it to equilibrium before water or plasticity are applied

```

round 0.5
block 0,0 0,2000 3663,2000 3663,0

; topography geometry
crack 0,1780 442,1965
crack 442,1965 568,1902
crack 568,1902 739,1772
crack 739,1772 1171,1546
crack 1171,1546 1305,1443
crack 1305,1443 1458,1370
crack 1458,1370 1509,1370
crack 1509,1370 1607,1299
crack 1607,1299 1996,1093
crack 1996 1093 2373,934
crack 2373,934 2713,802
crack 2713,802 3073,668
crack 3073,668 3161,643
crack 3161,643 3189,643
crack 3189,643 3254,609
crack 3254,609 3288,571
crack 3288,571 3382,567
crack 3382,567 3392,586
crack 3392,586 3663,598
;separate base into zones
crack 0,1200 2200,0
crack 0,1700 3000,0

;sliding surface
crack 750,1770 840,1612

```

crack 840,1612 1018,1383
crack 1018,1383 1133,1279
crack 1133,1279 1224,1215
crack 1224,1215 1372,1144
crack 1372,1144 1999,828
crack 1999,828 2806,570
crack 2806,570 2897,549
crack 2897,549 3099,483
crack 3099,483 3141,490
crack 3141,490 3174,512
crack 3174,512 3198,525
crack 3198,525 3221,548
crack 3221,548 3280,591

change mat=1
change jmat=1

; delete overburden
delete block 1108

; joint regions for later material and joint set assignment
jregion id 1 0,0 0,1200 2200,0 0,-1
jregion id 2 0,1200 0,1700 3000,0 2200,0
jregion id 3 3778,-454 0,1700 0, 2000 3778, 2000

; sub-vertical jointing in base
jset 90,0 1000,0 0,0 400,0 150,0 range jregion 1

; sub-horizontal jointing for flow connectivity in base
jset -30,0 5000,0 0,0 300,0 0,0 range jregion 1

; sub-vertical jointing in middle
jset 80,0 2000,0 0,0 100,0 25,0 range jregion 2

; sub-horizontal jointing for flow connectivity in middle
jset -30,0 5000,0 0,0 100,0 0,0 range jregion 2

change mat=5 range block 3588
change mat=4 range block 4541

; sub-vertical jointing in mass
jset 80,0 2000,0 0,0 100,0 0,0 range jregion 3

; sub-horizontal jointing for flow connectivity in mass
jset -30,0 5000,0 0,0 25,0 0,0 range jregion 3

```

jdelete

; delete small blocks and tunnel
delete range area 100

; mesh generation
gen quad 30
gen edge 30
gen edge 60

; material properties (base)
; granitic gneiss - E=30 GPa v=0.25
prop mat=1 dens=2600 k=20e9 g=12e9
prop mat=4 dens=2600 k=20e9 g=12e9
prop mat=5 dens=2600 k=20e9 g=12e9
prop jmat=1 jkn=1e10 jks=1e9 jfric=45.0
prop jmat=4 jkn=1e10 jks=1e9 jfric=45.0
prop jmat=5 jkn=1e10 jks=1e9 jfric=45.0
prop jmat=3 jkn=1e10 jks=1e9 jfric=45.0

;create groups above and below sliding surface
group block up range mat 4
group block low range mat 5

;assign sliding surface properties
change jmat=3 range gint up low

; boundary conditions
bound xvel=0 range -1,1 -1,2001
bound xvel=0 range 3662,3664 -1,2001
bound yvel=0 range -1,3664 -1,1

; in situ stress conditions (gravitational loading) assuming k=1/2
insitu str -25.1e6 0 -50.1e6 ygrad 0.0128e6 0 0.0255e6 &
      szz -25.1e6 zgrad 0 0.0255e6
grav 0 -10

; histories
hist unbal
hist xdis 3382 567 ; (toe)
hist ydis 3382 567 ; (toe)
solve
save faulted1.sav

```

B.4 Plasticity

The code in this section introduces plasticity to the geometry models above

B.4.1 Campo Vallemaggia Mohr Coulomb

```
reset displ jdispl hist
```

```
; elasto-plastic deformation of slide mass  
change cons=3 range mat=2  
change cons=3 range mat=4  
prop mat=2 dens=2250 k=5.5e9 g=1.85e9 coh=0.2e6 fric=30.0 ten=0.1e6  
prop mat=4 dens=2300 k=16.7e9 g=7.69e9 coh=1e6 fric=45.0 ten=0.5e6
```

```
; joint properties  
prop jmat=2 jkn=1e10 jks=1e9 jfric=35.0  
prop jmat=4 jkn=1e10 jks=1e9 jfric=40.0
```

```
; histories  
hist unbal  
hist xdis 3325,1180 ; (toe)  
hist ydis 3325,1180 ; (toe)
```

```
solve  
cycle 5000  
save mc.sav
```

B.4.2 Little Chief Mohr Coulomb

```
reset displ jdispl hist
```

```
; properties prior to plasticity  
prop mat=5 dens=2600 k=20e9 g=12e9  
prop jmat=5 jkn=1e10 jks=1e9 jfric=45.0  
prop mat=4 dens=2600 k=20e9 g=12e9  
prop jmat=4 jkn=1e10 jks=1e9 jfric=45.0  
prop jmat=3 jkn=1e10 jks=1e9 jfric=45.0
```

```
; elasto-plastic deformation of slide mass  
; change cons=3 range mat=5  
change cons=3 range mat=4  
; prop mat=5 dens=2600 k=11e9 g=3.7e9 coh=2.5e6 fric=34.0 ten=0.5e6  
prop mat=4 dens=2600 k=11e9 g=3.7e9 coh=2.5e6 fric=34.0 ten=0.5e6
```

```
; histories  
hist unbal  
hist xdis 3325,1180 ; (toe)  
hist ydis 3325,1180 ; (toe)  
solve  
save faulted2.sav
```

B.4.3 Little Chief Strain Softening

```
reset displ jdispl hist
```

```

prop mat=5 dens=2600 k=20e9 g=12e9
prop jmat=5 jkn=1e10 jks=1e9 jfric=45.0
prop mat=4 dens=2600 k=20e9 g=12e9
prop jmat=4 jkn=1e10 jks=1e9 jfric=45.0
prop jmat=3 jkn=1e10 jks=1e9 jfric=45.0

; tables of strain softening (strain, value)
table 5 0,3e6 0.001,0.05e6 0.002,0.05e6 ;cohesion
table 6 0,34 0.001,25 0.002,25 ;friction
table 7 0,0.3e6 0.001,0.005e6 0.002,0.005e6; tension =1/10 coh

; elasto-plastic deformation of slide mass with strain softening
zone model ss range mat 4

prop mat=4 dens=2600
zone bu=11e9 sh=3.7e9 coh=3e6 fric=34.0 ten=0.5e6
zone ctable=5 ftable=6 ttable=7

; histories
hist unbal
hist xdis 3325,1180 ; (toe)
hist ydis 3325,1180 ; (toe)

solve
save svalley2.sav

```